Chemical Engineering Science 153 (2016) 174–187

Contents lists available at ScienceDirect

Chemical Engineering Science

journal homepage: www.elsevier.com/locate/ces

# Describing diffusion in fluid mixtures at elevated pressures by combining the Maxwell–Stefan formulation with an equation of state

Rajamani Krishna [a,*], Jasper M. van Baten [b]

[a] Van't Hoff Institute for Molecular Sciences, University of Amsterdam, Science Park 904, 1098 XH Amsterdam, The Netherlands
[b] AmsterCHEM, Calle Las Rozas 32, Las Rozas, Cuevas del Almanzora, 04618 Almería, Spain

## HIGHLIGHTS

- Fugacity gradients are the appropriate driving forces for diffusion.
- Compressibility factor influences diffusion in dense gases.
- The thermodynamic corrections are important near supercritical pressures.
- Thermodynamic corrections are predominant near V/L phase transition regions.
- Mixture diffusion is often strongly coupled near phase transition regions.

## GRAPHICAL ABSTRACT

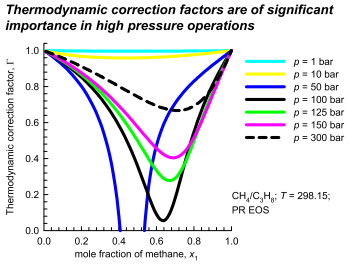


## ARTICLE INFO

*Article history:*
Received 1 June 2016
Received in revised form
18 July 2016
Accepted 20 July 2016
Available online 21 July 2016

*Keywords:*
Equation of state
Compressibility factor
Phase stability
Maxwell–Stefan formulation
Transient overshoots
Curvilinear trajectories

## ABSTRACT

Many operations of interest to chemical engineers require proper modeling of diffusion in fluid mixtures at operating pressures ranging to several megapascals. Examples include supercritical extraction, fractionation of natural gas liquids, enhanced oil recovery and exploitation of shale gas reserves. The Maxwell–Stefan (M–S) formulation, in combination with the Peng–Robinson equation of state, affords a convenient framework for modeling mixture diffusion. The primary objective of this article is to highlight a number of important and distinguishing diffusional characteristics of mixture diffusion at elevated pressures. For dense binary gas mixtures, the pressure-dependence of the M–S diffusivity $Đ_{ij}$ requires additional correction for the compressibility factor, $Z$; this correction introduces a composition dependence for the $Đ_{ij}$ that is absent for ideal gas mixtures. Also significant are influences of the thermodynamic correction factors $\Gamma_{ij}$, that are related to the derivatives of the fugacity coefficients with respect to the compositions. For operations near critical pressures, or close to vapor/liquid and solid/liquid phase transition regions, the thermodynamic factor for binary mixtures tend to reduce to near-zero values; this reduction has a direct and proportional impact on the Fick diffusivities. For ternary fluid mixtures, the $\Gamma_{ij}$ cause the individual diffusion fluxes to be strongly coupled. Such coupling effects can be of significant importance even for hydrocarbon mixtures; this conclusion is not intuitively obvious. Strongly coupled diffusion leads to curvilinear equilibration trajectories, and may cause uphill diffusion of species.



## 1. Introduction

Many separation and reaction processes of interest to chemical engineers are conducted at pressures in the range of 1–100 MPa. The ammonia synthesis reactor operates at pressures ranging to a few hundred bars; the catalyst effectiveness is strongly influenced

* Corresponding author.
*E-mail address:* r.krishna@contact.uva.nl (R. Krishna).

http://dx.doi.org/10.1016/j.ces.2016.07.025
0009-2509/

**Nomenclature**

| | |
|---|---|
| $[B]$ | matrix defined by Eq. (13) ($m^{-2}$ s) |
| $c_i$ | molar concentration of species $i$ (mol $m^{-3}$) |
| $c_t$ | total molar concentration of mixture (mol $m^{-3}$) |
| $C$ | empirical constant |
| $Đ_{12}$ | M–S diffusivity for binary pair 1–2 ($m^2$ $s^{-1}$) |
| $D_{12}$ | Fick diffusivity for binary mixture ($m^2$ $s^{-1}$) |
| $D_{i,eff}$ | Effective diffusivity in mixture ($m^2$ $s^{-1}$) |
| $[D]$ | Fick diffusivity matrix ($m^2$ $s^{-1}$) |
| $\|D\|$ | Determinant of the Fick diffusivity matrix ($m^4$ $s^{-2}$) |
| $E_i$ | Component Murphree efficiency (dimensionless) |
| $f_i$ | fugacity of species $i$ (Pa) |
| Fo | Fourier number (dimensionless) |
| $J_i$ | molar diffusion flux of species $i$ with respect to $u$ (mol $m^{-2}$ $s^{-1}$) |
| $M_i$ | molar mass of species $i$ (kg $mol^{-1}$) |
| $n$ | number of species in the mixture (dimensionless) |
| $N_i$ | molar flux of species $i$ in laboratory fixed reference frame (mol $m^{-2}$ $s^{-1}$) |
| $N_t$ | molar flux of total mixture in laboratory fixed reference frame (mol $m^{-2}$ $s^{-1}$) |
| $p$ | total system pressure (Pa) |
| $P_c$ | critical pressure (Pa) |
| $[Q]$ | matrix quantifying fractional unaccomplished change (dimensionless) |
| $r$ | radial direction coordinate (m) |
| $R$ | gas constant (8.314 J $mol^{-1}$ $K^{-1}$) |
| $t$ | time (s) |
| $T$ | absolute temperature (K) |
| $T_c$ | critical temperature (K) |
| $x_i$ | mole fraction of component $i$ in fluid phase (dimensionless) |
| $y_i$ | mole fraction of component $i$ in vapor phase (dimensionless) |
| $u$ | molar average mixture velocity (m $s^{-1}$) |
| $z$ | direction coordinate (m) |
| $Z$ | compressibility factor (dimensionless) |

*Greek letters*

| | |
|---|---|
| $\delta$ | slab thickness (m) |
| $\delta_{ij}$ | Kronecker delta (dimensionless) |
| $\phi_i$ | fugacity coefficient of component $i$ (dimensionless) |
| $\Gamma_{ij}$ | thermodynamic factors (dimensionless) |
| $[\Gamma]$ | matrix of thermodynamic factors (dimensionless) |
| $[\Lambda]$ | matrix defined by (Eqs. (13) and 15) ($m^2$ $s^{-1}$) |
| $\mu_i$ | molar chemical potential (J $mol^{-1}$) |
| $\mu_i^0$ | molar chemical potential at standard state (J $mol^{-1}$) |
| $\sigma$ | rate of entropy production (J $m^{-3}$ $s^{-1}$ $K^{-1}$) |

*Subscripts*

| | |
|---|---|
| $c$ | referring to critical parameter |
| $i$ | referring to component $i$ |
| $n$ | referring to component $n$ |
| $t$ | referring to total mixture |

by intra-particle diffusion (Dyson and Simon, 1968). Supercritical carbon dioxide ($CO_2$) is widely used as a solvent for extraction of trace quantities of compounds, such as lipids, and caffeine from substrates; such operations are conducted at pressures higher than the critical pressure of $CO_2$, which is 7.28 MPa. The design of supercritical extraction processes is crucially dependent on the proper estimation of the diffusion of solutes into the supercritical fluid phase. Savage et al. (1995) point out a number of advantages that are associated with carrying out reactions under supercritical conditions. Hydro-processing of petroleum fractions is carried out at pressures in the range of 50–100 bar (Sie and Krishna, 1998). Fractionation of natural gas liquids, enhanced oil recovery and exploitation of shale gas reserves are other examples of high pressure processing.

Under the prevailing pressures and temperature conditions, the fluid phases may exist either in the gaseous, liquid, or in a supercritical state. The proper description of the diffusion characteristics in the fluid mixtures is often of crucial importance for equipment design and process development. At elevated pressures, the diffusion characteristics often exhibit significant deviations from those normally observed for either ideal gas mixtures or liquid phase mixtures under ambient conditions. To set the scene and define the objectives of this article, we examine five experimental data sets to highlight departures from normal diffusion behaviors.

Fig. 1 shows the experimental data of Takahashi and Hongo (1982) for diffusivities of $CO_2$(trace amounts)/$C_2H_4$ mixtures, and $CO_2$/$C_2H_4$(trace amounts) mixtures at 323.2 K for pressures ranging to 180 bar. For an ideal gas mixture, the binary diffusivity is inversely proportional to the pressure, and is independent of composition. The dashed line in Fig. 1 shows the estimates of diffusivity using empirical (FSG) method of Fuller et al. (1966), based on the kinetic theory of gases, and widely used in chemical engineering practice

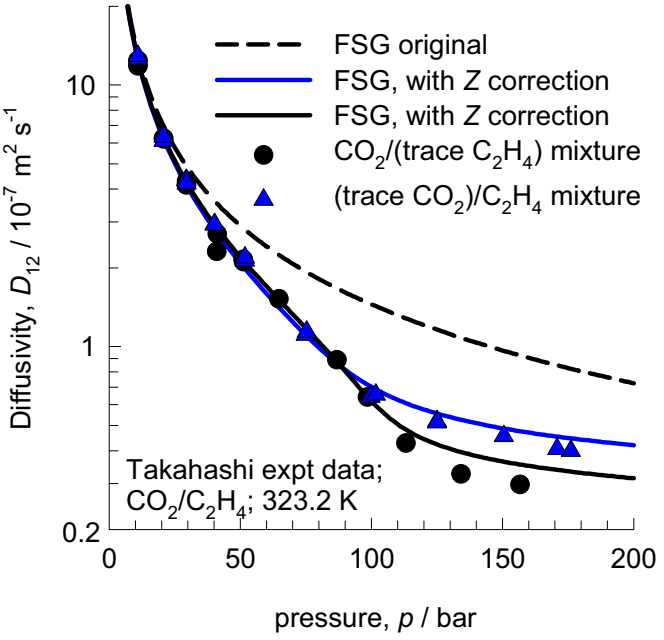


**Fig. 1.** Experimental data of Takahashi and Hongo (1982) for M–S diffusivities of $CO_2$(trace amounts)/$C_2H_4$ mixtures, and $CO_2$/$C_2H_4$(trace amounts) mixtures at 323.2 K for a range of pressures. The dashed line represents the estimations using the FSG Eq. (1). The continuous solid lines represent the estimations of the M–S diffusivities using Eq. (22).

$$D_{12}^{FSG} = C\frac{T^{1.75}}{p\sqrt{M_{12}}\left[\left(v_1^{1/3}\right)+\left(v_2^{1/3}\right)\right]^2}\ \text{m}^2\ \text{s}^{-1} \tag{1}$$

where $C$ is an empirical constant, $p$ is the pressure, $M_{12} = \frac{2}{\frac{1}{M_1}+\frac{1}{M_2}}$ is the mean molar mass of the mixture, $v_1$, and $v_2$ are the diffusion volume, whose values are obtained by summing the contributions of the volumes of the constituent atoms in the molecular species (the values are tabulated in Table 11.1 of Reid et al. (1986)). According to the FSG estimation procedure, the product of $D_{12}^{FSG}$ and the total pressure, $pD_{12}^{FSG}$ is a function only of temperature and is also independent of composition.

At $p=180$ bar, the FSG estimate is about five times higher than the experimentally determined values. Evidently, increasing pressure reduces the diffusivity more than proportionately. A further point to note is that for $p>100$ bar, the diffusivities of $CO_2$(trace amounts)/$C_2H_4$ mixtures is higher than that for $CO_2$/$C_2H_4$(trace amounts) mixtures. What are the reasons for significant deviations from the diffusivity characteristics of ideal gas mixtures? How do we quantify the $D_{12}$ vs $p$ characteristics?

Fig. 2 shows the experimental data of Tuan et al. (1999) for the dependence of the Fick diffusivity of methyl oleate (MO) (component 1) in supercritical $CO_2$ (component 2), on the mole fraction $x_1$. At $x_1 \approx 0.01$, the diffusivity reduces about an order of magnitude compared to the infinite dilution value. What causes this sharp reduction in MO diffusivity with small increase in $x_1$?

Fig. 3 shows the experimental data of Nishiumi and Kubota (2007) for diffusivity of benzene (component 1; $x_1 \approx 0.017$) in supercritical $CO_2$ (component 2) as a function of the reduced pressure, $p_r = p/P_{c2}$ where $P_{c2}=7.28$ MPa is the critical pressure of $CO_2$. We note that the diffusivity exhibits a deep well at $p_r \approx 1$. What are the physico-chemical principles that underlie the curious $D_{12}$ vs $p_r$ characteristics?

Fig. 4 shows the experimental data of Dysthe and Hafskjold (1995) for Fick diffusivities of $CH_4$(1)/n-$C_{10}H_{22}$(2) mixtures at $T=303.5$ K and $p=40$, 50 and 60 MPa. It is easy to check that the mixture is in the liquid state at the prevailing conditions. Normally, we would expect the thermodynamics of mixtures of $n$-alkanes to conform to ideal solution behaviors. It is interesting to note the deep well in diffusivity values at a methane mole fraction, $x_1 \approx 0.9$. The well-depth gets shallower with increasing $p$. How do we rationalize the well-depth in the $D_{12}$ vs $x_1$ dependence? Is there a link between the well-depths in Figs. 3 and 4?

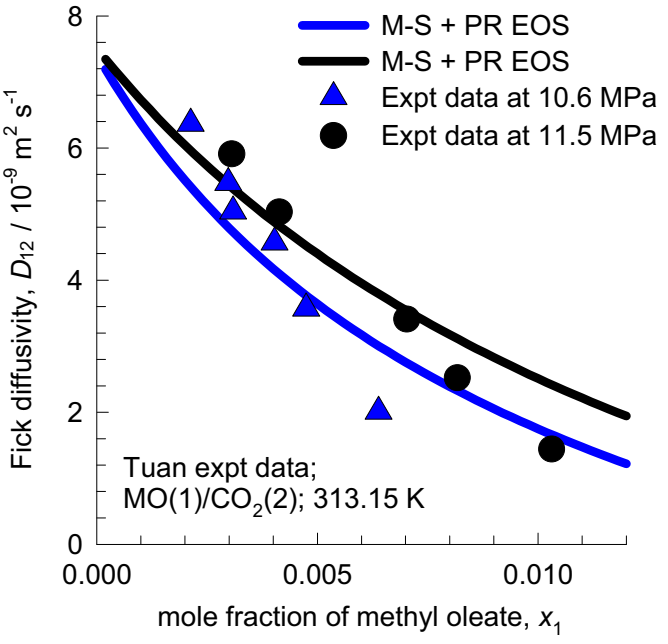


**Fig. 2.** Experimental data of Tuan et al. (1999) for the dependence of the Fick diffusivity of methyl oleate (MO) (component 1) in supercritical $CO_2$ (component 2), on the mole fraction of MO for $T=313.15$ K, $p=10.6$ MPa, and $p=11.5$ MPa. The continuous solid lines are the estimations of the Fick diffusivity using Eq. (23).

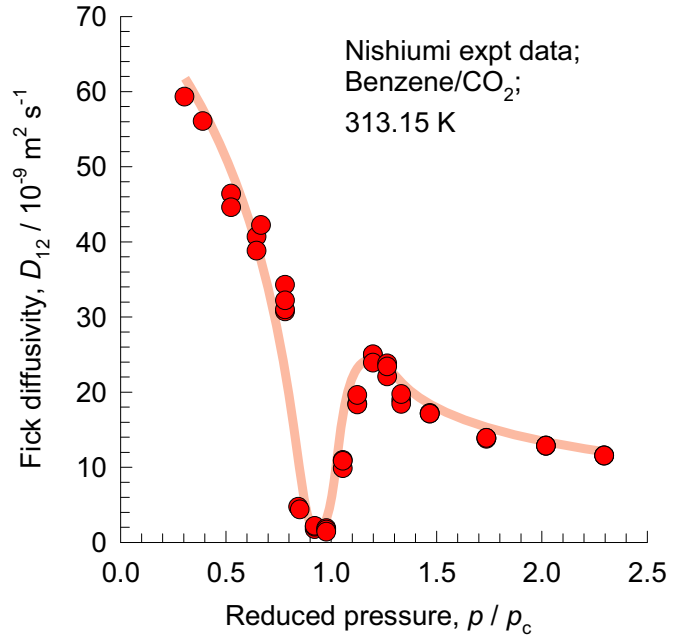


**Fig. 3.** Experimental data of Nishiumi and Kubota (2007) for diffusivity of benzene (component 1) in supercritical $CO_2$ (component 2) as a function of the reduced pressure, $p_r = p/P_{c2}$ where $P_{c2}=7.28$ MPa is the critical pressure of $CO_2$.

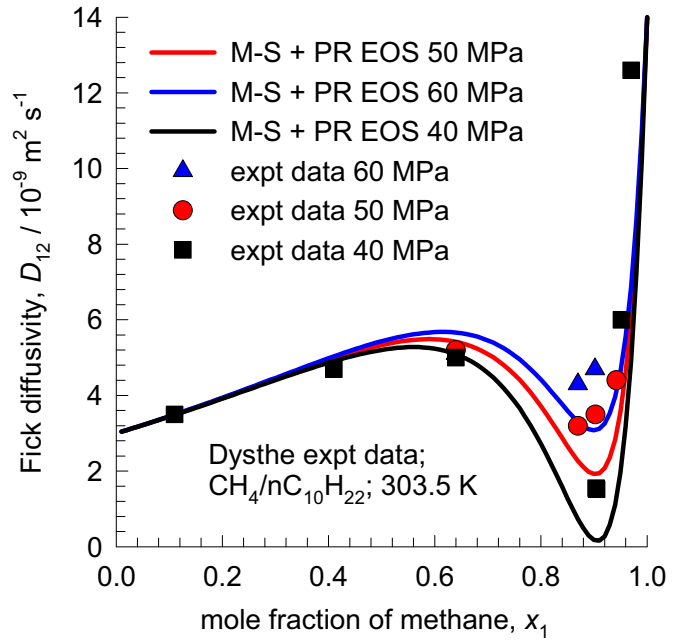


**Fig. 4.** Experimental data of Dysthe and Hafskjold (1995) for Fick diffusivities of $CH_4$(1)/n-$C_{10}H_{22}$(2) mixtures at $T=303.5$ K and $p=40$, 50 and 60 MPa. The continuous solid lines are the estimations of the Fick diffusivity using Eq. (26).

For diffusion in ternary fluid mixtures, the diffusion fluxes, $J_i$, are related to the composition gradients $dx_i/dz$ by the generalized Fick's law, expressed in two-dimensional matrix notation as

$$\begin{pmatrix} J_1 \\ J_2 \end{pmatrix} = -c_t \begin{bmatrix} D_{11} & D_{12} \\ D_{21} & D_{22} \end{bmatrix} \frac{d\begin{pmatrix} x_1 \\ x_2 \end{pmatrix}}{dz} \tag{2}$$

Finite, non-zero, values of the off-diagonal elements $D_{12}$, and $D_{21}$ cause the diffusion fluxes to be coupled; the extent of coupling is particularly strong in non-ideal liquid mixtures that are encountered in liquid–liquid extraction processes (Krishna, 2015b, 2016b). For hydrocarbon mixtures, made up of species of similar sizes, we would normally expect the off-diagonal elements $D_{12}$, and $D_{21}$ to be a small fraction of the magnitudes of the diagonal elements $D_{11}$, and $D_{22}$. For the ternary liquid mixture of $nC_8H_{18}(1)/nC_{10}H_{22}(2)/1$-methylnapthalene(3) at the composition $x_1=0.384$, $x_2=0.308$, $x_3=0.308$ at 296.15 K, Leahy-Dios et al. (2005) report experimental data on the Fick diffusivity matrix in the molar average reference velocity frame: $[D]=\begin{bmatrix} 1.92 & -1.07 \\ -0.333 & 2.47 \end{bmatrix}\times 10^{-9}$ m$^2$ s$^{-1}$. We note that the magnitude of $D_{12}$ is about half the magnitude of $D_{11}$; this implies strong coupling. The molar masses of the three species are 0.114, 0.142, and 0.142 kg mol$^{-1}$. What is the reason for the large magnitude of the off-diagonal elements for this ternary system in which the molar masses differ by only 20%?

The primary objective of this article is to address all of the questions posed in the foregoing paragraphs, and provide a unified framework for describing mixture diffusion that is applicable to dense fluids in high pressure operations. Towards this end, we use the Maxwell–Stefan (M–S) diffusion formulation in combination with the Peng Robinson equation of state (PR EOS) to describe phase equilibrium thermodynamics. While the combination of the M–S and PR EOS concepts is well established in the literature for binary mixture diffusion (Leahy-Dios and Firoozabadi, 2007; Tuan et al., 1999), this article aims to highlight the strong influence of phase equilibrium thermodynamics on coupling effects in multicomponent diffusion.

This Supplementary material accompanying the article provides details of (a) derivations of the Maxwell–Stefan equations, (b) further background information and insights on diffusivities, (d) details of the calculations of the compressibility factor and thermodynamic factors using the Peng–Robinson EOS, and (e) input data, and simulation results.

## 2. The Maxwell–Stefan diffusion formulation

For $n$-component fluid mixtures, the M–S equations represent a balance between the force exerted per mole of species $i$ with the drag, or friction, experienced with each of the partner species in the mixture (Krishna, 2015a, 2016a; Standart et al., 1979). We may expect that the frictional drag to be proportional to differences in the velocities of the diffusing species $(u_i-u_j)$. For component 1, for example, we write

$$-\frac{d\mu_1}{dz}=\frac{RT}{Đ_{12}}x_2(u_1-u_2)+\frac{RT}{Đ_{13}}x_3(u_1-u_3)+\ldots\ldots+\frac{RT}{Đ_{1n}}x_n(u_1-u_n) \tag{3}$$

The corresponding relations for components 2, 3,..$n$ are written down in an intuitively obvious manner. The left member of Eq. (3) is the negative of the gradient of the chemical potential, with the units N mol$^{-1}$; it represents the driving force acting per mole of species 1. The term $RT/Đ_{ij}$ is interpreted as the drag coefficient for the $i$–$j$ pair. The multiplier $x_j$ in each of the right members represents the mole fraction of component $j$; this factor is introduced because we expect the friction to be dependent on the number of molecules of $j$ relative to that of component 1. The M–S diffusivity $Đ_{ij}$ has the units m$^2$ s$^{-1}$ and the physical significance of an *inverse* drag coefficient.

The modeling and design of separation and reaction equipment requires calculation of the diffusion fluxes, $J_i$; these are defined with respect to an arbitrarily chosen reference velocity of the fluid mixture, $u$:

$$J_i\equiv c_i(u_i-u);\quad i=1,2,..n \tag{4}$$

Most commonly, we choose $u$ as the molar average velocity of the mixture

$$u=x_1u_1+x_2u_2+\cdots x_nu_n \tag{5}$$

Only $n-1$ of the fluxes $J_i$ are independent because the diffusion fluxes sum to zero

$$\sum_{i=1}^{n}J_i=0 \tag{6}$$

The molar fluxes $N_i$ in the laboratory fixed reference frame are related to the diffusion fluxes $J_i$ by

$$N_i\equiv c_iu_i=J_i+x_iN_t;\quad N_t=\sum_{i=1}^{n}N_i \tag{7}$$

By multiplying both sides of Eq. (3) by $x_i$ after introducing the expressions for fluxes, we obtain

$$-\frac{x_i}{RT}\frac{d\mu_i}{dz}=\sum_{\substack{j=1\\ j\neq i}}^{n}\frac{x_jN_i-x_iN_j}{c_tĐ_{ij}}=\sum_{\substack{j=1\\ j\neq i}}^{n}\frac{x_jJ_i-x_iJ_j}{c_tĐ_{ij}};\qquad i=1,2,\ldots n \tag{8}$$

For describing segregation in petroleum reservoirs, the left member of Eq. (8) needs to be augmented to include the contributions of the pressure gradients (induced by gravity) and the temperature gradient (Soret effect) (Galliéro and Montel, 2008; Standart et al., 1979; Touzet et al., 2011). The calculations presented in Figs. S32–S35 of Supplementary material illustrate the relative influences of the segregation due to the influences of gravity and thermal diffusion.

Only $(n-1)$ of the chemical potential gradients $\frac{d\mu_i}{dz}$ in Eq. (8) are independent, because of the Gibbs–Duhem relationship

$$x_1\frac{d\mu_1}{dz}+x_2\frac{d\mu_2}{dz}+\cdots x_n\frac{d\mu_n}{dz}=0 \tag{9}$$

The Onsager Reciprocal Relations imply that the M–S pair diffusivities are symmetric

$$Đ_{ij}=Đ_{ji}\quad;\quad i,j=1,2\ldots n \tag{10}$$

For fluid mixtures, the chemical potential of component $i$, $\mu_i$ is related to the component fugacity,

$$\mu_i=\mu_i^0+RT\ \ln(f_i)=\mu_i^0+RT\ \ln(\phi_ix_ip) \tag{11}$$

where $\phi_i$ is the activity coefficient and $p$ is the total pressure.

It is helpful to express the left member of Eq. (8) in terms of the mole fraction gradients by introducing an $(n-1)\times(n-1)$ matrix of thermodynamic factors $[\Gamma]$:

$$\frac{x_i}{RT}\frac{d\mu_i}{dz}=x_i\frac{d\ \ln\ f_i}{dz}=\sum_{j=1}^{n-1}\Gamma_{ij}\frac{dx_j}{dz};\qquad \Gamma_{ij}=\delta_{ij}+x_i\frac{\partial\ \ln\ \phi_i}{\partial x_j};\quad i,j=1,2\ldots n-1 \tag{12}$$

The elements of $[\Gamma]$ can be calculated by analytic differentiation of an equation of state (EOS) such as the Peng–Robinson (PR) EOS. For binary mixtures, explicit analytic expressions for $\Gamma=x_1\frac{\partial\ \ln\ f_1}{\partial x_1}=1+x_1\frac{\partial\ \ln\ \phi_1}{\partial x_1}$ for PR EOS are provided by Tuan et al. (1999).

We also define a $(n-1)\times(n-1)$ matrix of inverse diffusivities $[B]$ whose elements are given by

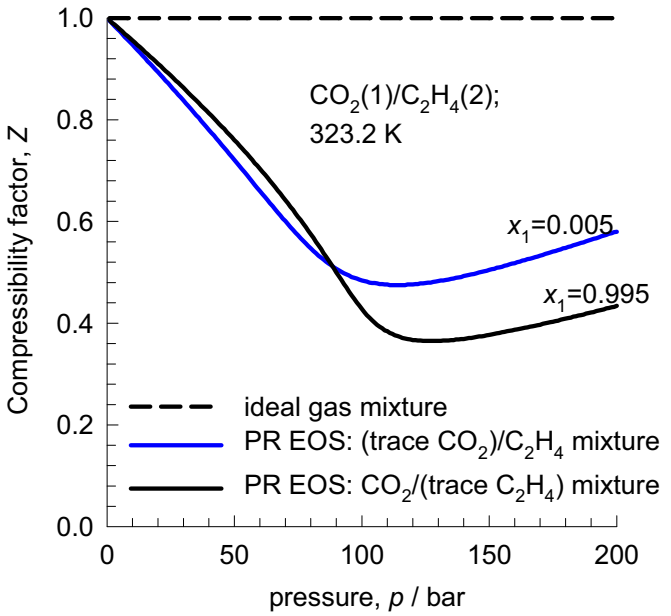


**Fig. 5.** Calculations of the compressibility factor using the Peng–Robinson equation of state (PR EOS) of $CO_2$(trace amounts)/$C_2H_4$ mixtures, and $CO_2$/$C_2H_4$(trace amounts) mixtures at 323.2 K, for a range of pressures.

$$B_{ii} = \frac{x_i}{Đ_{in}} + \sum_{\substack{k=1 \\ k\neq i}}^{n} \frac{x_k}{Đ_{ik}}; \qquad B_{ij(i\neq j)} = -x_i\left(\frac{1}{Đ_{ij}} - \frac{1}{Đ_{in}}\right);$$
$$i, j = 1, 2 \ldots n-1 \tag{13}$$

Combining (Eqs. (8), (12), and 13), we can re-cast Eq. (8) into $(n-1)$ dimensional matrix notation

$$(J) = -c_t[B]^{-1}[\Gamma]\frac{d(x)}{dz} = -c_t[\Lambda][\Gamma]\frac{d(x)}{dz} \tag{14}$$

where we have additionally defined

$$[\Lambda] = [B]^{-1} \tag{15}$$

If we define a $(n-1)\times(n-1)$ dimensional Fick diffusivity matrix $[D]$

$$(J) = -c_t[D]\frac{d(x)}{dz} \tag{16}$$

we obtain the inter-relationship

$$[D] = [B]^{-1}[\Gamma] = [\Lambda][\Gamma] \tag{17}$$

For a binary mixture, $n=2$, we get

$$D_{12} = Đ_{12}\Gamma \tag{18}$$

For a ternary mixture, $n=3$, we derive

$$\begin{bmatrix} D_{11} & D_{12} \\ D_{21} & D_{22} \end{bmatrix} = \begin{bmatrix} \Lambda_{11} & \Lambda_{12} \\ \Lambda_{21} & \Lambda_{22} \end{bmatrix}\begin{bmatrix} \Gamma_{11} & \Gamma_{12} \\ \Gamma_{21} & \Gamma_{22} \end{bmatrix}$$
$$= \frac{\begin{bmatrix} Đ_{13}\left(x_1Đ_{23} + (1-x_1)Đ_{12}\right) & x_1Đ_{23}\left(Đ_{13} - Đ_{12}\right) \\ x_2Đ_{13}\left(Đ_{23} - Đ_{12}\right) & Đ_{23}\left(x_2Đ_{13} + (1-x_2)Đ_{12}\right) \end{bmatrix}}{x_1Đ_{23} + x_2Đ_{13} + x_3Đ_{12}}$$
$$\times \begin{bmatrix} \Gamma_{11} & \Gamma_{12} \\ \Gamma_{21} & \Gamma_{22} \end{bmatrix} \tag{19}$$

For stable single phase fluid mixtures, we must have $|\Gamma| \geq 0$ (Krishna, 2015b, 2016b). In view of Eq. (17), the condition of phase stability translates to

$$|D| \geq 0; \quad |\Gamma| \geq 0; \quad \text{phase stability} \tag{20}$$

The condition for phase stability in a binary fluid mixture is

$$D_{12} \geq 0; \quad \Gamma \geq 0; \quad \text{phase stability} \tag{21}$$

The occurrence of $\Gamma < 0$ implies vapor/liquid, liquid/liquid, or liquid/solid phase transitions (Krishna, 2015b, 2016b).

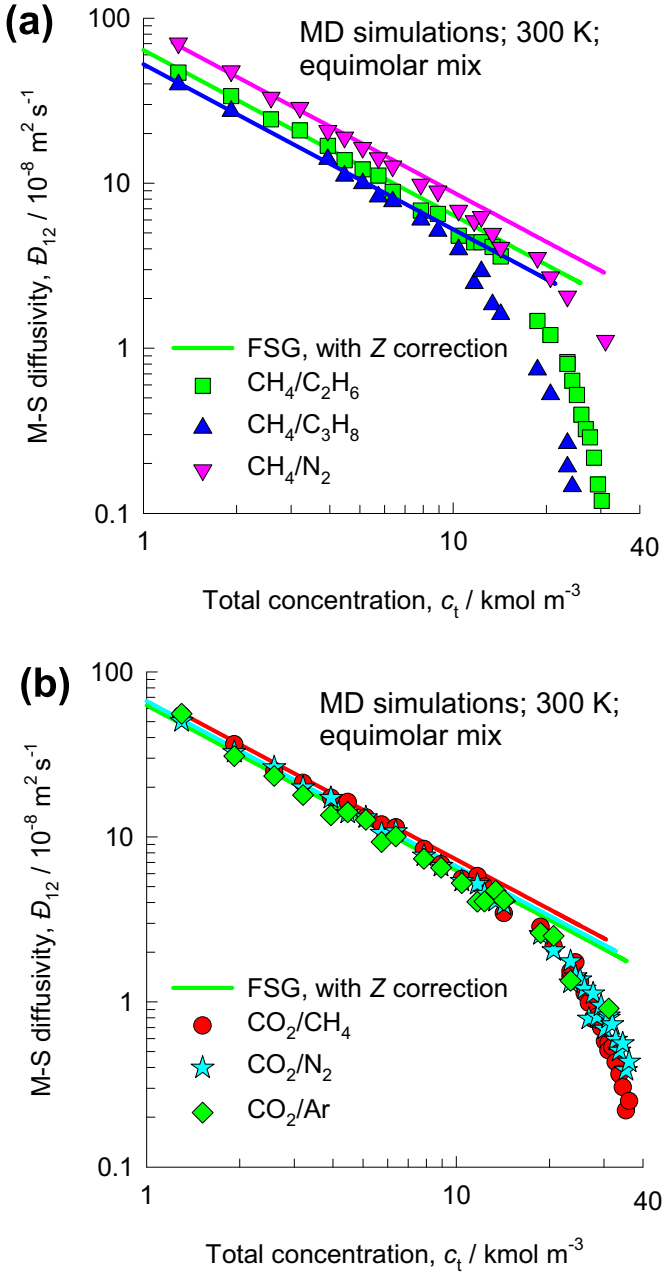


**Fig. 6.** Data on MD simulations (Krishna and van Baten, 2009) for the Maxwell–Stefan diffusivity, $Đ_{12}$, for equimolar binary mixtures $CH_4(1)/C_2H_6(2)$, $CH_4(1)/C_3H_8(2)$, $CH_4(1)/N_2(2)$, $CO_2(1)/CH_4(2)$, $CO_2(1)/N_2(2)$, $CO_2(1)/Ar(2)$ at 300 K. The straight lines are the estimations of $Đ_{12}$, for Eq. (22).

## 3. Diffusivities in dense binary gas mixtures

In generalizing the FSG method to dense gas mixtures, it is

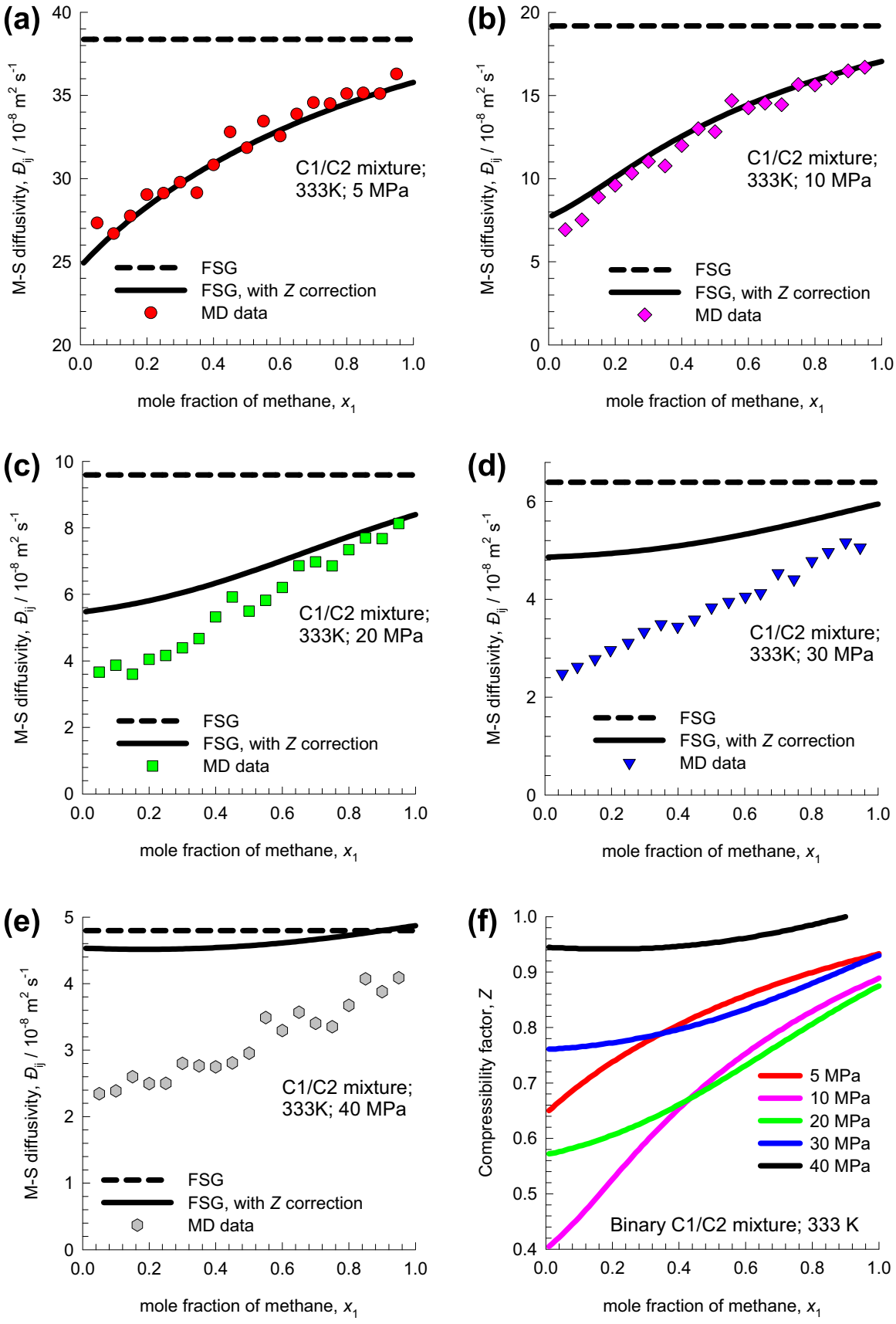


**Fig. 7.** MD simulations for the Maxwell–Stefan diffusivity, $Đ_{12}$, for binary $CH_4(1)/C_2H_6(2)$ mixtures at 333 K at (a) 5 MPa, (b) 10 MPa, (c) 20 MPa, (d) 30 MPa, and (e) 30 MPa with varying compositions of methane $x_1$. The simulation methodology is the same as that used in the work of Krishna and van Baten (2005). The continuous solid lines are the estimations of the M–S diffusivities using Eq. (22). Also shown by the dashed lines are the FSG estimations, using Eq. (1). (f) Variation of the compressibility factor $Z$ with $x_1$ at different total pressures.

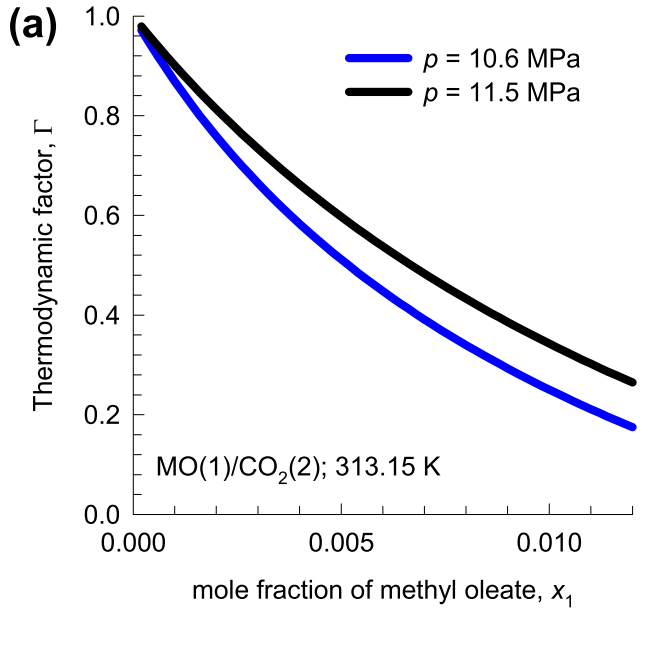


**Fig. 8.** (a) PR EOS calculations of the thermodynamic factor, $\Gamma$, for methyl oleate (MO) (component 1) in supercritical $CO_2$ (component 2), on the mole fraction of MO at $T=313.15$ K, $p=10.6$ MPa, and $p=11.5$ MPa. (b) Calculations of the thermodynamic factor, $\Gamma$, for naphthalene (component 1) in supercritical $CO_2$ (component 2), as a function of the mole fraction of naphthalene, at $T=308.2$ K, $p=8.25$ MPa, and $p=10.4$ MPa.

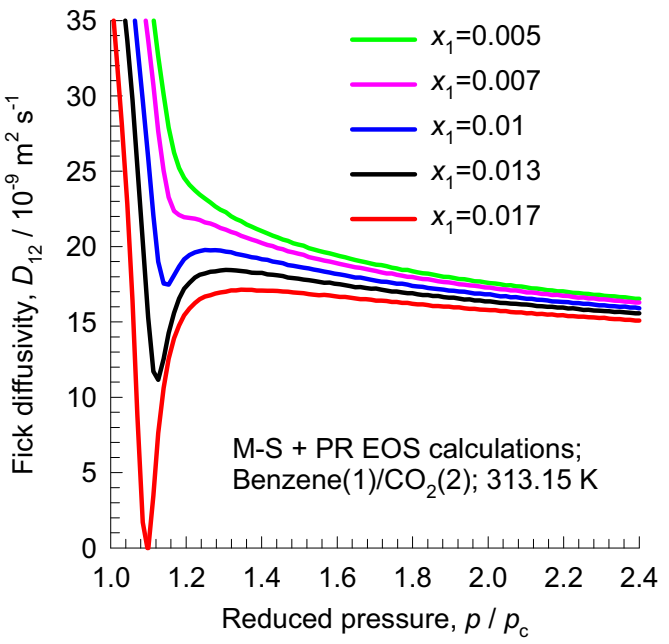


**Fig. 9.** Calculations of the Fick diffusivity of benzene (component 1) in $CO_2$ (component 2), as a function of the reduced pressure, $p/p_c$ and composition of benzene in the mixture.

important realize that Eq. (1) implies that at constant temperature, the M–S diffusivity is inversely proportional to the molar density of the gas phase. The total mixture molar density of the gas phase is $c_t = \frac{p}{ZRT}$ where $Z$ is the compressibility factor. Consequently, the M–S diffusivity for dense gases can be estimated by correcting the original FSG equation by introducing the compressibility factor $Z$:

$$Đ_{ij} = D_{ij}^{FSG} Z \tag{22}$$

Due to the introduction of the compressibility factor, the M–S diffusivity $Đ_{ij}$ becomes dependent on mixture composition. The molar density of the mixture is $c_t = \frac{p}{ZRT}$, and therefore Eq. (22) anticipates that $c_t Đ_{ij}$ is constant at constant temperature $T$.

Fig. 5 presents calculations of the compressibility factor, $Z$, using the Peng–Robinson equation of state (PR EOS) for $CO_2$(trace amounts)/$C_2H_4$ mixtures, and $CO_2$/$C_2H_4$ (trace amounts) mixtures. The $Z$ values are same at $p > 100$ bar; this explains the differences in the corresponding diffusivity values in Fig. 1. This implies, that the departures from the FSG prescription, Eq. (1) (these calculation are shown by the dashed lines in Fig. 1), is primarily to be attributed to the departures of fluid densities from the ideal gas prescription. The experimental data of Takahashi and Hongo (1982) conforms quite well with the modified prescription of Eq. (22); the calculations are shown by the continuous solid lines in Fig. 1.

In order to determine the limits of applicability Eq. (22), Fig. 6 presents comparisons of the estimates with MD simulation data (Krishna and van Baten, 2009) for the M–S diffusivity, $Đ_{12}$, for six different equimolar binary mixtures at 300 K determined as a function of the total molar concentration $c_t$. The estimations of $Đ_{12}$ using Eq. (22) are accurate up to a total molar concentration $c_t \approx 10$ kmol m$^{-3}$, corresponding to a system pressure of about 10 MPa. Put another way, the product $c_t Đ_{12}$ is constant for a given binary mixture only up to a molar density of 10 kmol m$^{-3}$. For molar densities, $c_t > 10$ kmol m$^{-3}$, the MD simulated data are significantly lower than the $Đ_{12}$ values estimated from Eq. (22).

The limits of applicability of Eq. (22) are emphasized further in the MD simulation data for the M–S diffusivity, $Đ_{12}$, for binary $CH_4(1)/C_2H_6(2)$ mixtures at 333 K at 5, 10, 20, 30, and 40 MPa with varying compositions of methane $x_1$; see Fig. 7. The continuous solid lines are the estimations of the M–S diffusivities using Eq. (22). Also shown by the dashed lines are the FSG estimations, using Eq. (1). For system pressures below 10 MPa, Eq. (22) provides accurate estimates of $Đ_{12}$ vs $x_1$; the composition dependence of $Đ_{12}$ is entirely caused due to the variation of the compressibility factor Z with $x_1$. For system pressures exceeding 10 MPa, the MD data show a much stronger composition dependence than anticipated by the $Z$ correction introduced in Eq. (22). For the purposes of this article, we refer to systems with $c_t > 10$ kmol m$^{-3}$ as "dense fluid mixtures", and use the term "dense gas mixtures" to indicate systems for which Eq. (22) is of adequate accuracy.

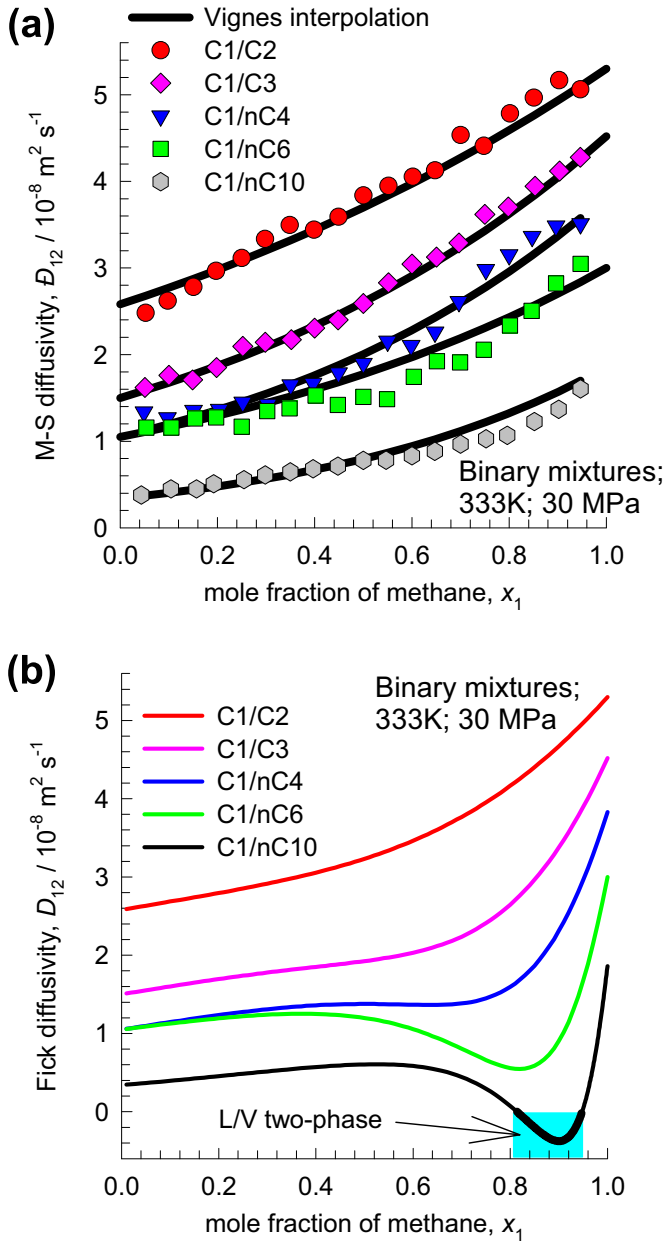


**Fig. 10.** (a) MD simulation data of Krishna and van Baten (2005) on $Đ_{12}$ for the binary mixtures of methane with ethane, propane, n-butane, n-hexane, and n-decane at 333 K and 30 MPa as function of the mole fraction of methane. The continuous solid lines are the calculations of $Đ_{12}$ using the Vignes interpolation formula (25). (b) Calculations of the Fick diffusivity using Eq. (26), where the thermodynamic factor is calculated using the PR EOS.

## 4. Diffusivities in supercritical $CO_2$

The Fick diffusivity for dense gas mixtures can be estimated by multiplying M–S diffusivity $Đ_{12}$, determined from Eq. (22), with the thermodynamic correction factor $\Gamma$:

$$D_{12} = Đ_{12}\Gamma = D_{12}^{FSG} Z\Gamma; \quad \Gamma \equiv \left(1 + \frac{\partial \ln \phi_1}{\partial \ln x_1}\right) \tag{23}$$

Fig. 8a presents calculations of $\Gamma$ for methyl oleate (MO) (component 1) in supercritical $CO_2$ (component 2) at pressures of $p = 10.6$ MPa, and $p = 11.5$ MPa. The strong decrease in $\Gamma$ with increasing $x_1$ provides a rationalization of the strong diffusivity in the Fick diffusivity with small increase in the mole fraction of MO, observed in Fig. 2. The continuous solid lines in Fig. 2 are estimates using Eq. (23); there is reasonably good agreement between the experimental data and the combined Maxwell–Stefan-PR EOS model.

Higashi et al. (2002) report an analogous set of experimental data for Fick diffusivity of naphthalene (component 1) in supercritical $CO_2$. Their data show significant reduction in the naphthalene diffusivity for increase in the naphthalene composition to the level of $x_1 \approx 0.01$. Their experimental observations can be rationalized by PR EOS calculations of the thermodynamic correction factor; see Fig. 8b. The strong reduction in $\Gamma$ with increasing $x_1$ provides a rationalization of the experimental trends observed in the data reported by Higashi et al. (2002).

For benzene/$CO_2$ mixtures, Fig. 9 shows calculations of the Fick diffusivity $D_{12}$ using Eq. (23), as a function of the reduced pressure, $p/p_c$, for $x_1 = 0.005$, 0.007, 0.01, 0.013, and 0.017. The depth of the well increases with increasing mole fraction of benzene in the fluid phase mixture. The combined influence of the compressibility factor $Z$ and $\Gamma$ provides an explanation of the experimentally observed well in the experimental $D_{12}$ vs $p_r$ data in Fig. 3.

The important message emerging from the data in Figs. 8 and 9 is that the corrections due the thermodynamic factor on the values of the Fick diffusivity are significant even when the solute concentrations are at the level of $x_1 \approx 0.01$.

## 5. Diffusion in binary fluid mixtures with $c_t > 10$ kmol m$^{-3}$

We turn our attention to diffusion in binary mixtures for which the molar densities, $c_t > 10$ kmol m$^{-3}$; these are normally termed as "liquid" mixtures. The M–S diffusivity of component 1, that is present in infinitely dilute concentrations in component 2, $Đ_{12}^{x_2 \to 1}$, can be estimated using a number of procedures that are discussed in Reid et al. (1986) and Taylor and Krishna (1993). The most well-known estimation method is due to (Wilke and Chang, 1955)

$$Đ_{12}^{x_2 \to 1} = C\frac{(\psi M_2)^{1/3} T}{\eta_2 V_1^{0.6}} \tag{24}$$

In Eq. (24), $C$ is an empirical constant, $M_2$ is the molar mass of component 2, $\eta_2$ is the (dynamic) viscosity of component 2, $V_1$ is the molar volume of component 1 at its normal boiling temperature, $\psi$ is the *association* factor of the solvent 2. An analogous relation holds for $Đ_{12}^{x_1 \to 1}$.

Leahy-Dios and Firoozabadi (2007) present an empirical model for estimation of $Đ_{12}^{x_2 \to 1}$, valid for $c_t > 10$ kmol m$^{-3}$ that reduces to the FSG correlation for dilute gases in the limit of low molar densities.

The composition dependence of the M–S diffusivity is then determined using the Vignes interpolation formula (Krishna and van Baten, 2005, 2009)

$$Đ_{12} = \left(Đ_{12}^{x_1 \to 1}\right)^{x_1} \left(Đ_{12}^{x_2 \to 1}\right)^{x_2} \tag{25}$$

Cullinan (1966) has derived the Vignes interpolation formula using the Eyring theory of rate processes as a fundamental basis. As illustration of the accuracy of the Vignes interpolation formula, Fig. 10a presents MD simulation data of Krishna and van Baten (2005) on $Đ_{12}$ for the binary mixtures of methane with ethane, propane, n-butane, n-hexane, and n-decane as function of the mole fraction of methane. The continuous solid lines are the calculations of $Đ_{12}$ using the Vignes interpolation formula (25). The interpolation formula is of good accuracy for all five binary mixtures; Figs. S12–S16 provide validation of other binary alkane mixtures.

The Fick diffusivity for binary liquid mixtures can be calculated

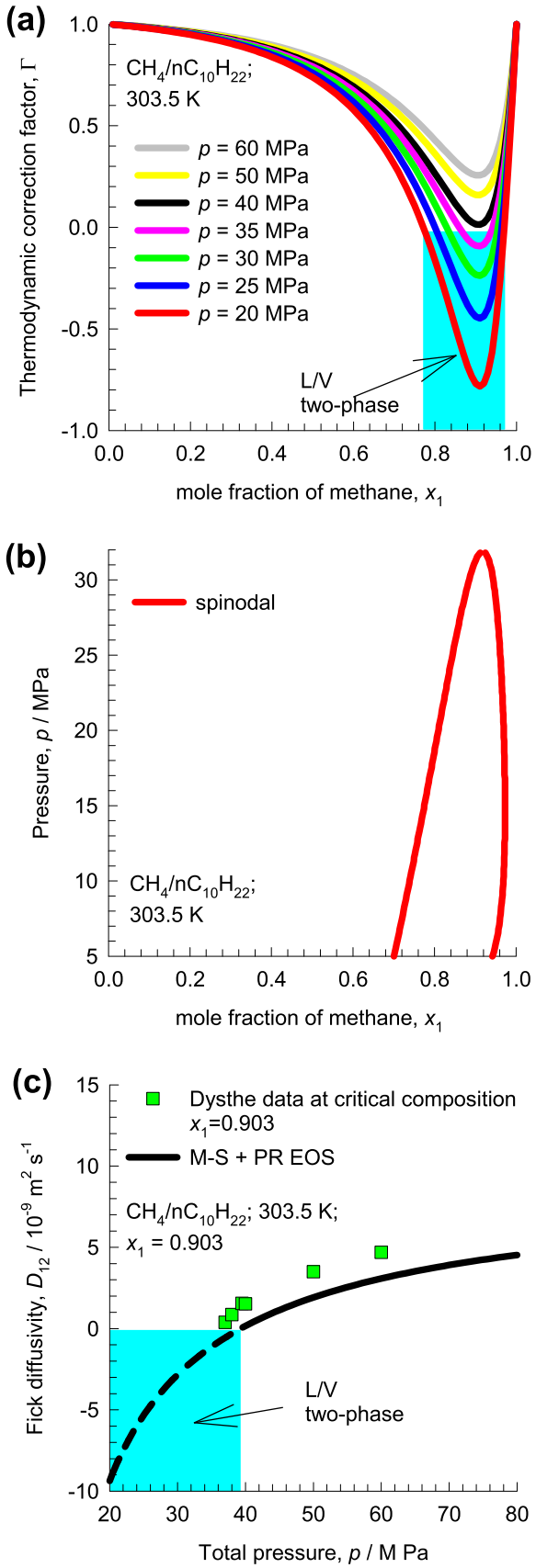


**Fig. 11.** (a) Calculations of the thermodynamic factor, $\Gamma$, for $CH_4(1)$/n-$C_{10}H_{22}(2)$ mixtures using PR EOS at $p=20$, 25, 30, 35, 40, 50 and 60 MPa. (b) Spinodal compositions for $CH_4(1)$/n-$C_{10}H_{22}(2)$ mixtures at $T=303.5$ K. (c) Experimental data of Dysthe and Hafskjold (1995) for Fick diffusivities of $CH_4(1)$/n-$C_{10}H_{22}(2)$ mixtures at $T=303.5$ K with varying total pressures; the mole fractions of methane $x_1=0.903$.

by correcting the M–S diffusivity for the thermodynamic factor

$$D_{12} = \left(Đ_{12}^{x_1\to 1}\right)^{x_1}\left(Đ_{12}^{x_2\to 1}\right)^{x_2}\left(1+\frac{\partial \ln \phi_1}{\partial \ln x_1}\right) \tag{26}$$

Fig. 10b presents calculations of the Fick diffusivity using Eq. (26), where the thermodynamic factor is calculated using the PR EOS. At methane mole fractions, $x_1$, in the range 0.8–0.9, we note that the Fick diffusivity of C1–nC6, and C1–nC10 mixtures shows a pronounced minimum. For C1–nC10 mixtures, the minimum in the Fick diffusivity appears to be in qualitative agreement with the experimental data of Dysthe and Hafskjold (1995) shown in Fig. 4. We now attempt to obtain a quantitative match with their experiments.

D'Agostino et al. (2012) have considered examples of binary liquid mixture diffusion near the critical point in which the Fick diffusivity exhibits a power-law dependence on $\Gamma$; this aspect deserves further research scrutiny.

Fig. 11a presents calculations of the thermodynamic factor, $\Gamma$, for $CH_4(1)$/n-$C_{10}H_{22}(2)$ mixtures at $p=20$, 25, 30, 35, 40, 50 and 60 MPa. We note that for pressures below 40 MPa, there is a range of compositions for which $\Gamma<0$; this signifies phase instability. The condition $\Gamma=0$, defines the limits of phase stability and the resulting spinodal compositions are plotted in Fig. 11b. The deep well in the $\Gamma$ values are caused by the proximity to V/L transitions. The Fick diffusivity, estimated using Eq. (26), are shown by the continuous solid lines in Fig. 4. All of the essential characteristics of the Fick diffusivities are captured quantitatively; the clue lies in the $\Gamma$ corrections.

Fig. 11c shows the experimental data of Dysthe and Hafskjold (1995) for Fick diffusivities of $CH_4(1)$/n-$C_{10}H_{22}(2)$ mixtures at $T=303.5$ K with varying total pressures at the critical composition $x_1=0.903$. The experimental data show that the Fick diffusivity progressively decreases in magnitude as the pressure is reduced, and $D_{12}\approx 0$ at $p\approx 36$ MPa. Eq. (26) provides a reasonable description of the experimentally observed pressure dependence.

## 6. Influence of thermodynamic coupling in ternary liquid mixtures

Eq. (19) allows the estimation of the elements of the Fick diffusivity matrix $[D]$, obtained as a product of the matrix $[\Lambda]$ and the matrix of thermodynamic factors $[\Gamma]$. Each of these matrices $[\Lambda]$ and $[\Gamma]$ have non-zero off-diagonal elements, and therefore the product of the two matrices, $[D]=[\Lambda][\Gamma]$ is strongly coupled. Differentiation of the PR EOS, allow the calculation of the $\Gamma_{ij}=\delta_{ij}+x_i\frac{\partial \ln \phi_i}{\partial x_j}; \qquad i,j=1,2.$

For estimation of the elements of $[\Lambda]$, Krishna and van Baten (2005) have suggested the following extension of the Vignes interpolation formula (25):

$$Đ_{ij} = \left(Đ_{ij}^{x_i\to 1}\right)^{x_i}\left(Đ_{ij}^{x_j\to 1}\right)^{x_j}\left(Đ_{ij}^{x_k\to 1}\right)^{x_k} \tag{27}$$

For the estimation of $Đ_{ij}^{x_k\to 1}$, the $i$–$j$ pair diffusivity when both $i$ and $j$ are present in infinitely dilute concentration, Krishna and van Baten (2005) suggest

$$\begin{aligned} Đ_{12}^{x_3\to 1} &= \left(Đ_{13}^{x_3\to 1}\right)^{x_1/(x_1+x_2)}\left(Đ_{23}^{x_3\to 1}\right)^{x_2/(x_1+x_2)} \\ Đ_{13}^{x_2\to 1} &= \left(Đ_{12}^{x_2\to 1}\right)^{x_1/(x_1+x_3)}\left(Đ_{23}^{x_2\to 1}\right)^{x_3/(x_1+x_3)} \\ Đ_{23}^{x_1\to 1} &= \left(Đ_{12}^{x_1\to 1}\right)^{x_2/(x_2+x_3)}\left(Đ_{13}^{x_1\to 1}\right)^{x_3/(x_2+x_3)} \end{aligned} \tag{28}$$

For the special case of an equimolar mixture we obtain

$$Đ_{12}^{x_3\to 1} = \sqrt{\left(Đ_{13}^{x_3\to 1} Đ_{23}^{x_3\to 1}\right)}$$
$$Đ_{13}^{x_2\to 1} = \sqrt{\left(Đ_{12}^{x_2\to 1} Đ_{23}^{x_2\to 1}\right)}$$
$$Đ_{23}^{x_3\to 1} = \sqrt{\left(Đ_{12}^{x_1\to 1} Đ_{13}^{x_1\to 1}\right)} \quad (29)$$

The simplified interpolation formula (29) was proposed by Wesselingh and Bollen (1997).

Consider liquid phase diffusion in the ternary methane(1)/propane(2)/n-hexane (3) mixture at 333 K and 8.5 MPa. In ternary composition space, there is a composition region in which we have V/L phase splitting. This region is indicated in Fig. 12. The compositions of the vapor and liquid phases in equilibrium with each other are indicated by the tie-lines. The region to the left of the two-phase region consists of the liquid phase region.

Thermodynamic coupling effects become increasingly significant as the liquid phase compositions approach the phase transition region. In order to demonstrate this, we performed calculations for the determinant $|\Gamma|$ as a function of the composition of n-hexane, $x_3$, keeping the ratio $x_1/x_2$ at a constant value of unity; see inset to Fig. 12. At the pure hexane vertex, $x_3=1$, $|\Gamma|=1$. As $x_3$ decreases in value and the two-phase region is approach, the magnitude of $|\Gamma|$ progressively decreases. The condition $|\Gamma|=0$ signifies the limit of phase stability; at this point we must have $\Gamma_{11}\Gamma_{22} = \Gamma_{12}\Gamma_{21}$, i.e. the product of the off-diagonal elements is equal in magnitude to the product of the diagonal elements. This situation implies significant degree of thermodynamic coupling. Strong coupling of the thermodynamic factor $[\Gamma]$ contributes to strong coupling of the Fick matrix $[D]$. At the composition, $x_1=0.1$, $x_2=0.2$, $x_3=0.7$, that is far removed from the V/L phase transition region, we calculate $[\Gamma] = \begin{bmatrix} 0.9397 & -0.0249 \\ -0.0333 & 0.9885 \end{bmatrix}$, and $[D] = \begin{bmatrix} 5.24 & -0.139 \\ -0.381 & 4.42 \end{bmatrix} \times 10^{-8}$ m$^2$ s$^{-1}$. The contributions of the off-diagonal elements is less than about 10%. At the composition $x_1=0.333532$, $x_2=0.521103$, $x_3=0.145365$ that is at the V/L transition point, we calculate $[\Gamma] = \begin{bmatrix} 0.2937 & -0.3546 \\ 0.2594 & 1.135 \end{bmatrix}$, and $[D] = \begin{bmatrix} 2.53 & -3.84 \\ 1.47 & 9.29 \end{bmatrix} \times 10^{-8}$ m$^2$ s$^{-1}$; in this case diffusional coupling is extremely strong and $D_{12}/D_{11} \approx -1.5$. Furthermore, we note that the sign of the off-diagonal elements of matrix $[D]$ are the same as the corresponding ones for $[\Gamma]$ at both compositions. Indeed, multiplying $[\Gamma]$ by a scalar diffusivity offers a simple and fairly reliable procedure for the estimation of $[D]$; this has been demonstrated in earlier work (Krishna, 2015b, 2016b).

We can now address the fifth question raised in the Introduction regarding the strong diffusional coupling of the Fick diffusivity matrix for the ternary liquid phase mixture of $nC_8H_{18}(1)/nC_{10}H_{22}(2)$/1-methylnapthalene(3) at 295.65 K. The pressure and temperature conditions are far removed for V/L transition points. We note that the melting points of $nC_8H_{18}(1)$, $nC_{10}H_{22}(2)$, and 1MN(3) are 216 K, 243 K, and 251 K, respectively. On cooling, crystals of 1MN will be first to come out of solution and the 1MN can be separated from linear alkanes by fractional crystallization. To demonstrate the possibility of phase separation, Fig. 13 presents calculations for the determinant $|\Gamma|$ for the ternary mixture of $nC_8H_{18}(1)/nC_{10}H_{22}(2)$/1-methylnapthalene(3) as a function of the composition of 1MN, $x_3$, keeping the ratio $x_1/x_2$ at a constant value of unity. The calculations are presented for three different temperatures $T=295.65$ K, 240 K, and 200 K. We note that at the lowest temperature, $T=200$ K, there is a range of compositions for which $|\Gamma| < 0$, indicating phase instability and crystal formation. We conclude that thermodynamic coupling is strong in the $nC_8H_{18}(1)/nC_{10}H_{22}(2)$/1-methylnapthalene

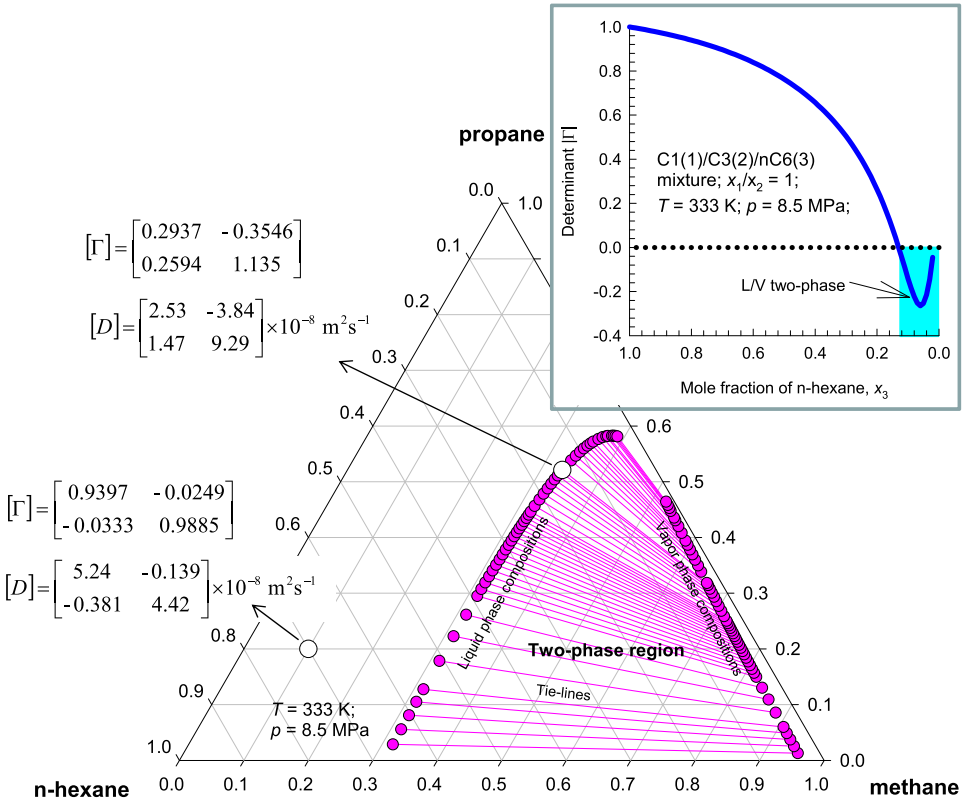


**Fig. 12.** Ternary diagram delineating the two-phase V/L region for methane(1)/propane(2)/n-hexane (3) mixtures at 333 K and 8.5 MPa. The compositions of the vapor and liquid phases in equilibrium with each other are indicated by the tie-lines. The region to the left of the two-phase region consists of the liquid region. The inset shows the calculations for the determinant $|\Gamma|$ as a function of the composition of n-hexane, $x_3$, keeping the ratio $x_1/x_2$ at a constant value of unity.

(3) because of the proximity to liquid/solid phase transition regions. At a liquid mixture composition $x_1=0.384$, $x_2=0.308$, $x_3=0.308$, we can evaluate the matrix of thermodynamic factors, $[\Gamma]=\begin{bmatrix} 0.486 & -0.305 \\ -0.068 & 0.9 \end{bmatrix}$. Multiplying $[\Gamma]$ by a scalar $3.4\times10^{-9}$ m$^2$ s$^{-1}$, corresponding to the self-diffusivity of $nC_{10}H_{22}$ as determined by MD simulations (Krishna and van Baten, 2005), yields $[D]=\begin{bmatrix} 1.65 & -1.03 \\ -0.23 & 3.06 \end{bmatrix}\times10^{-9}$ m$^2$ s$^{-1}$. This estimated value is close to the experimentally determined value $[D]=\begin{bmatrix} 1.92 & -1.07 \\ -0.333 & 2.47 \end{bmatrix}\times10^{-9}$ m$^2$ s$^{-1}$ of Leahy-Dios et al. (2005). We conclude that the large off-diagonal elements of $[D]$ are ascribable to strong thermodynamic coupling.

## 7. Influence of diffusional coupling effects on transient equilibration trajectories

We shall demonstrate the strong influence of diffusional coupling on the transient diffusion equilibration in the ternary liquid phase of the methane(1)/propane(2)/n-hexane (3) mixture at 333 K and 8.5 MPa. At time $t=0$, a liquid slab of composition $x_{10}=0.05$, $x_{20}=0.55$, $x_{30}=0.4$ is exposed to a vapor phase mixture of composition $y_1=0.659033$, $y_2=0.318393$, $y_3=0.022574$. The vapor composition is held constant for the duration of the transient equilibration process in the liquid of half-thickness $\delta$ ($=1$ mm). The liquid slab is considered to be of "infinite" length in the vertical direction and the diffusion is limited to the transverse ($z$) direction. The composition of the liquid phase in equilibrium with the vapor phase is $x_{1\delta}=0.333532$, $x_{2\delta}=0.521103$, $x_{3\delta}=0.145365$.

Fig. 14a presents the calculation results of the transient equilibration for liquid phase diffusion in methane(1)/propane(2)/n-hexane (3) mixtures at 333 K and 8.5 MPa; the simulation details are provided in Supplementary material accompanying this publication. It is noteworthy that propane (component 2) experiences

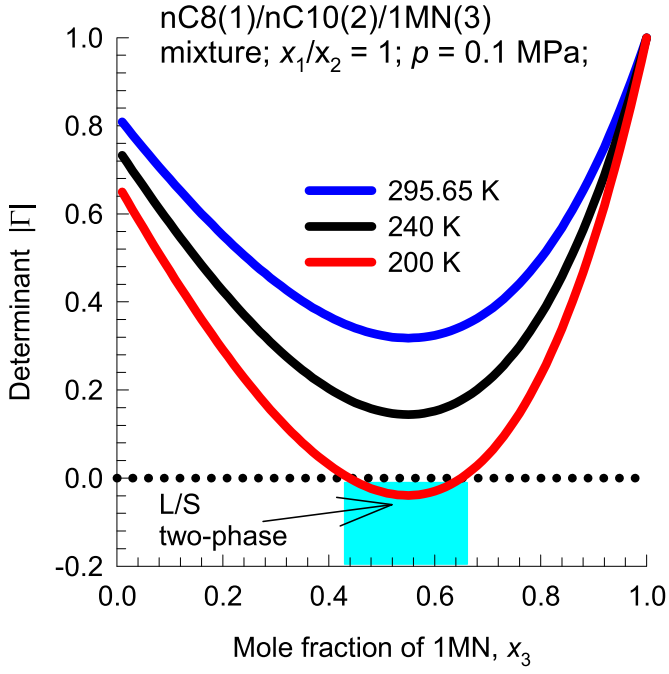


**Fig. 13.** Calculations for the determinant $|\Gamma|$ for the ternary mixture of $nC_8H_{18}$(1)/$nC_{10}H_{22}$(2)/1-methylnapthalene(3) as a function of the composition of 1MN, $x_3$, keeping the ratio $x_1/x_2$ at a constant value of unity. The calculations are presented for three different temperatures $T=295.65$ K, 240 K, and 200 K.

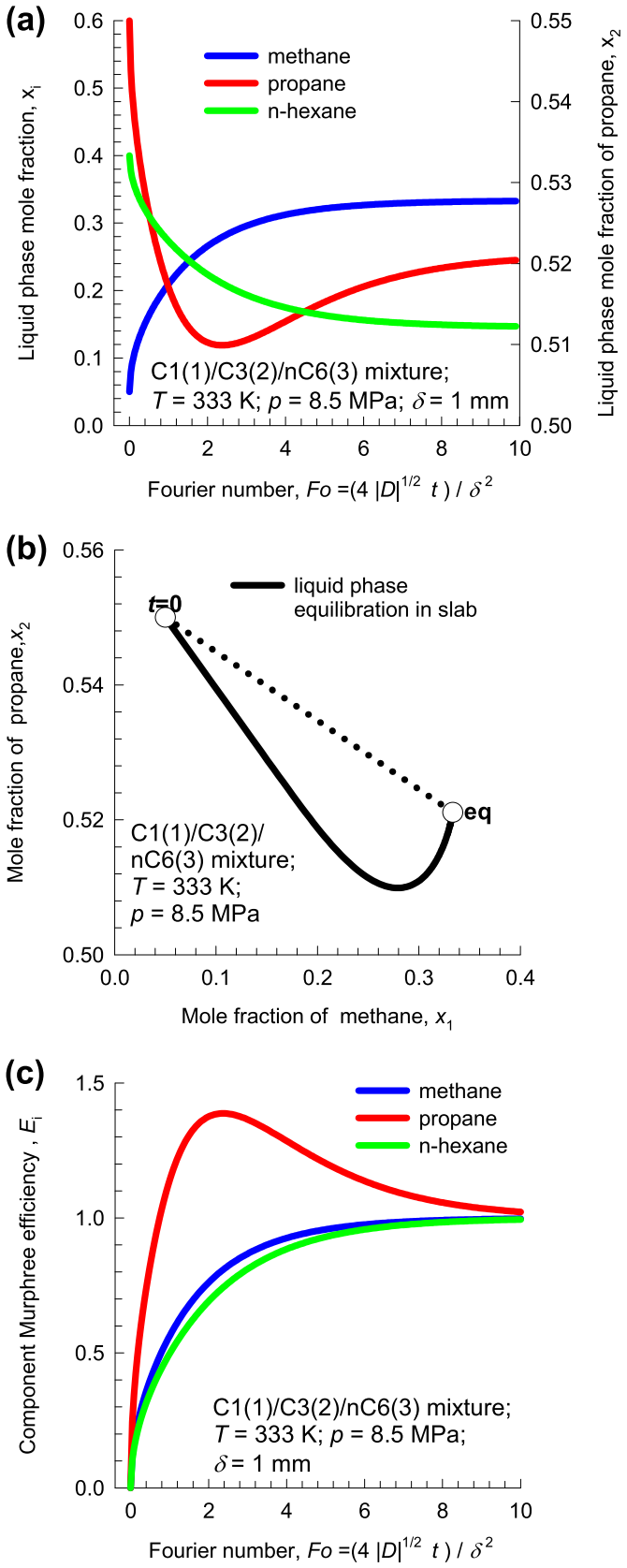


**Fig. 14.** (a) Transient equilibration for liquid phase diffusion in methane(1)/propane(2)/n-hexane (3) mixtures at 333 K and 8.5 MPa using Eq. (19) for the estimation of the elements of the Fick diffusivity matrix $[D]$. (b) The equilibration trajectory plotted in composition space. (c) Component Murphree efficiencies plotted as a function of the Fourier number, $\frac{4|D|^{1/2}t}{\delta^2}$, wherein the value of the characteristics diffusivity is chosen as the square root of the determinant of the Fick matrix, $|D|^{1/2}=5.5\times10^{-8}$ m$^2$ s$^{-1}$.

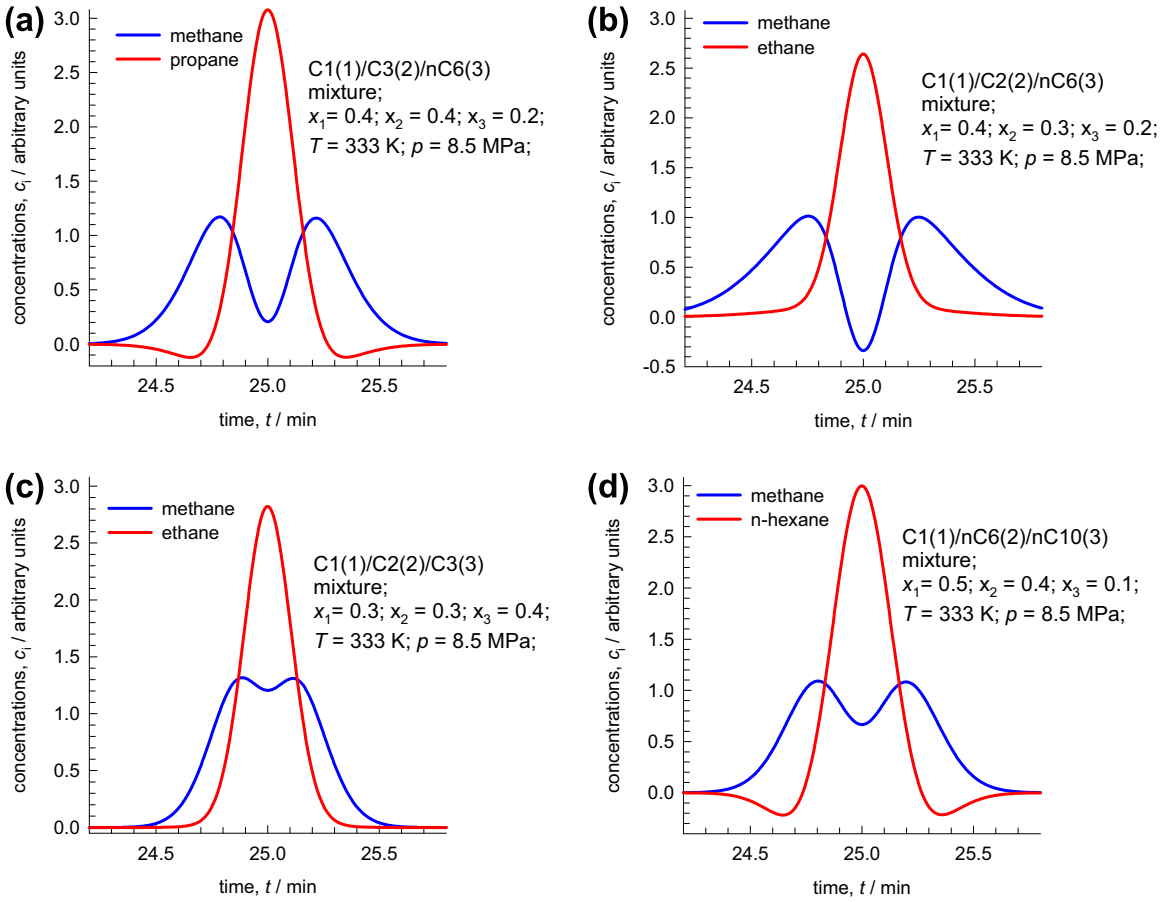


**Fig. 15.** Simulation results for Taylor dispersion for four different liquid phase mixtures at 333 K and 8.5 MPa. (a) Methane(1)/propane(2)/n-hexane (3) mixtures, (b) methane (1)/ethane(2)/n-hexane (3), (c) methane(1)/ethane(2)/propane (3), and (d) methane(1)/n-hexane(2)/n-decane (3). Eq. (19) is used for the estimation of the elements of the Fick diffusivity matrix $[D]$. At time $t=0$, Dirac δ-pulses $M1=M2=10^{-7}$ mol of components 1 and 2 are injected at the inlet.

an undershoot during transient equilibration. The equilibration trajectory follows a curvilinear path in composition space; see Fig. 14b. Transient overshoots/undershoots, and curvilinear equilibration trajectories are characteristic signatures of uphill diffusion (Krishna, 2015a, 2015b, 2016a, 2016b, 2016c).

The fractional approaches to equilibrium, also termed as the Murphree efficiencies (Murphree, 1925a, 1925b; Robbins and Cusack, 1999; Seader et al., 2011; Treybal, 1980), are calculated from

$$E_1 = \frac{x_{10}-x_1}{x_{10}-x_{1\delta}} = 1 - Q_{11} - Q_{12}\frac{x_{20}-x_{2\delta}}{x_{10}-x_{1\delta}};$$
$$E_2 = \frac{x_{20}-x_2}{x_{20}-x_{2\delta}} = 1 - Q_{22} - Q_{21}\frac{x_{10}-x_{1\delta}}{x_{20}-x_{2\delta}};$$
$$E_3 = \frac{x_{30}-x_3}{x_{30}-x_{3\delta}} = \frac{\frac{x_{10}-x_{1\delta}}{x_{20}-x_{2\delta}}E_1 + E_2}{\frac{x_{10}-x_{1\delta}}{x_{20}-x_{2\delta}}+1} \tag{30}$$

In Fig. 14c the component Murphree efficiencies are plotted as a function of the Fourier number defined as, $\frac{4|D|^{1/2}t}{\delta^2}$, wherein the value of the characteristics diffusivity is chosen as the square root of the determinant of the Fick matrix, At the averaged composition, we get $|D|^{1/2} = 5.5\times10^{-8}\ \mathrm{m^2\,s^{-1}}$. We note that Murphree efficiency of propane exceeds unity during most of the equilibration time span. An important reason for this is that the driving force for propane $(x_{20}-x_{2\delta})=(0.55-0.521103)=0.029$ is significantly lower than the driving forces of the partner species. Consequently, the transfer of propane is strongly influenced by the driving force of methane.

## 8. Taylor dispersion of ternary hydrocarbon liquid mixtures

A different demonstration of coupling effects in ternary hydrocarbon liquid mixtures is by consideration of Taylor dispersion in a tube (Price, 1988; Rutten, 1992); the modeling details are provided in Supplementary material. Fig. 15a shows the simulation results for Taylor dispersion for liquid phase methane(1)/propane (2)/n-hexane (3) mixtures at 333 K and 8.5 MPa, using Eq. (19) for the estimation of the elements of the Fick diffusivity matrix $[D]$. The liquid mixture flowing in the tube has the (cross-sectional averaged) composition $x_1=0.4$, $x_2=0.4$, $x_3=0.2$. At time $t=0$, Dirac δ-pulse containing $M1=M2=10^{-7}$ excess amounts (arbitrary units) of components 1 and 2 are injected at the inlet. The excess concentration of methane, and propane at the exit of the tube are shown as a function of time elapsed. Due to diffusional coupling, the transient methane concentration displays double-hump, non-Gaussian characteristics. Propane, on the other hand, experiences transient undershoots.

Analogous non-Gaussian peaks are obtained for Taylor dispersion in methane(1)/ethane(2)/n-hexane (3), methane(1)/ethane (2)/propane (3), and methane(1)/n-hexane(2)/n-decane (3) mixtures; Fig. 15b–d.

The Taylor dispersion analysis based on a linearized set of Maxwell–Stefan equations are commonly used for determination of the Fick diffusivity matrix in multicomponent mixtures (Price, 1988; Rutten, 1992). The Taylor dispersion analysis is also of relevance in the recovery of hydrocarbons from shale gas reserves an in enhanced oil recovery.

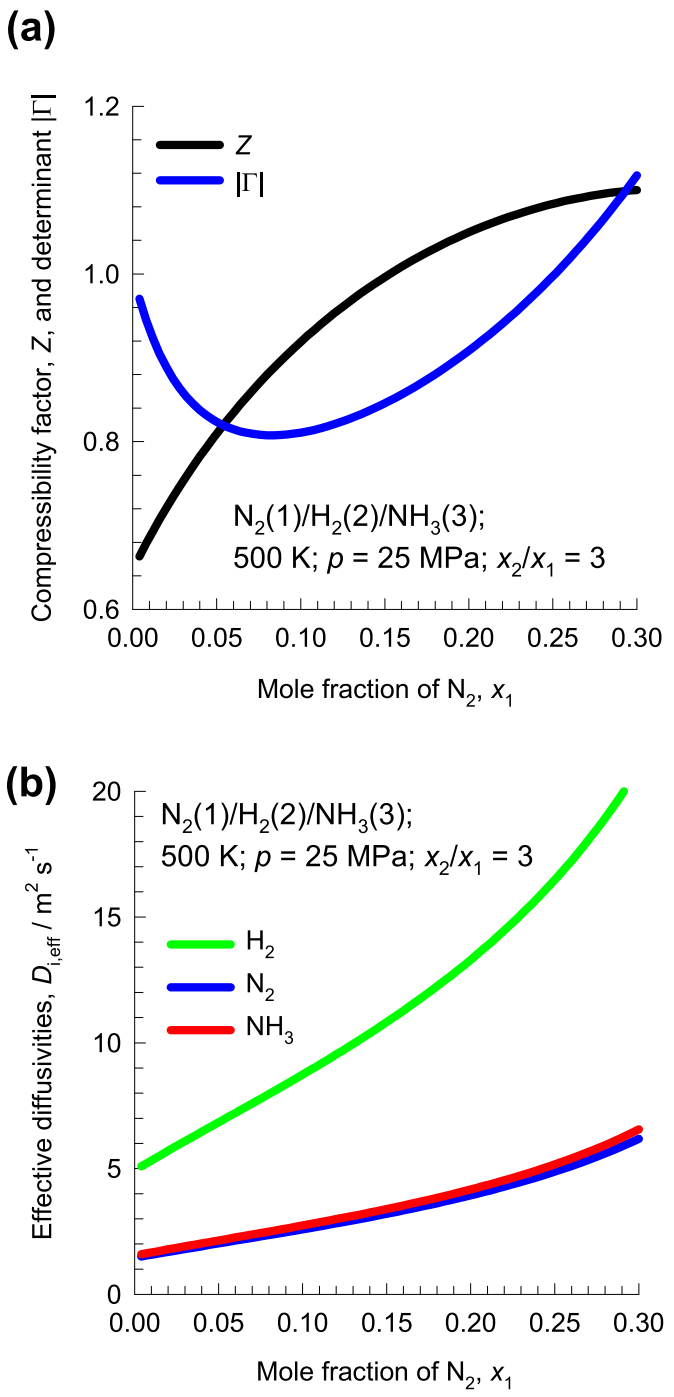


**Fig. 16.** (a) Calculation of the compressibility factor, $Z$, and the determinant $|\Gamma|$ in the gaseous mixture $N_2/H_2/NH_3$ at a temperature of 500 K and total pressure of 25 MPa; the ratio of the compositions $x_2/x_1=3$. (b) Calculation of the effective diffusivities in the gaseous mixture $N_2/H_2/NH_3$ at a temperature of 500 K and total pressure of 25 MPa. The M–S pair diffusivities are calculated using Eq. (22).

## 9. Diffusion with heterogeneous chemical reaction

For mixture diffusion with a heterogeneous reaction

$$\nu_1 A_1 + \nu_2 A_2 + \nu_3 A_3 + \ldots\ldots \nu_n A_n = 0 \tag{31}$$

the ratios of the fluxes $N_i$, in the laboratory fixed reference velocity frame, are determined by the reaction stoichiometry and so

$$\frac{N_1}{\nu_1} = \frac{N_2}{\nu_2} = \frac{N_3}{\nu_3} = \ldots. = \frac{N_n}{\nu_n} \tag{32}$$

For ammonia synthesis reaction $N_2 + 3H_2 \rightarrow 2NH_3$, for example, we have the constraint $\frac{N_1}{1} = \frac{N_2}{3} = \frac{N_3}{-2}$. In such cases, it is convenient to re-write the Maxwell–Stefan diffusion formulation (8) in a different manner by defining effective diffusivities, $D_{i,eff}$ for each component $i$ as follows

$$N_i = -c_t D_{i,eff}\left(\frac{x_i}{RT}\frac{d\mu_i}{dz}\right) \quad ; \quad i = 1, 2, \ldots n \tag{33}$$

Eq. (8) allows us to obtain an explicit expression for the effective diffusivity

$$\frac{1}{D_{i,eff}} = \sum_{\substack{j=1 \\ j\neq i}}^{n} \frac{x_j}{Đ_{ij}}\left(1 - \frac{x_i N_j}{x_j N_i}\right) = \sum_{\substack{j=1 \\ j\neq i}}^{n} \frac{x_j}{Đ_{ij}}\left(1 - \frac{x_i \nu_j}{x_j \nu_i}\right); \quad i = 1, 2, \ldots n \tag{34}$$

For dense gas mixtures, with $c_t < 10$ kmol m$^{-3}$, the M–S pair diffusivities can be estimated from the FSG equation, and subsequently applying the $Z$-correction using Eq. (22).

The ammonia synthesis reactor operates at pressures ranging to a few hundred bars, and fugacity coefficient corrections are important (Dyson and Simon, 1968). To demonstrate this, Fig. 16a shows calculations of the compressibility factor, $Z$, and the determinant $|\Gamma|$ in the gaseous mixture $N_2/H_2/NH_3$ at a temperature of 500 K and total pressure of 25 MPa. In these calculations, the ratio of the compositions $x_2/x_1=3$. Both $Z$, and $|\Gamma|$ show significant deviations from unity demonstrating the non-ideal gas behavior and the importance of fugacity coefficient corrections. Fig. 16b presents calculations of the effective diffusivities in the gaseous mixture $N_2/H_2/NH_3$ using Eq. (34). Interestingly, we note that the effective diffusivity of $N_2$ is practically the same as that of $NH_3$.

## 10. Conclusions

The following major conclusions can be drawn from the investigations reported in this work.

(1) The Maxwell–Stefan (M–S) equations, in combination with the Peng–Robinson equation of state, provide a convenient and practical framework of describing mixture diffusion in dense fluid mixtures.
(2) The Fick diffusivity for binary fluid mixtures, $D_{12}$, is obtained by multiplying the M–S diffusivity with the thermodynamic factor $\Gamma$. For operation near critical pressures, or near phase transition regions, $\Gamma \rightarrow 0$, and correspondingly $D_{12} \rightarrow 0$.
(3) For diffusion of solutes in supercritical $CO_2$, the corrections due to $\Gamma$ are significant even when the solute concentrations are at the level of $x_1 \approx 0.01$.
(4) For binary mixtures with molar densities $c_t < 10$ kmol m$^{-3}$, the M–S diffusivity $Đ_{12}$ can be estimated with good accuracy by introducing the correction for the compressibility factor $Z$ in the Fuller–Schettler–Giddings procedure as in Eq. (22). This correction introduces a composition dependence for the $Đ_{ij}$ that is absent for ideal gas mixtures.
(5) For binary mixtures with molar densities $c_t > 10$ kmol m$^{-3}$, the M–S diffusivity $Đ_{12}$ can be estimated using the Vignes interpolation formula (25); the infinite dilution diffusivities can be estimated using procedures such as the Wilke–Chang correlation.
(6) For ternary fluid mixtures, the matrix of Fick diffusivities $[D]$ is the product of $[\Lambda]$, calculable from the binary pair M–S diffusivities, $Đ_{ij}$, and the matrix of thermodynamic factors $[\Gamma]$. The off-diagonal elements of $[\Gamma]$ become of increasing importance as the compositions approach those corresponding

to V/L, or L/S phase transitions. This results in strong coupling of the diffusion fluxes.

(7) Strongly coupled diffusion of ternary mixtures leads to curvilinear equilibration trajectories. For Taylor dispersion of ternary hydrocarbon mixtures in tubes, coupling effects leads to non-Gaussian peaks at the tube exit.

## Appendix A. Supplementary material

Supplementary data associated with this article can be found in the online version at http://dx.doi.org/10.1016/j.ces.2016.07.025.

## References


Cullinan, H.T., 1966. Concentration dependence of the binary diffusion coefficient. Ind. Eng. Chem. Fundam. 5, 281–283.

D'Agostino, C., Mantle, M.D., Gladden, L.F., Moggridge, G.D., 2012. Prediction of mutual diffusion coefficients in non-ideal mixtures from pulsed field gradient NMR data: triethylamine–water near its consolute point. Chem. Eng. Sci. 74, 105–113.

Dyson, D.C., Simon, J.M., 1968. A kinetic expression with diffusion correction for ammonia synthesis on industrial catalyst. Ind. Eng. Chem. Fundam. 7, 605–610.

Dysthe, D.K., Hafskjold, B., 1995. Inter- and intradiffusion in liquid mixtures of methane and n-decane. Int. J. Thermophys. 16, 1213–1224.

Fuller, E.N., Schettler, P.D., Giddings, J.C., 1966. A new method for prediction of binary gas-phase diffusion coefficients. Ind. Eng. Chem. 58, 19–27.

Galliéro, G., Montel, F., 2008. Nonisothermal gravitational segregation by molecular dynamics simulations. Phys. Rev. E 78, 041203.

Higashi, H., Iwai, Y., Oda, T., Nakamura, Y., Arai, Y., 2002. Concentration dependence of diffusion coefficients for supercritical carbon dioxide + naphthalene system. Fluid Phase Equilib. 194–197, 1161–1167.

Krishna, R., 2015a. Uphill diffusion in multicomponent mixtures. Chem. Soc. Rev. 44, 2812–2836.

Krishna, R., 2015b. Serpentine diffusion trajectories and the Ouzo effect in partially miscible ternary liquid mixtures. Phys. Chem. Chem. Phys. 17, 27428–27436.

Krishna, R., 2016a. Diffusing uphill with James Clerk Maxwell and Josef Stefan. Curr. Opin. Chem. Eng. 12, 106–119.

Krishna, R., 2016b. Highlighting diffusional coupling effects in ternary liquid extraction and comparisons with distillation. Ind. Eng. Chem. Res. 55, 1053–1063.

Krishna, R., 2016c. Tracing the origins of transient overshoots for binary mixture diffusion in microporous crystalline materials. Phys. Chem. Chem. Phys. 18, 15482–15495.

Krishna, R., van Baten, J.M., 2005. The darken relation for multicomponent diffusion in liquid mixtures of linear alkanes. An investigation using molecular dynamics (MD) simulations. Ind. Eng. Chem. Res. 44, 6939–6947.

Krishna, R., van Baten, J.M., 2009. Unified Maxwell–Stefan description of binary mixture diffusion in micro- and meso-porous materials. Chem. Eng. Sci. 64, 3159–3178.

Leahy-Dios, A., Bou-Ali, M.M., Platten, J.K., Firoozabadi, A., 2005. Measurements of molecular and thermal diffusion coefficients in ternary mixtures. J. Chem. Phys. 122, 234502.

Leahy-Dios, A., Firoozabadi, A., 2007. Unified model for nonideal multicomponent molecular diffusion coefficients. AIChE J. 53, 2932–2939.

Murphree, E.V., 1925a. Rectifying column calculations with particular reference to n-component mixtures. Ind. Eng. Chem. 17, 747–750.

Murphree, E.V., 1925b. Graphical rectifying column calculations. Ind. Eng. Chem. 17, 960–964.

Nishiumi, H., Kubota, T., 2007. Fundamental behavior of benzene–$CO_2$ mutual diffusion coefficients in the critical region of $CO_2$. Fluid Phase Equilib. 261, 146–151.

Price, W.F., 1988. Theory of the Taylor dispersion technique for three-component-system diffusion measurements. J. Chem. Soc. Faraday Trans. 1 (84), 2431–2439.

Reid, R.C., Prausnitz, J.M., Poling, B.E., 1986. The Properties of Gases and Liquids, 4th ed. McGraw-Hill, New York.

Robbins, L.A., Cusack, R.W., 1999. Chaper 15, Liquid–liquid extraction operations and equipment. In: Perry, R.H., Green, D.W. (Eds.), Perry's Chemical Engineers' Handbook. McGraw-Hill, New York, pp. 15-11–15-47.

Rutten, P.W.M., 1992. Diffusion in Liquids (Ph.D. Thesis, Dissertation). Delft University of Technology, Delft.

Savage, P.E., Gopalan, S., Mizan, T.I., Martino, C.J., Brock, E.E., 1995. Reactions at supercritical conditions: applications and fundamentals. AIChE J. 41, 1723–1778.

Seader, J.D., Henley, E.J., Roper, D.K., 2011. Separation Process Principles, 3rd ed. John Wiley, New York.

Sie, S.T., Krishna, R., 1998. Process development and scale up: III. Scale-up and scale-down of trickle bed processes. Rev. Chem. Eng. 14, 203–252.

Standart, G.L., Taylor, R., Krishna, R., 1979. The Maxwell–Stefan formulation of irreversible thermodynamics for simultaneous heat and mass transfer. Chem. Eng. Commun. 3, 277–289.

Takahashi, S., Hongo, M., 1982. Diffusion coefficients of gases at high pressures in the $CO_2$–$C_2H_4$ system. J. Chem. Eng. Jpn. 15, 57–59.

Taylor, R., Krishna, R., 1993. Multicomponent Mass Transfer. John Wiley, New York.

Touzet, M., Galliero, G., Lazzeri, V., Saghir, M.Z., Montel, F., Legros, J.-C., 2011. Thermodiffusion: from microgravity experiments to the initial state of petroleum reservoirs. C. R. Mec. 339, 318–323.

Treybal, R.E., 1980. Mass-Transfer Operations, 3rd ed. McGraw-Hill, New York.

Tuan, D.Q., Zollweg, J.A., Rizvi, S.S.H., 1999. Concentration dependence of the diffusion coefficient of lipid in supercritical carbon dioxide. Ind. Eng. Chem. Res. 38, 2787–2793.

Wesselingh, J.A., Bollen, A.M., 1997. Multicomponent diffusivities from the free volume theory. Chem. Eng. Res. Des. 75, 590–602.

Wilke, C.R., Chang, P., 1955. Correlation of diffusion coefficients in dilute solutions. AIChE J. 1, 264–270.

*Supplementary material to accompany:*

# Describing Diffusion in Fluid Mixtures at Elevated Pressures by Combining the Maxwell-Stefan Formulation with an Equation of State

**Rajamani Krishna***

Van 't Hoff Institute for Molecular Sciences, University of Amsterdam, Science Park 904,

1098 XH Amsterdam, The Netherlands

and

**Jasper M. van Baten**

AmsterCHEM, Calle Las Rozas 32,

04618 Las Rozas, Cuevas del Almanzora,

Almería, SPAIN

*email: r.krishna@contact.uva.nl

**Table of Contents**

# 1. Preamble

This Supplementary material accompanying the article *Describing Diffusion in Fluid Mixtures at Elevated Pressures by Combining the Maxwell-Stefan Formulation with an Equation of State* provides details of (a) derivations of the Maxwell-Stefan equations, (b) some background information and insights on diffusivities, (d) details of the calculations of the compressibility factor and thermodynamic factors using the Peng-Robinson EOS, and (e) all input data, and simulation data results.

All the calculations and simulations were performed using MathCad 15.[1]

For ease of reading, this Supplementary material is written as a stand-alone document; as a consequence, there is some overlap of material with the main manuscript.

# 2. The Maxwell-Stefan formulation for diffusion in *n*-component fluid mixtures

The Maxwell-Stefan (M-S) formulation is widely used in chemical engineering practice to describe *n*-component diffusion in bulk fluid mixtures. For *n*-component fluid mixtures, the M-S equations represent a balance between the force exerted per mol of species *i* with the drag, or friction, experienced with each of the partner species in the mixture. We may expect that the frictional drag to be proportional to differences in the velocities of the diffusing species $\left(u_i - u_j\right)$. For component 1, for example, we write

$$-\frac{d\mu_1}{dz} = \frac{RT}{Đ_{12}} x_2\left(u_1 - u_2\right) + \frac{RT}{Đ_{13}} x_3\left(u_1 - u_3\right) + ..... + \frac{RT}{Đ_{1n}} x_n\left(u_1 - u_n\right) \tag{1}$$

The corresponding relations for components 2, 3, ..*n* are written down in an intuitively obvious manner. The left member of equation (1) is the negative of the gradient of the chemical potential, with the units N mol$^{-1}$; it represents the driving force acting per mole of species 1. The term $RT/Đ_{ij}$ is interpreted as the drag coefficient for the *i*-*j* pair. The multiplier $x_j$ in each of the right members represents the mole fraction of component *j*; this factor is introduced because we expect the friction to be dependent on the number of molecules of *j* relative to that of component 1. The M-S diffusivity $Đ_{ij}$

has the units $m^2\ s^{-1}$ and the physical significance of an *inverse* drag coefficient. The magnitudes of the M-S diffusivities $Đ_{ij}$ do not depend on the choice of the mixture reference velocity because Equation (1) is set up in terms of velocity differences.

The modelling and design of separation and reaction equipment requires calculation of the diffusion fluxes, $J_i$; these are defined with respect to an arbitrarily chosen reference velocity of the fluid mixture, $u$:

$$J_i \equiv c_i(u_i - u); \quad i = 1,2,..n \tag{2}$$

Most commonly, we choose $u$ as the molar average velocity of the mixture

$$u = x_1u_1 + x_2u_2 + \cdots x_nu_n \tag{3}$$

Only $n$-1 of the fluxes $J_i$ are independent because the diffusion fluxes sum to zero

$$\sum_{i=1}^{n} J_i = 0 \tag{4}$$

The molar fluxes $N_i$ in the laboratory fixed reference frame are related to the diffusion fluxes $J_i$ by

$$N_i \equiv c_i u_i = J_i + x_i N_t; \quad N_t = \sum_{i=1}^{n} N_i \tag{5}$$

Equation (1) may be re-written as

$$-\frac{1}{RT}\frac{d\mu_i}{dz} = \sum_{\substack{j=1 \\ j\neq i}}^{n} \frac{x_j(u_i - u_j)}{Đ_{ij}} \tag{6}$$

Multiplying both sides of equation (6) by $x_i$ we get

$$-\frac{x_i}{RT}\frac{d\mu_i}{dz} = \sum_{\substack{j=1 \\ j\neq i}}^{n} \frac{x_i x_j(u_i - u_j)}{Đ_{ij}} = \sum_{\substack{j=1 \\ j\neq i}}^{n} \frac{(x_j x_i u_i - x_i x_j u_j)}{Đ_{ij}} = \sum_{\substack{j=1 \\ j\neq i}}^{n} \frac{(x_j c_i u_i - x_i c_j u_j)}{c_t Đ_{ij}} \tag{7}$$

Introducing the expressions for fluxes in equation (7), we obtain

$$-\frac{x_i}{RT}\frac{d\mu_i}{dz}=\sum_{\substack{j=1\\ j\neq i}}^{n}\frac{x_j N_i - x_i N_j}{c_t Đ_{ij}}=\sum_{\substack{j=1\\ j\neq i}}^{n}\frac{x_j J_i - x_i J_j}{c_t Đ_{ij}};\quad i=1,2,\ldots n \tag{8}$$

where the second equality arises from application of equations (4) and (5).

Only ($n$-1) of the chemical potential gradients $\frac{d\mu_i}{dz}$ are independent, because of the Gibbs-Duhem relationship

$$x_1\frac{d\mu_1}{dz}+x_2\frac{d\mu_2}{dz}+\cdots x_n\frac{d\mu_n}{dz}=0 \tag{9}$$

The second law of thermodynamics dictates that the rate of entropy production must be positive

$$\sigma=-\frac{1}{T}\sum_{i=1}^{n}\frac{d\mu_i}{dz}J_i=-\frac{1}{T}\sum_{i=1}^{n-1}\frac{d\left(\mu_i-\mu_n\right)}{dz}J_i\geq 0 \tag{10}$$

The Maxwell-Stefan diffusion formulation (8) is consistent with the Onsager formulation in which the ($n$-1) independent diffusion fluxes are postulated as linear functions of the ($n$-1) independent chemical potential gradients

$$(J)=-c_t\left[L\right]\frac{1}{RT}\left(\frac{d\left(\mu-\mu_n\right)}{dz}\right) \tag{11}$$

The units of the elements $L_{ij}$ are the same as those for Fick diffusivities, i.e. $m^2\ s^{-1}$. The matrix of Onsager coefficients $\left[L\right]$ is symmetric because of the Onsager Reciprocal Relations (ORR)[2]

$$L_{ij}=L_{ji} \tag{12}$$

The Onsager Reciprocal Relations imply that the M-S pair diffusivities are symmetric

$$Đ_{ij}=Đ_{ji};\quad i,j=1,2...n \tag{13}$$

Insertion of the Maxwell-Stefan diffusion eq. (1) into (10) we obtain on re-arrangement[3]

$$\sigma=\frac{1}{2}c_t R\sum_{i=1}^{n}\sum_{j=1}^{n}\frac{x_i x_j}{Đ_{ij}}\left|u_i-u_j\right|^2\geq 0 \tag{14}$$

The term $\frac{x_i}{RT}\frac{d\mu_i}{dz}$ on the left hand member of equation (8) is the generalization of the mole fraction gradients, used as driving forces for ideal gas mixtures. Indeed, for ideal gas ternary mixtures, equation (8) simplify to yield

$$\begin{aligned}
-\frac{dx_1}{dz} &= \frac{x_2N_1-x_1N_2}{c_t Đ_{12}} + \frac{x_3N_1-x_1N_3}{c_t Đ_{13}};\\
-\frac{dx_2}{dz} &= \frac{x_1N_2-x_2N_1}{c_t Đ_{12}} + \frac{x_3N_2-x_2N_3}{c_t Đ_{23}}\\
-\frac{dx_3}{dz} &= \frac{x_1N_3-x_3N_1}{c_t Đ_{13}} + \frac{x_2N_3-x_3N_2}{c_t Đ_{23}}
\end{aligned} \tag{15}$$

For mixtures of ideal gases for which the $Đ_{ij}$ are independent of composition the condition (14) can only be satisfied if

$$Đ_{ij} \geq 0; \quad \text{(ideal gas mixtures)} \tag{16}$$

Equation (16) was first derived by Hirschfelder, Curtiss and Bird.[4] For non-ideal lfluid mixtures the $Đ_{ij}$ are composition dependent in general and a result analogous to eq. (16) cannot be derived.[3]

For fluid mixtures containing uncharged neutral species, the chemical potential of component *i*, $\mu_i$ is related to the component fugacity, $f_i = \phi_i p_i = \phi_i x_i p$:

$$\mu_i = \mu_i^0 + RT\ln(f_i) = \mu_i^0 + RT\ln(\phi_i x_i p) \tag{17}$$

where $\phi_i$ is the activity coefficient and *p* is the total pressure.

It is helpful to express the left member of equation (8) in terms of the mole fraction gradients by introducing an (*n*-1) × (*n*-1) matrix of thermodynamic factors $[\Gamma]$:

$$\frac{x_i}{RT}\frac{d\mu_i}{dz} = x_i\frac{d\ln f_i}{dz} = \sum_{j=1}^{n-1}\Gamma_{ij}\frac{dx_j}{dz}; \quad \Gamma_{ij} = \delta_{ij} + x_i\frac{\partial\ln\phi_i}{\partial x_j}; \quad i,j = 1,2\ldots n-1 \tag{18}$$

The elements of $[\Gamma]$ can be calculated by analytic differentiation of an Equation of State (EOS) such as the Peng-Robinson (PR) EOS. For binary mixtures, explicit analytic expressions for $\Gamma = x_1 \frac{\partial \ln f_1}{\partial x_1} = 1 + x_1 \frac{\partial \ln \phi_1}{\partial x_1}$ for PR EOS are provided in the paper by Tuan et al.[5]

We also define a ($n$-1) × ($n$-1) matrix of inverse diffusivities $[B]$ whose elements are given by

$$B_{ii} = \frac{x_i}{Đ_{in}} + \sum_{\substack{k=1 \\ k \neq i}}^{n} \frac{x_k}{Đ_{ik}}; \quad B_{ij(i \neq j)} = -x_i \left( \frac{1}{Đ_{ij}} - \frac{1}{Đ_{in}} \right); \quad i, j = 1,2...n-1 \tag{19}$$

Combining equations (8), (18), and (19), we can re-cast equation (8) into ($n$-1) dimensional matrix notation

$$(J) = -c_t [B]^{-1} [\Gamma] \frac{d(x)}{dz} = -c_t [\Lambda][\Gamma] \frac{d(x)}{dz} \tag{20}$$

where we have additionally defined

$$[\Lambda] = [B]^{-1} \tag{21}$$

If we define a ($n$-1) × ($n$-1) dimensional Fick diffusivity matrix $[D]$

$$(J) = -c_t [D] \frac{d(x)}{dz} \tag{22}$$

we obtain the inter-relationship

$$[D] = [B]^{-1} [\Gamma] = [\Lambda][\Gamma] \tag{23}$$

For an ideal gas mixture, we have

$$[\Lambda] = [B]^{-1} = [D]; \quad \text{ideal gas mixture} \tag{24}$$

Equation (23) underscores the direct influence of mixture thermodynamics on the Fick diffusivites $D_{ij}$.

For a binary mixture, $n$ = 2, equation (8) simplifies to yield

$$-\frac{x_1}{RT} \frac{d\mu_1}{dz} = \frac{(x_2 J_1 - x_1 J_2)}{c_t Đ_{12}} \tag{25}$$

Introducing the constraints $J_2 = -J_1$, and $x_2 = 1 - x_1$, equation () simplies to yield

$$J_1 = -c_t Đ_{12} \frac{x_1}{RT} \frac{d\mu_1}{dz} = -c_t Đ_{12} \Gamma \frac{dx_1}{dz} = -c_t D_{12} \frac{dx_1}{dz} \tag{26}$$

in which the Fick diffusivity for binary mixture is

$$D_{12} = Đ_{12} \Gamma \tag{27}$$

For a ternary mixture, $n = 3$, we derive

$$\begin{bmatrix} D_{11} & D_{12} \\ D_{21} & D_{22} \end{bmatrix} = \frac{1}{B_{11}B_{22} - B_{12}B_{21}} \begin{bmatrix} \dfrac{x_2}{Đ_{23}} + \dfrac{x_1}{Đ_{12}} + \dfrac{x_3}{Đ_{23}} & x_1\left(\dfrac{1}{Đ_{12}} - \dfrac{1}{Đ_{13}}\right) \\ x_2\left(\dfrac{1}{Đ_{12}} - \dfrac{1}{Đ_{23}}\right) & \dfrac{x_1}{Đ_{13}} + \dfrac{x_2}{Đ_{12}} + \dfrac{x_3}{Đ_{13}} \end{bmatrix} \begin{bmatrix} \Gamma_{11} & \Gamma_{12} \\ \Gamma_{21} & \Gamma_{22} \end{bmatrix} \tag{28}$$

Equation (28) simplifies to yield

$$\begin{bmatrix} D_{11} & D_{12} \\ D_{21} & D_{22} \end{bmatrix} = \begin{bmatrix} \Lambda_{11} & \Lambda_{12} \\ \Lambda_{21} & \Lambda_{22} \end{bmatrix} \begin{bmatrix} \Gamma_{11} & \Gamma_{12} \\ \Gamma_{21} & \Gamma_{22} \end{bmatrix} = \frac{\begin{bmatrix} Đ_{13}\left(x_1 Đ_{23} + (1-x_1) Đ_{12}\right) & x_1 Đ_{23}\left(Đ_{13} - Đ_{12}\right) \\ x_2 Đ_{13}\left(Đ_{23} - Đ_{12}\right) & Đ_{23}\left(x_2 Đ_{13} + (1-x_2) Đ_{12}\right) \end{bmatrix}}{x_1 Đ_{23} + x_2 Đ_{13} + x_3 Đ_{12}} \begin{bmatrix} \Gamma_{11} & \Gamma_{12} \\ \Gamma_{21} & \Gamma_{22} \end{bmatrix} \tag{29}$$

The determinant of $[B]$ for a ternary mixture is

$$|B| = \frac{x_1}{Đ_{12}Đ_{13}} + \frac{x_2}{Đ_{12}Đ_{23}} + \frac{x_3}{Đ_{13}Đ_{23}} = \frac{1}{|\Lambda|}; \quad |\Lambda| = \frac{Đ_{12}Đ_{13}Đ_{23}}{x_1 Đ_{23} + x_2 Đ_{13} + x_3 Đ_{12}} \tag{30}$$

We also have

$$|\Lambda|^{1/2} = \sqrt{\frac{Đ_{12}Đ_{13}Đ_{23}}{x_1 Đ_{23} + x_2 Đ_{13} + x_3 Đ_{12}}} \tag{31}$$

The quantity $|\Lambda|^{1/2}$ can be interpreted as an "average" magnitude of M-S diffusivity in the ternary mixture.

For stable single phase fluid mixtures, we must have $|\Gamma| \geq 0$. In view of equation (23), the condition of phase stability translates to

$$|D| \geq 0; \quad |\Gamma| \geq 0; \quad \text{phase stability} \tag{32}$$

Equation (32) implies that all the eigenvalues of the Fick matrix [$D$] are positive. It is interesting to note that thermodynamic stability considerations do not require the diagonal elements $D_{ii}$ to be positive. If recourse is made to the kinetic theory of gases, it can be shown that the diagonal elements $D_{ii}$ are individually positive for mixtures of ideal gases. The off-diagonal elements $D_{ij}(i \neq j)$ can be either positive or negative, even for ideal gas mixtures. Indeed, the sign of $D_{ij}(i \neq j)$ also depends on the component numbering.

The condition for phase stability in a binary fluid mixture is

$$D_{12} \geq 0; \quad \Gamma \geq 0; \quad \text{phase stability} \tag{33}$$

The occurrence of $\Gamma < 0$ implies vapor/liquid or liquid/solid phase transitions.

# 3. Other choices of reference velocities in the definition of the Fick diffusivity matrix

The Fick diffusivity matrix $[D]$ is defined in equation (22) in terms of molar diffusion fluxes, $J_i$, that are, in turn, defined with respect to the molar average reference velocity frame $u$. Other choice of fluxes and reference velocities are encountered in the chemical engineering literature; see Section 3.2.2 of Taylor and Krishna.[6]

For mass diffusion fluxes, $j_i \equiv \rho_i\left(u_i - u^{mass}\right); \quad i = 1,2,..n; \quad \sum_{i=1}^{n} j_i = 0$ defined with respect the mass average mixture velocity $u^{mass} = \sum_{i=1}^{n} \omega_i u_i$, we write $(j) = -\rho_t\left[D^{mass}\right]\frac{d(\omega)}{dz}$.

The mass fractions are related to the mole fractions $x_i$

$$\omega_i = \frac{\rho_i}{\rho_t} = \frac{x_i M_i}{\sum_{i=1}^{n} x_i M_i} = \frac{x_i M_i}{\overline{M}}; \quad x_i = \frac{c_i}{c_t} = \frac{\frac{\omega_i}{M_i}}{\sum_{i=1}^{n} \frac{\omega_i}{M_i}} = \frac{\omega_i}{M_i}\overline{M} \tag{34}$$

where $M_i$ is the molar mass of species $i$, with the units kg mol$^{-1}$, and $\overline{M}$ is the mean molar mass of the mixture is

$$\overline{M} = \sum_{i=1}^{n} x_i M_i = \frac{1}{\sum_{i=1}^{n} \frac{\omega_i}{M_i}} \tag{35}$$

The mixture mass density is related to the total molar concentration of the mixture

$$\rho_t = c_t \overline{M} \tag{36}$$

For molar diffusion fluxes, $J_i^{volume} \equiv c_i\left(u_i - u^{volume}\right); \quad i = 1,2,..n; \quad \sum_{i=1}^{n} \overline{V}_i J_i^{volume} = 0$ defined with respect the volume average mixture velocity $u^{volume} = \sum_{i=1}^{n} c_i \overline{V}_i u_i$, we write $(J^{volume}) = -\left[D^{volume}\right]\frac{d(c)}{dz}$. This is a common choice in the experimental determination of diffusivities.

The formulae for transformation of the Fick diffusivity matrix from one reference frame to another are provided in Section 3.2.4 of Taylor and Krishna.[6]

For *n*-component mixtures, the numerical values of the elements of $[D]$, $\left[D^{mass}\right]$, and $\left[D^{volume}\right]$ are different. However, the determinants of the corresponding matrices are equal to one another.[6]

$$|D| = \left|D^{mass}\right| = \left|D^{volume}\right| \tag{37}$$

For the special case of a binary mixture, $dx_1 = \frac{\frac{1}{M_1 M_2}}{\left(\frac{\omega_1}{M_1} + \frac{\omega_2}{M_2}\right)^2} d\omega_1; \quad d\omega_1 = \frac{M_1 M_2}{\left(x_1 M_1 + x_2 M_2\right)^2} dx_1$, and the Fick diffusivity is the same for the three different choice of reference velocity frames[6]

$$\begin{aligned} j_1 &\equiv \rho_1\left(u_1 - u^{mass}\right) = -\rho_t D_{12} \frac{d\omega_1}{dz} \\ J_1 &\equiv c_1\left(u_1 - u\right) = -c_t D_{12} \frac{dx_1}{dz} \\ J_1^{volume} &\equiv c_i\left(u_1 - u^{volume}\right) = -D_{12} \frac{dc_1}{dz} \end{aligned} \tag{38}$$

# 4. Generalization of the M-S equations to include pressure gradients and body forces

The important persuasive advantage of the M-S diffusion formulation (8) is that it can be extended to include the contribution of pressure gradients, that is important in the context of gravitational segregation in petroleum reservoirs.[7] The treatment below closely follows earlier works.[6, 8, 9]

The chemical potential gradient term may be expanded to explicitly include the contribution of the pressure gradient

$$\nabla_T \mu_i = \nabla_{T,p} \mu_i + \overline{V}_i \nabla p \tag{39}$$

Here $\overline{V}_i$ is the partial molar volume of species *i*. The molar volume of the mixture is $\overline{V} = \sum_{k=1}^{m} x_k \overline{V}_k = \frac{1}{c_t}$ where $c_t$ is the total molar concentration of the mixture, containing *n* species.

Let $\tilde{F}_i$ represent the body force acting per kg of species *i*. Expressed per volume of mixture the generalized driving force $d_i$ for diffusion is defined by

$$-c_t RT d_i \equiv -c_i \frac{d\mu_i}{dz} - c_i \overline{V}_i \frac{dp}{dz} + \rho_i \tilde{F}_i \tag{40}$$

The molar concentration of the mixture is

$$c_t = \sum_{i=1}^{n} c_i; \quad x_i = \frac{c_i}{c_t} \tag{41}$$

Under the action of external body forces, linear momentum will be conserved

$$-\frac{1}{\rho_t}\frac{dp}{dz} + \sum_{i=1}^{n} \omega_i \tilde{F}_i = \frac{d\mathbf{v}}{dt} + \nabla \bullet \tau \tag{42}$$

where **v** is the mass average mixture velocity, $\boldsymbol{\tau}$ is the stress tensor and $\omega_i$ is the mass fraction of species *i*.

In diffusion processes of relevance to chemical engineering mechanical equilibrium is established far quicker than thermodynamic equilibrium and we may safely assume

$$\frac{d\mathbf{v}}{dt} + \nabla \bullet \tau \approx 0 = -\frac{1}{\rho_t}\frac{dp}{dz} + \sum_{i=1}^{n} \omega_i \tilde{F}_i \tag{43}$$

It is convenient to incorporate the mechanical equilibrium constraint (43) by redefining the generalized driving force in eq. (40) as follows

$$-c_t RTd_i \equiv -c_i \frac{d\mu_i}{dz} - c_i \overline{V_i}\frac{dp}{dz} + \rho_i \tilde{F}_i + \rho_i \left( \frac{1}{\rho_t}\frac{dp}{dz} - \sum_{i=1}^{n} \omega_i \tilde{F}_i \right) \tag{44}$$

where we add a vanishing contribution[6, 8, 9] to the driving force defined by eq. (40).

On re-arrangement we obtain the following expression for the generalized driving force

$$-d_i \equiv -\frac{x_i}{RT}\frac{d\mu_i}{dz} - \frac{1}{c_t RT}\left(c_i \overline{V_i} - \omega_i\right)\frac{dp}{dz} + \frac{\rho_i}{c_t RT}\left( \tilde{F}_i - \sum_{i=1}^{n} \omega_i \tilde{F}_i \right) \tag{45}$$

where we note that $c_i \overline{V_i}$ is the volume fraction of species *i*.

If the body forces $F_i$ represent the force acting per mole of species *i*, i.e. $\rho_i \tilde{F}_i = c_i F_i$, the corresponding expressions for the generalized driving force is

$$-d_i \equiv -\frac{x_i}{RT}\frac{d\mu_i}{dz} - \frac{1}{c_t RT}\left(c_i \overline{V_i} - \omega_i\right)\frac{dp}{dz} + \frac{1}{c_t RT}\left( c_i F_i - \omega_i \sum_{k=1}^{n} c_k F_k \right) \tag{46}$$

For transport in electrolyte systems, for example, the body force $F_i$ acting per mol of species *i* is

$$F_i = -z_i \mathrm{F}\frac{d\Phi}{dz} \tag{47}$$

where $z_\mathrm{i}$ is the ionic charge of species *i* and F is the Faraday constant. Except in regions close to electrode surfaces, where there will be charge separation (the double layer phenomena), the condition of electro-neutrality is met

$$\sum_{i=1}^{n} c_i z_i = 0 \tag{48}$$

and therefore

$$\sum_{k-1}^{n} c_k F_k == \left( \sum_{k=1}^{n} c_k z_k \right) \mathrm{F} \frac{d\Phi}{\mathrm{dz}} = 0 \tag{49}$$

In view of equations (47) and (49), the expression for the generalized driving force simplifies to yield

$$-d_i \equiv -\frac{x_i}{RT}\frac{d\mu_i}{dz} - \frac{1}{c_t RT}\left(c_i \overline{V_i} - \omega_i\right)\frac{dp}{dz} - \frac{x_i z_i \mathrm{F}}{RT}\frac{d\Phi}{dz} \tag{50}$$

The generalization of the M-S diffusion formulation (8) with the inclusion of pressure gradients and electrostatic potential gradients is

$$-\frac{x_i}{RT}\frac{d\mu_i}{dz} - \frac{1}{c_t RT}\left(c_i \overline{V_i} - \omega_i\right)\frac{dp}{dz} - \frac{x_i z_i \mathrm{F}}{RT}\frac{d\Phi}{dz} = \sum_{\substack{j=1 \\ j\neq i}}^{n} \frac{x_j N_i - x_i N_j}{c_t Đ_{ij}} = \sum_{\substack{j=1 \\ j\neq i}}^{n} \frac{x_j J_i - x_i J_j}{c_t Đ_{ij}}; \quad i = 1,2,\ldots n \tag{51}$$

For diffusion inside porous materials, the friction experienced by species *i* with the wall (w) needs to be accounted for by adding the term representing the drag with the pore walls $RT\left(u_i - u_w\right)/Đ_{iw}$ where $Đ_{\mathrm{iw}}$ is the pore diffusivity.

## 5. Diffusivities in dense binary gas mixtures

The M-S pair diffusivities $Đ_{\mathrm{ij}}$ for gaseous mixtures at low pressures, below about 10 bar, can be estimated to a good level of accuracy using the Fuller-Schettler-Giddings (FSG)[10] method.

$$Đ_{12} = \frac{1.43\times 10^{-7} T^{1.75}}{p\sqrt{M_{12}}\left[\left(v_1^{1/3}\right) + \left(v_2^{1/3}\right)\right]^2} \quad \mathrm{m^2 s^{-1}} \tag{52}$$

where $p$ is the pressure (expressed in bars), $M_{12} = \dfrac{2}{\dfrac{1}{M_1} + \dfrac{1}{M_2}}$ is the mean molecular weight of the mixture (expressed in g $\mathrm{mol^{-1}}$), $v_1$, and $v_2$ are the diffusion volumes (expressed in $\mathrm{cm^3\ mol^{-1}}$) whose values are obtained by summing the contributions of the volumes of the constituent atoms in the molecular species (the values are tabulated in Table 11.1 of Reid, Prausnitz, and Poling[11]). According to the FSG estimation procedure, the product of $Đ_{12}$ and the total pressure, $p$, is a function only of temperature and is also independent of composition.

In generalizing the FSG method to dense gas mixtures, it is important realize that equation (52) implies that, *at constant temperature*, the M-S diffusivity is *inversely* proportional to the molar density of the gas phase. For dense gases, the total mixture molar density of the gas phase is $c_t = \frac{p}{ZRT}$ where $Z$ is the compressibility factor. Consequently, the M-S diffusivity for dense gases can be estimated by correcting the original FSG equation by introducing the compressibility factor $Z$:

$$Đ_{12} = \frac{1.43\times10^{-7}T^{1.75}}{p\sqrt{M_{12}}\left[\left(v_1^{1/3}\right)+\left(v_2^{1/3}\right)\right]^2}Z \tag{53}$$

where $p$ is the pressure (expressed in bars). Due to the introduction of the compressibility factor, the M-S diffusivity $Đ_{12}$ becomes dependent on mixture composition. The molar density of the mixture is $c_t = \frac{p}{ZRT}$, and therefore Equation (53) anticipates that $c_t Đ_{12}$ is constant at constant temperature $T$.

In order to demonstrate the composition dependence of the $Đ_{12}$, Figure 1 presents calculations of combined FSG and PR EOS models for thermodynamics and diffusion in $CO_2(1)/C_2H_4(2)$ mixtures at $T$ = 323.2 K with varying compositions $x_1$, and total pressure, $p$. Figure 1a shows that the compressibility factor, $Z$, reduces slightly with increasing mole fraction $x_1$ of $CO_2(1)$. The thermodynamic correction factor, $\Gamma \equiv \left(1+\frac{\partial \ln \phi_1}{\partial \ln x_1}\right)$, is practically equal to unity for the entire range of pressures and compositions; see Figure 1b. The calculations of $\Gamma = x_1\frac{\partial \ln f_1}{\partial x_1} = 1 + x_1\frac{\partial \ln \phi_1}{\partial x_1}$ use the analytic expressions provided in the paper by Tuan et a;[5] we have also confirmed the validity of these expressions by comparison with calculations using numerical derivatives, programmed in MathCad 15.[1] The small composition dependence of compressibility factor, $Z$, results in a corresponding, small, composition dependence of the Maxwell-Stefan diffusivity, $Đ_{12}$ on $x_1$; see Figure 1c.

The Fick diffusivity for dense gas mixtures can be estimated by multiplying the estimates of the $Đ_{12}$ using Equation (53) with the thermodynamic correction factor $\Gamma$:

$$D_{12} = Đ_{12}\Gamma; \quad \Gamma \equiv \left(1 + \frac{\partial \ln \phi_1}{\partial \ln x_1}\right) \tag{54}$$

For $CO_2(1)/C_2H_4(2)$ mixtures, the thermodynamic correction factors are practically unity, and therefore the Fick diffusivity values are indistinguishable from the M-S diffusivity, $Đ_{12}$; see Figure 1d.

Figure 2 presents calculations of combined FSG and PR EOS models for thermodynamics and diffusion in $CO_2(1)/C_2H_4(2)$ equimolar mixtures ($x_1$=0.5) with varying reduced pressures $p_r$ and reduced temperatures $T_r$. In conformity with the results presented in Figure 1b, the thermodynamic correction factor, $\Gamma \equiv \left(1 + \frac{\partial \ln \phi_1}{\partial \ln x_1}\right)$, is practically equal to unity for the entire range of pressures and temperatures; see Figure 2b. The calculations of the M-S and Fick diffusivities as functions of $p_r$ and $T_r$ are presented in Figure 2c, and Figure 2d; these values are indistinguishable from each other because the thermodynamic correction factors are virtually unity.

The compressibility factor, $Z$, on the other hand, is strongly dependent on the reduced pressures $p_r$ and reduced temperatures $T_r$; see Figure 2a. Indeed, the dependence of $Z$ on $p_r$ and $T_r$ is the predominant cause of the strong dependence of the M-S and Fick diffusivities on $p_r$ and $T_r$. The compressibility factor $Z$ is the appropriate "correction factor" for translating FSG estimations of diffusivities, valid for *low-density* gases, to binary pair diffusivities in *dense* gaseous mixtures.

A generalized chart for this "correction factor", developed using empirical fits of experimental diffusivity data, is presented in Figure 2 of the paper Takahashi[12]; this generalized chart is also recommended for use in the influential book of Reid, Prausnitz, and Poling[11] (see Figure 11.7 of Reid book). The reader will find it easy to verify that the dependence of $Z$ on $p_r$ and $T_r$ as presented in Figure 2a is practically indistinguishable from the generalized chart in Figure 2 of the Takahashi[12] paper.

For gaseous mixtures at high pressures, the experimental data of Takahashi and Hongo[13] for M-S diffusivities of $CO_2$(trace amounts)/$C_2H_4$ mixtures, and $CO_2/C_2H_4$(trace amounts) mixtures at 298.2 K, 323.2 K, and 348.2 K demonstrate quite clearly, and dramatically, that the assumption $p\,Đ_{ij}$ = constant, implicit in the FSG estimation with Equation (52), becomes increasingly poor as $p$ increases; see

Figures 3a, 3b, and 3c. The departures from the FSG Equation (52) (these calculation are shown by the dashed lines in Figures 3a,b,c), is primarily to be attributed to the departures of fluid densities from the ideal gas prescription. The experimental data of Takahashi and Hongo[13] conforms quite well with the modified prescription of equation (53); the calculations are shown by the continuous solid lines in Figures 3a, 3b, and 3c. It is noteworthy that the experimental data for $CO_2$(trace amounts)/$C_2H_4$ mixtures, and $CO_2$/$C_2H_4$(trace amounts) mixtures are not coincidental. To understand the departures from the FSG prescription, Figures 3d, 3e, and 3f present calculations of the compressibility factor, $Z$, using the Peng-Robinson Equation of State (PR EOS) at the three different temperatures. In these calculations, the mole fraction of the trace component is arbitrarily chosen as 0.005. The compressibility factors for $CO_2$(trace amounts)/$C_2H_4$ mixtures, and $CO_2$/$C_2H_4$ (trace amounts) mixtures are not the same, and this explains the differences in the corresponding diffusivity values.

Figure 4 presents MD simulation data for the Maxwell-Stefan diffusivity, $Đ_{12}$, culled from Krishna and van Baten[14], for six different equimolar binary mixtures at 300 K determined as a function of the total molar concentration $c_t$ in the simulation box. The six binary mixtures are (a) $CH_4(1)/C_2H_6(2)$, (b) $CH_4(1)/C_3H_8(2)$, (c) $CH_4(1)/N_2(2)$, (d) $CO_2(1)/CH_4(2)$, (e) $CO_2(1)/N_2(2)$, and (d) $CO_2(1)$/Ar(2). For MD simulation data, the $x$-axis is the total molar concentration, $c_t$, in the simulation box; note that this value is *not* calculated from the ideal gas law. The estimations of $Đ_{12}$ using Equation (53) are accurate up to a total molar concentration $c_t \approx 10$ kmol m$^{-3}$, corresponding to a system pressure of about 10 MPa. Put another way, the product $c_t Đ_{12}$ is constant for a given binary mixture only up to a molar density of 10 kmol m$^{-3}$. For molar densities, $c_t > 10$ kmol m$^{-3}$, the MD simulated data are significantly lower than the $Đ_{12}$ values estimated from Equation (53).

The limits of applicability of Equation (53) are emphasized further in the MD simulation data for the Maxwell-Stefan diffusivity, $Đ_{12}$, for binary $CH_4(1)/C_2H_6(2)$ mixtures at 333 K at (a) 5 MPa, (b) 10 MPa, (c) 20 MPa, (d) 30 MPa, and (e) 40 MPa and with varying compositions of methane $x_1$; see Figure 5. The continuous solid lines are the estimations of the M-S diffusivities using Equation (53). Also shown by the dashed lines are the FSG estimations, using equation (52). For system pressures below 10 MPa,

Equation (53) provides accurate estimates of $Đ_{12}$ vs $x_1$; the composition dependence of $Đ_{12}$ is entirely caused due to the variation of the compressibility factor Z with $x_1$. For system pressures exceeding 10 MPa, the MD data show a much stronger composition dependence than anticipated by the $Z$ correction introduced in Equation (53). For the purposes of this article, we refer to systems with $c_t > 10$ kmol m$^{-3}$ as "dense fluid mixtures", and use the term "dense gas mixtures" to indicate systems for which Equation (53) is of adequate accuracy.

The proper modelling of the composition and pressure dependence of $Đ_{12}$ for dense fluid mixtures are discussed in Section 5 below.

## 6. Diffusion of solutes in supercritical $CO_2$

Supercritical carbon dioxide ($CO_2$) is widely used as a solvent for extraction of trace quantities of compounds, such as lipids, and caffeine from substrates. The design of supercritical extraction processes is crucially dependent on the proper estimation of the diffusion of solutes into the supercritical gas phase.

Figures 6a presents the experimental data of Tuan et al.[5] for the dependence of the Fick diffusivity of methyl oleate (MO) (component 1) in supercritical $CO_2$ (component 2) on the mole fraction of MO for $T$ = 313.15 K at pressures of $p$ = 10.6 MPa, and $p$ = 11.5 MPa. The strong decrease in the Fick diffusivity with increasing mole fraction of MO, even to the level of $x_1 \approx 0.01$, is noteworthy. The composition dependence can be rationalized by PR EOS calculations of the compressibility factor $Z$, and the thermodynamic correction factor, $\Gamma = \left(1 + \frac{\partial \ln \phi_1}{\partial \ln x_1}\right)$; see Figures 6b,c. The compressibility factor $Z$ is virtually composition independent. However, $\Gamma$ decreases sharply with increasing $x_1$. The continuous solid line in Figure 6a,b represent calculations using Equation (54): $D_{12} = (Đ_0)\left(1 + \frac{\partial \ln \phi_1}{\partial \ln x_1}\right)Z$ with input data for the infinite dilution M-S diffusivity value (at $Z$ = 1) of $Đ_0 = 25 \times 10^{-9}$ m$^2$s$^{-1}$; there is reasonably good agreement between the combined Maxwell-Stefan-PR EOS model and the experimental data.

Higashi et al.[15] report experimental data for diffusivity of naphthalene (component 1) in supercritical ($CO_2$). Their data show significant reduction in the naphthalene diffusivity for increase in the naphthalene composition to the level of $x_1 \approx 0.01$. Their experimental observations can be rationalized by PR EOS calculations of the thermodynamic correction factor $\Gamma = \left(1 + \frac{\partial \ln \phi_1}{\partial \ln x_1}\right)$; see Figure 7. The decrease in the thermodynamic factor, $\Gamma$, is much more prominent at $p$ = 8.25 MPa that at $p$ = 10.4 MPa. The thermodynamic factor provides a rationalization of the experimental trends observed in the data reported b Higashi et al.[15]

The important message emerging from the data in Figures 6 and 7 is that the corrections due the thermodynamic factor on the values of the Fick diffusivity are significant even when the solute concentrations are at the level of $x_1 \approx 0.01$.

Figure 8a presents experimental data of Ago and Nishiumi[16] for diffusivity of benzene in supercritical $CO_2$ as a function of the reduced pressure, $p/p_c$ where $p_c$ = 7.28 MPa is the critical pressure of $CO_2$. The measurements were made in a Taylor dispersion tube with varying amounts of benzene injection into the tube, expressed in μL. We note that with increased injection of benzene, the variation of the diffusivity with the total system pressure $p$ is significantly affected. For injection of 5.7 μL and 13.1 μL of benzene, we note a sharp increase in the diffusivity at the reduced pressure, $p/p_c \approx 1$. In order to rationalize the experimental results we use PR EOS calculations of the compressibility factor $Z$, and the thermodynamic correction factor, $\Gamma = \left(1 + \frac{\partial \ln \phi_1}{\partial \ln x_1}\right)$; see Figures 8b, and 8c. These calculations have been performed at four different benzene compositions, $x_1$ = 0.005, 0.007, 0.01, and 0.013 that correspond to the four different amounts of Benzene injected in the Taylor dispersion experiments. Particularly noteworthy is the deep well in $\Gamma$ at the reduced pressure, $p/p_c \approx 1$. The depth of the well increases with increasing mole fraction of benzene in the fluid phase mixture. The calculations of the Fick diffusivity based on combining the FSG calculations with the PR EOS: $D_{ij} = \frac{8 \times 10^{-7}}{p} Z \left(1 + \frac{\partial \ln \phi_1}{\partial \ln x_1}\right)$ $\mathrm{m^2\,s^{-1}}$ where

$p$ is the pressure (expressed in bars) are shown in Figure 8d for $x_1$ = 0.005, 0.007, 0.01, and 0.013. These model calculations are able to rationalize the characteristics of the experimental diffusivities in Figure 8a; the key factor appears to be deep well in the thermodynamic factor, Γ.

Figure 9a presents an analogous set of experimental data of Nishiumi and Kubota[17] for diffusivity of benzene in supercritical $CO_2$ as a function of the reduced pressure, $p/p_c$. The deep well in the experimental Fick diffusivity at the reduced pressure, $p/p_c \approx 1$ can be rationalized by model predictions (indicated by the continuous solid lines) based on combining the FSG calculations with the PR EOS:

$$D_{ij} = \frac{8\times 10^{-7}}{p} Z\left(1+\frac{\partial \ln \phi_1}{\partial \ln x_1}\right) \quad \mathrm{m^2\,s^{-1}} \text{ for } x_1 = 0.005,\ 0.007,\ 0.01,\ 0.013, \text{ and } 0.017; \text{ see Figure 9b.}$$

## 7. Diffusion in binary fluid mixtures with $c_t$ > 10 kmol m$^{-3}$

We turn our attention to diffusion in binary mixtures for which the molar densities, $c_t$ > 10 kmol m$^{-3}$; these are normally termed as "liquid" mixtures. The M-S diffusivity of component 1, that is present in infinitely dilute concentrations in component 2, $Đ_{12}^{x_2\to 1}$, can be estimated using a number of procedures that are discussed in Reid, Prausnitz, and Poling,[11] and Taylor and Krishna.[6] The most well-known estimation method is due to Wilke and Chang:[18]

$$Đ_{12}^{x_2\to 1} = C\frac{(\psi M_2)^{1/3} T}{\eta_2 V_1^{0.6}} \tag{55}$$

In equation (55), $C$ is an empirical constant, $M_2$ is the molar mass of component 2, $\eta_2$ is the (dynamic) viscosity of component 2, $V_1$ is the molar volume of component 1 at its normal boiling temperature, $\psi$ is the *association* factor of the solvent 2. An analogous relation holds for $Đ_{12}^{x_1\to 1}$.

The composition dependence of the M-S diffusivity is then determined using the Vignes interpolation formula[14, 19]

$$Đ_{12} = \left(Đ_{12}^{x_1\to 1}\right)^{x_1}\left(Đ_{12}^{x_2\to 1}\right)^{x_2} \tag{56}$$

Leahy-Dios and Firoozabadi[20] present an empirical model for estimation of $Đ_{12}^{x_2\to 1}$,valid for $c_t$ > 10 kmol m$^{-3}$ that reduces to the FSG correlation for dilute gases in the limit of low molar densities.

The Fick diffusivity for binary liquid mixtures can be calculated by correcting the M-S diffusivity for the thermodynamic factor

$$D_{12} = \left(Đ_{12}^{x_1\to 1}\right)^{x_1}\left(Đ_{12}^{x_2\to 1}\right)^{x_2}\left(1+\frac{\partial \ln \phi_1}{\partial \ln x_1}\right) \tag{57}$$

We now highlight some characteristics of diffusion in binary mixtures that have the propensity to undergo vapor/liquid phase transitions.

As illustration, the PR EOS calculations for the compressibility factor, $Z$, and the thermodynamic correction factor, $\Gamma = \left(1+\frac{\partial \ln \phi_1}{\partial \ln x_1}\right)$ are shown in Figure 10a, and 10b for $CH_4(1)/C_3H_8(2)$ mixtures at 298.15 K and $x_1$ = 0.7; the calculations are for varying reduced pressures $p_r$ and reduced temperatures $T_r$. For stable single phase mixtures, we have the stability constraint in Equation (33). The occurrence of $\Gamma < 0$ implies vapor/liquid phase transitions. From Figure 10b, we note that there is a range of values of $p_r$ and $T_r$ for which $\Gamma < 0$. For reduced pressures $p_r$ > 2, i.e. $p$ larger than about 100 bar, the mixtures are in the liquid phase over the entire range of compositions.

Figure 11 presents calculations of the compressibility factor, $Z$, and the thermodynamic correction factor, $\Gamma = \left(1+\frac{\partial \ln \phi_1}{\partial \ln x_1}\right)$ in $CH_4(1)/C_3H_8(2)$ mixtures at $T$ = 298.15 K with varying compositions $x_1$, and total pressure, $p$. There is a range of fluid mixture compositions for which we experience phase transitions, signified by $\Gamma < 0$; see Figure 11b. For pressures $p$ larger than about 100 bar, no phase transitions are experienced and the mixtures are in the liquid phase.

The M-S diffusivities for binary mixtures in the liquid phase are composition dependent. For illustration purposes, Figures 12, 13, 14, 15, 16, and 17a present MD simulation data of Krishna and van Baten[19] for binary mixtures containing linear alkanes at 333 K and 30 MPa. For the chosen pressure and temperature, the mixtures are in the *liquid phase* for the entire range of compositions; this

can be verified for the calculations of the thermodynamic correction factor, $\Gamma = \left(1 + \frac{\partial \ln \phi_1}{\partial \ln x_1}\right)$ in $CH_4(1)/C_3H_8(2)$ mixtures that is presented in Figure 10b, and Figure 11b.

Figure 12 presents the MD simulation data of Krishna and van Baten[19] on the Maxwell-Stefan diffusivity $Đ_{ij}$ for methane(1)/ethane(2), methane(1)/n-hexane(3), and ethane(2)/n-hexane(3) binary mixtures. For the three binary mixtures methane(1)/ethane(2), methane(1)/n-hexane(3), and ethane(2)/n-hexane(3), we can determine the M-S diffusivities (units: $10^{-8}$ $m^2$ $s^{-1}$) at the limiting compositions as follows:

methane(1)/ethane(2): $Đ_{12}^{x_1 \to 1} = 5.3$; $Đ_{12}^{x_2 \to 1} = 2.58$

methane(1)/n-hexane(3): $Đ_{13}^{x_1 \to 1} = 3$; $Đ_{13}^{x_3 \to 1} = 1.05$

ethane(2)/n-hexane(3): $Đ_{23}^{x_2 \to 1} = 1.09$; $Đ_{23}^{x_3 \to 1} = 0.84$

In terms of the self-diffusivities in the binary mixtures, the limiting values of the M-S diffusivities are

$$D_{2,self}^{x_1 \to 1} = Đ_{12}^{x_1 \to 1}; \quad D_{1,self}^{x_2 \to 1} = Đ_{12}^{x_2 \to 1} \tag{58}$$

Also shown in Figure 12 are the calculations using Vignes interpolation formula (56) along with the infinite dilution M-S diffusivity values at either ends of the composition range. The interpolation formula is of good accuracy.

Figure 13 presents the MD simulation data of Krishna and van Baten[19] on $Đ_{ij}$ for the binary methane(1)/ethane(2), methane(1)/propane(3), and ethane(2)/propane (3) mixtures. The continuous solid lines are the calculations of $Đ_{ij}$ using the Vignes interpolation formula (56). The interpolation formula is of good accuracy.

Figure 14 presents MD simulation data of Krishna and van Baten[19] on $Đ_{ij}$ for the binary methane(1)/propane(2), methane(1)/n-hexane(3), and propane(2)/n-hexane (3) mixtures. The continuous solid lines are the calculations of $Đ_{ij}$ using the Vignes interpolation formula (56). The interpolation formula is of good accuracy.

Figure 15 presents MD simulation data of Krishna and van Baten[19] on $Đ_{ij}$ for the binary ethane(1)/propane(2), ethane(1)/n-butane(3), and propane(2)/n-butane (3) mixtures. The continuous solid lines are the calculations of $Đ_{ij}$ using the Vignes interpolation formula (56). The interpolation formula is of good accuracy.

Figure 16 presents MD simulation data of Krishna and van Baten[19] on $Đ_{ij}$ for the binary propane(1)/n-butane(2), propane(1)/n-pentane(3), and n-butane(2)/n-pentane (3) mixtures. The continuous solid lines are the calculations of $Đ_{ij}$ using the Vignes interpolation formula (56). The interpolation formula is of good accuracy.

Figure 17a presents MD simulation data of Krishna and van Baten[19] on $Đ_{ij}$ for the binary mixtures of methane with ethane, propane, n-butane, n-hexane, and n-decane at at 333 K and 30 MPa as function of the mole fraction of methane. The continuous solid lines are the calculations of $Đ_{ij}$ using the Vignes interpolation formula (56). The interpolation formula is of good accuracy for all five binary mixtures.

Figure 17b presents calculations of the Fick diffusivity using Equation (57), where the thermodynamic factor is calculated using the PR EOS, using the binary interaction parameters in Table 2.

At methane mole fractions, $x_1$, in the range 0.8 – 0.9, we note that the Fick diffusivity of C1-nC6, and C1-nC10 mixtures shows a pronounced minimum.

In order to test the validity of the estimations using Equation (57) and the trends of the Fick diffusivity predicted in Figure 17b, we examine published experimental data.

Firstly, let us consider thermodynamics and diffusion in $CH_4(1)/C_3H_8(2)$ mixtures at $T$ = 311 K and 206.8 bar. Figure 18a shows calculations of the thermodynamic factor, $\Gamma$, using analytic differentiation of the PR EOS. With the MD simulation data as guidelines for the limiting M-S diffusivities for $CH_4(1)/C_3H_8(2)$ mixtures, we choose: $Đ_{12}^{x_1\to 1} = 5.4$; $Đ_{12}^{x_2\to 1} = 1.8$ (units of $10^{-8}$ $m^2$ $s^{-1}$). Figure 18b compares the experimental data of Sigmund, as reported in Figure 2c of Leahy-Dios and Firoozabadi,[20] for Fick diffusivities of $CH_4(1)/C_3H_8(2)$ mixtures at $T$ = 311 K and $p$ = 206.8 bar with the estimations using Equation (57). The agreement is reasonably good.

We now examine the characteristics of diffusivities in binary liquid phase $CH_4(1)$/n-$C_{10}H_{22}(2)$ mixtures in regions close to vapor/liquid phase transitions. Figures 19a, and 19b present experimental data of Dysthe and Hafskjold[21] for Fick diffusivities of $CH_4(1)$/n-$C_{10}H_{22}(2)$ mixtures at $T$ = 303.5 K and $p$ = 40, 50 and 60 MPa. The experimental data show a deep well in the Fick diffusivities at $x_1 \approx 0.9$; the depth of the well is higher at lower pressures; these characteristics correlate with the composition dependence of the thermodynamic factor $\Gamma = \left(1 + \frac{\partial \ln \phi_1}{\partial \ln x_1}\right)$; see Figure 19c. In order to rationalize the deep well at $x_1 \approx 0.9$, we determined the compositions for which $\Gamma = \left(1 + \frac{\partial \ln \phi_1}{\partial \ln x_1}\right) = 0$; the spinodal curve obtained from PR EOS is plotted in Figure 19d.

The sharp well in the Fick diffusivity data at $x_1 \approx 0.9$ is caused by the proximity to the spinodal compositions.

Also shown in Figures 19a, and 19b are the estimations of the Fick diffusivities using Equation (57); for the purposes of the estimations we use the values $Đ_{12}^{x_1 \to 1} = 14 \times 10^{-9}$ m$^2$s$^{-1}$, and $Đ_{12}^{x_2 \to 1} = 3 \times 10^{-9}$ m$^2$s$^{-1}$ that are estimated from the Dysthe and Hafskjold[21] experimental data. Equation (57) quantitatively captures the composition variation of the Fick diffusivities at various pressures.

Figure 19e shows the experimental data of Dysthe and Hafskjold[21] for Fick diffusivities of $CH_4(1)$/n-$C_{10}H_{22}(2)$ mixtures at $T$ = 303.5 K with varying total pressures at the critical composition $x_1$= 0.903. The experimental data show that the Fick diffusivity progressively decreases in magnitude as the pressure is reduced, and $D_{12} \approx 0$ at $p \approx 36$ MPa. Equation (57) provides a reasonable description of the pressure dependence.

# 8. Estimation of Fick diffusivity matrix in ternary liquid mixtures

Equation (29) allows the estimation of the elements of the Fick diffusivity matrix $[D]$, obtained as a product of the matrix $[\Lambda]$ and the matrix of thermodynamic factors $[\Gamma]$. Each of these matrices $[\Lambda]$ and $[\Gamma]$ have non-zero off-diagonal elements, and therefore the product of the two matrices, $[D] = [\Lambda][\Gamma]$ is

strongly coupled. Differentiation of the PR EOS, allow the calculation of the $\Gamma_{ij} = \delta_{ij} + x_i \dfrac{\partial \ln \phi_i}{\partial x_j}; \quad i, j = 1,2$.

For the ternary mixture $nC_{12}H_{26}(1)/nC_{16}H_{34}(2)/n\text{-}C_6H_{14}$ (3) at the composition $x_1 = 0.35$, $x_2 = 0.317$, $x_3 = 0.333$ at 298.15 K, Kett and Anderson[22] report experimental data on the Fick diffusivity matrix: $[D] = \begin{bmatrix} 0.969 & 0.266 \\ 0.225 & 1.031 \end{bmatrix} \times 10^{-9}$ m$^2$s$^{-1}$. The estimations of the matrix of thermodynamic factors using the PR EOS, yields $[\Gamma] = \begin{bmatrix} 0.7 & -0.026 \\ 0.137 & 1.03 \end{bmatrix}$, suggesting that off-diagonal elements of $[D]$ are strongly influenced by thermodynamic coupling.

For the ternary mixture of $nC_8H_{18}(1)/nC_{10}H_{22}(2)$/1-methylnapthalene(3) at a liquid mixture composition with mass fractions $\omega_1 = 0.3333$, $\omega_2 = 0.3333$, $\omega_3 = 0.3333$ at 295.65 K, Leahy-Dios et al.[23] report experimental data on the Fick diffusivity matrix in the mass average reference velocity frame: $[D^{mass}] = \begin{bmatrix} 1.99 & -0.93 \\ -0.42 & 2.4 \end{bmatrix} \times 10^{-9}$ m$^2$s$^{-1}$; the large magnitudes of the off-diagonal elements are particular noteworthy. The corresponding mole fractions of the three components are $x_1 = 0.384$, $x_2 = 0.308$, $x_3 = 0.308$. We use the molar average reference velocity frame consistently in this article, and therefore we need to transform the values $[D^{mass}]$; the transformation formula are provided in Section 3.2.4 of Taylor and Krishna;[6] see Figure 20.

On transformation, we obtain the matrix of Fick diffusivities in the molar average reference velocity frame $[D] = \begin{bmatrix} 1.92 & -1.07 \\ -0.333 & 2.47 \end{bmatrix} \times 10^{-9}$ m$^2$s$^{-1}$.

The estimations of the matrix of thermodynamic factors at this composition using the PR EOS, yields $[\Gamma] = \begin{bmatrix} 0.486 & -0.305 \\ -0.068 & 0.9 \end{bmatrix}$, suggesting that off-diagonal elements of $[D]$ emanate primarily because of the strong thermodynamic coupling.

The MD simulation data of Krishna and van Baten[19] for self-diffusivities of nC8 and nC10 are close to one another $\approx 3.4\times10^{-9}$ $m^2s^{-1}$ (see Table 1). Multiplication of $[\Gamma]$, with this scalar diffusivity yields $[D]=\begin{bmatrix} 1.65 & -1.03 \\ -0.23 & 3.06 \end{bmatrix}\times10^{-9}$ $m^2s^{-1}$, that is close to the experimentally determined values. We conclude that thermodynamic coupling is the major source of diffusional coupling in mixtures of liquid hydrocarbons.

To understand the reason for the strong thermodynamic coupling, we note that the melting points of $nC_8H_{18}$(1), $nC_{10}H_{22}$(2), and 1MN(3) are 216 K, 243 K, and 251 K, respectively. On cooling, crystals of 1MN will be first to come out of solution and the 1MN can be separated from linear alkanes by fractional crystallization. To demonstrate the possibility of phase separation, Figure 21 presents calculations for the determinant $|\Gamma|$ for the ternary mixture of $nC_8H_{18}$(1)/$nC_{10}H_{22}$(2)/1-methylnapthalene(3) as a function of the composition of 1MN, $x_3$, keeping the ratio $x_1/x_2$ at a constant value of unity. The calculations are presented for three different temperatures $T$ = 295.65 K, 240 K, and 200 K. We note that at the lowest temperature, $T$ = 200 K, there is a range of compositions for which $|\Gamma| < 0$, indicating phase instability and crystal formation. Thermodynamic coupling is strong in the $nC_8H_{18}$(1)/$nC_{10}H_{22}$(2)/1-methylnapthalene(3) because of the proximity to liquid/solid phase transition temperature.

For estimation of the elements of $[\Lambda]$, Krishna and van Baten[19] has suggested the following extension of the Vignes interpolation formula (56):

$$Đ_{ij} = \left(Đ_{ij}^{x_i\to1}\right)^{x_i}\left(Đ_{ij}^{x_j\to1}\right)^{x_j}\left(Đ_{ij}^{x_k\to1}\right)^{x_k} \tag{59}$$

For the estimation of $Đ_{ij}^{x_k\to1}$, the $i$ - $j$ pair diffusivity when both $i$ and $j$ are present in infinitely dilute concentration, Krishna and van Baten[19] suggest

$$
\begin{aligned}
Đ_{12}^{x_3\to 1} &= \left(Đ_{13}^{x_3\to 1}\right)^{x_1/(x_1+x_2)}\left(Đ_{23}^{x_3\to 1}\right)^{x_2/(x_1+x_2)}\\
Đ_{13}^{x_2\to 1} &= \left(Đ_{12}^{x_2\to 1}\right)^{x_1/(x_1+x_3)}\left(Đ_{23}^{x_2\to 1}\right)^{x_3/(x_1+x_3)}\\
Đ_{23}^{x_1\to 1} &= \left(Đ_{12}^{x_1\to 1}\right)^{x_2/(x_2+x_3)}\left(Đ_{13}^{x_1\to 1}\right)^{x_3/(x_2+x_3)}
\end{aligned}
\tag{60}
$$

For the special case of an equimolar mixture we obtain

$$
\begin{aligned}
Đ_{12}^{x_3\to 1} &= \sqrt{\left(Đ_{13}^{x_3\to 1}Đ_{23}^{x_3\to 1}\right)}\\
Đ_{13}^{x_2\to 1} &= \sqrt{\left(Đ_{12}^{x_2\to 1}Đ_{23}^{x_2\to 1}\right)}\\
Đ_{23}^{x_3\to 1} &= \sqrt{\left(Đ_{12}^{x_1\to 1}Đ_{13}^{x_1\to 1}\right)}
\end{aligned}
\tag{61}
$$

The simplified interpolation formula (61) was proposed by Wesselingh and Bollen.[24]

Krishna and van Baten[19] and Krishna[25] provide detailed validation of the interpolation formula (59) by comparison with MD simulations of a wide variety of ternary mixtures consisting of n-alkanes. For illustration, in Figure 22 we present the MD data for $|\Lambda|^{1/2}$ for three different ternary mixtures:

methane(1)/ethane(2)/n-hexane(3)

methane(1)/ethane(2)/propane(3)

methane(1)/propane (2)/n-hexane(3)

The open circles in Figure 22 represent calculations using Equations (31), (59), and (61).There is good agreement between the two sets.

Consider liquid phase diffusion in the ternary methane(1)/propane(2)/n-hexane (3) mixture at 333 K and 8.5 MPa. In ternary composition space, there is a region in which we have V/L phase splitting. This region is indicated in Figure 23. The compositions of the vapor and liquid phases in equilibrium with each other are indicated by the tie-lines. The region to the left of the two-phase region consists of the liquid phase region.

Thermodynamic coupling effects become increasingly significant as the liquid phase compositions approach the phase transition region. In order to demonstrate this, we performed calculations for the determinant $|\Gamma|$ as a function of the composition of n-hexane, $x_3$, keeping the ratio $x_1/x_2$ at a constant value of unity; see inset to Figure 23. At the pure hexane vertex, $x_3 = 1$, $|\Gamma| = 1$. As $x_3$ decreases in

value and the two-phase region is approach, the magnitude of $|\Gamma|$ progressively decreases. The condition $|\Gamma| = 0$ signifies the limit of phase stability; at this point we must have $\Gamma_{11}\Gamma_{22} = \Gamma_{12}\Gamma_{21}$, i.e the product of the off-diagonal elements is equal in magnitude to the product of the diagonal elements. This situation implies a significant degree of thermodynamic coupling. A large degree of thermodynamic coupling has a significant influence of the diffusion equilibration trajectory when operating close to the two-phase region.

# 9. Influence of diffusional coupling effects on transient equilibration trajectories

We shall demonstrate the strong influence of the off-diagonal elements of the matrix of thermodynamic factors $[\Gamma]$ on the transient diffusion equilibration in the ternary liquid phase of the methane(1)/propane(2)/n-hexane (3) mixture at 333 K and 8.5 MPa. At time $t$ = 0, a liquid slab of composition $x_{10}$ = 0.05, $x_{20}$ = 0.55, $x_{30}$ = 0.4 is exposed to a vapor phase mixture of composition $y_1$ = 0.659033, $y_2$ = 0.318393, $y_3$ = 0.022574; see schematic in Figure 24. The vapor composition is held constant for the duration of the transient equilibration process in the liquid of half-thickness $\delta$ (= 1 mm). The liquid slab is considered to be of "infinite" length in the vertical direction and the diffusion is limited to the transverse ($z$) direction.

The composition of the liquid phase in equilibrium with the vapor phase is $x_{1\delta}$ = 0.333532, $x_{2\delta}$ = 0.521103, $x_{3\delta}$ = 0.145365.

For a binary liquid mixture, the fractional *unaccomplished change* is given by[26]

$$\bar{x}(t) - x_{z=\delta} = Q\left(x_0 - x_{z=\delta}\right); \quad Q \equiv \sum_{m=0}^{\infty} \frac{8}{(2m+1)^2 \pi^2} \exp\left[-(2m+1)^2 \pi^2 \frac{Dt}{4\delta^2}\right] \tag{62}$$

The $\bar{x}(t)$ is the spatial-averaged composition in the slab at time $t$.

This expression can be generalized for ternary liquid mixtures by using two-dimensional matrix notation by replacing the binary mixture diffusivity $D$ by the Fick matrix $[D]$; the justification for this procedure is provided in earlier works.[6, 27, 28]

The expression for fractional *unaccomplished change* for ternary liquid mixtures is written using two-dimensional matrix notation as

$$\left(\overline{x}(t) - x_{z=\delta}\right) = [Q]\left(x_0 - x_{z=\delta}\right); \quad [Q] \equiv \sum_{m=0}^{\infty} \frac{8}{(2m+1)^2 \pi^2} \exp\left[ -(2m+1)^2 \pi^2 \frac{[D]t}{4\delta^2} \right] \tag{63}$$

The Sylvester theorem, detailed in Appendix A of Taylor and Krishna,[6] is required for explicit calculation of $[Q]$. For the case of distinct eigenvalues, $\lambda_1$ and $\lambda_2$ of the 2-dimensional square matrix $[D]$, the Sylvester theorem yields

$$[Q] = \frac{f(\lambda_1)[[D] - \lambda_2 [I]]}{(\lambda_1 - \lambda_2)} + \frac{f(\lambda_2)[[D] - \lambda_1 [I]]}{(\lambda_2 - \lambda_1)} \tag{64}$$

In equation (64), $[I]$ is the identity matrix with elements $\delta_{ik}$. The functions $f(\lambda_i)$ are obtained by substituting the eigenvalues $\lambda_1$ and $\lambda_2$ in place of the binary diffusivity in equation (62):

$$f(\lambda_i) = \sum_{m=0}^{\infty} \frac{8}{(2m+1)^2 \pi^2} \exp\left[ -(2m+1)^2 \pi^2 \frac{\lambda_i t}{4\delta^2} \right] \tag{65}$$

The calculations are implemented in MathCad 15.[1] In the MathCad implementation, the matrix $[D]$ is evaluated at the average between the initial compositions $x_{10}$ = 0.05, $x_{20}$ = 0.55, $x_{30}$ = 0.4 and the final equilibrated composition $x_{1\delta}$ = 0.333532, $x_{2\delta}$ = 0.521103, $x_{3\delta}$ = 0.145365. The matrix $[D]$ is assumed to be constant during the equilibration process.

Figure 25a presents the calculation results of the transient equilibration for liquid phase diffusion in methane(1)/propane(2)/n-hexane (3) mixtures at 333 K and 8.5 MPa. It is noteworthy that propane (component 2) experiences an undershoot during transient equilibration. The equilibration trajectory follows a curvilinear path in composition space; see Figure 25b. Transient overshoots/undershoots, and curvilinear equilibration trajectories are characteristic signatures of uphill diffusion.[25, 28-31]

The fractional approaches to equilibrium, also termed as the Murphree efficiencies,[32-36] are calculated from

$$E_1 = \frac{x_{10} - x_1}{x_{10} - x_{1\delta}} = 1 - Q_{11} - Q_{12}\frac{x_{20} - x_{2\delta}}{x_{10} - x_{1\delta}};$$
$$E_2 = \frac{x_{20} - x_2}{x_{20} - x_{2\delta}} = 1 - Q_{22} - Q_{21}\frac{x_{10} - x_{1\delta}}{x_{20} - x_{2\delta}}; \qquad (66)$$
$$E_3 = \frac{x_{30} - x_3}{x_{30} - x_{3\delta}} = \frac{\frac{x_{10} - x_{1\delta}}{x_{20} - x_{2\delta}}E_1 + E_2}{\frac{x_{10} - x_{1\delta}}{x_{20} - x_{2\delta}} + 1}$$

In Figure 25c the component Murphree efficiencies are plotted as a function of the Fourier number defined as, $\frac{4|D|^{1/2}t}{\delta^2}$, wherein the value of the characteristics diffusivity is chosen as the square root of the determinant of the Fick matrix, At the averaged composition, we get $|D|^{1/2} = 5.5\times10^{-8}$ m$^2$ s$^{-1}$. We note that Murphree efficiency of propane exceeds unity during most of the equilibration time span. An important reason for this is that the driving force for propane ($x_{20}$ - $x_{2\delta}$) = (0.55 - 0.521103) = 0.029 is significantly lower than the driving forces of the partner species. Consequently, the transfer of propane is strongly coupled with the transfer fluxes of methane.

## 10. Taylor dispersion of ternary hydrocarbon liquid mixtures for laminar flow in a circular tube

A different demonstration of coupling effects in ternary hydrocarbon liquid mixtures is by consideration of Taylor dispersion in a tube. For laminar flow in a circular tube of length *L*, and radius *R* the concentration development following the Dirac $\delta$-pulse injection of a tracer of a *binary* mixture with Fick diffusivity *D* is

$$C = \frac{M}{2\pi R^2\sqrt{\pi\frac{u^2R^2}{48D}t}}\exp\left(-\frac{(L-ut)^2}{4\frac{u^2R^2}{48D}t}\right) \qquad (67)$$

In equation (67), *M* is the excess amount of component (moles) injected, above the concentration in the flowing stream at the inlet; *R* is the tube radius (not the gas constant !). The details of the derivation

are provided, for example, by Price[37] and Rutten;[38] these authors also provide details of the extension of the model to multicomponent mixtures.

Following, Rutten,[38] our Taylor dispersion calculations are for the following set of conditions:

Length of tube, $L$ = 15 m;

Cross-sectional averaged velocity in tube, $u$ = 0.01 m $s^{-1}$;

Radius of tube, $R$ = 0.265 mm

Figure 26 shows the simulation results for Taylor dispersion for liquid phase methane(1)/propane(2)/n-hexane (3) mixtures at 333 K and 8.5 MPa, using Equation (29) for the estimation of the elements of the Fick diffusivity matrix $[D]$. The liquid mixture flowing in the tube has the (cross-sectional averaged) composition $x_1$ = 0.4, $x_2$ = 0.4, $x_3$ = 0.2. At time $t$ = 0, Dirac $\delta$-pulse containing M1 = M2 = $10^{-7}$ excess amounts (arbitrary units) of components 1 and 2 are injected at the inlet. The excess concentration of methane, and propane at the exit of the tube are shown as a function of time elapsed. Due to diffusional coupling, the transient methane concentration displays double-hump characteristics. Propane, on the other hand, experiences transient undershoots.

Figure 27 shows the corresponding Taylor dispersion simulation results for (a) methane(1)/ethane(2)/n-hexane (3), (b) methane(1)/ethane(2)/propane(3), (c) propane(1)/n-butane(2)/n-pentane, and (d) methane(1)/n-hexane(2)/n-decane (3) mixtures at 333 K and 8.5 MPa, using Equation (29) for the estimation of the elements of the Fick diffusivity matrix $[D]$. Except for propane(1)/n-butane(2)/n-pentane(3) mixtures that have chain lengths close to one another, the diffusional coupling effects have a significant influence on the dispersion characteristics.

# 11. Diffusion with heterogeneous chemical reaction

For mixture diffusion with a heterogeneous reaction

$$\nu_1 \mathrm{A}_1 + \nu_2 \mathrm{A}_2 + \nu_3 \mathrm{A}_3 + .....\nu_n \mathrm{A}_n = 0 \tag{68}$$

the ratios of the fluxes $N_i$, in the laboratory fixed reference velocity frame, are determined by the reaction stoichiometry and so

$$\frac{N_1}{\nu_1} = \frac{N_2}{\nu_2} = \frac{N_3}{\nu_3} = .... = \frac{N_n}{\nu_n} \tag{69}$$

For ammonia synthesis reaction $N_2 + 3H_2 \rightarrow 2NH_3$, for example, we have the constraint $\frac{N_1}{1} = \frac{N_2}{3} = \frac{N_3}{-2}$. In such cases, it is convenient to re-write the Maxwell-Stefan diffusion formulation (8) in a different manner by defining effective diffusivities, $D_{i,eff}$ for each component *i* as follows

$$N_i = -c_t D_{i,eff}\left(\frac{x_i}{RT}\frac{d\mu_i}{dz}\right); \quad i = 1,2,\ldots n \tag{70}$$

Equation (8) allows us to obtain an explicit expression for the effective diffusivity

$$\frac{1}{D_{i,eff}} = \sum_{\substack{j=1 \\ j\neq i}}^{n} \frac{x_j}{Đ_{ij}}\left(1 - \frac{x_i N_j}{x_j N_i}\right) = \sum_{\substack{j=1 \\ j\neq i}}^{n} \frac{x_j}{Đ_{ij}}\left(1 - \frac{x_i \nu_j}{x_j \nu_i}\right); \quad i = 1,2,\ldots n \tag{71}$$

For dense gas mixtures, with $c_t < 10$ kmol m$^{-3}$, the M-S pair diffusivities can be estimated from the FSG equation, and subsequently applying the *Z*-correction using Equation (53).

The ammonia synthesis reactor operates at pressures ranging to a few hundred bars, and fugacity coefficient corrections are important.[39] To demonstrate this, Figure 28a shows the calculation of the compressibility factor, *Z*, and the determinant $|\Gamma|$ in the gaseous mixture $N_2/H_2/NH_3$ at a temperature of 500 K and total pressure of 25 MPa. In these calculations, the ratio of the compositions $x_2/x_1 = 3$. Both *Z*, and $|\Gamma|$ show significant deviations from unity demonstrating the non-ideal gas behaviour and the importance of fugacity coefficient corrections. Figure 28b presents calculations of the effective diffusivities in the gaseous mixture $N_2/H_2/NH_3$ using Equation (71); in these calculations, the M-S pair diffusivities are calculated using Equation (53). Interestingly, we note that the effective diffusivity of $N_2$ is practically the same as that of $NH_3$.

It must be remarked here that the Wilke formula[40]

$$D_{i,eff} = (1 - x_i) / \sum_{\substack{k=1 \\ k\neq i}}^{n} (x_k / Đ_{ik}) \tag{72}$$

is often used to calculate the effective diffusivity of component *i* in a multicomponent mixture, even though its general validity is restricted to the situation wherein the species *i* diffuses in a mixture of stagnant, non-transferring, species, i.e. when $N_j$ $(j \neq i)$ = 0. For example, Dyson and Simon[39] use equation (72) in effectiveness factor calculations for ammonia synthesis. A cautionary note against the use of equation (72) to describe diffusion in the ammonia synthesis process has been flagged.[41]

We illustrate the effective diffusivity approach using Equation (71) by considering: chemical vapor deposition (CVD). Consider the specific example of the CVD process for deposition of tungsten, by surface reaction on a wafer

$$WF_6 + 3H_2 \rightarrow W_{(s)} + 6HF \tag{73}$$

The gas phase mixture consists of four species $WF_6$, $H_2$, HF, along with inert gas Ar. The molar masses of the four species are, respectively: 297.83, 2, 20, and 40 kg mol$^{-1}$. For example, in a tungsten CVD reactor with the species $WF_6$ (1), $H_2$ (2), HF (3) and inert Ar (4), the flux ratios are $\nu_2/\nu_1 = 3$; $\nu_3/\nu_1 = -6$; $\nu_4/\nu_1 = 0$. Calculations of the effective diffusivities according to eq. (70) are illustrated in Figure **29** for conditions in which the ratio of the compositions $x_2/x_1 = 3$, and the composition of Ar is held constant at $x_4 = 0.3$. At the chosen temperature (673 K) and pressure conditions (100 Pa), use of the Peng-Robinson equation of state reveals that ideal gas behavior prevails despite the presence of the "heavy" $WF_6$. The effective diffusivity of $H_2$ is about an order of magnitude higher than that of $WF_6$. Also noteworthy is that the effective diffusivities are practically composition independent. The large differences in the effective diffusivities of $WF_6$ (1), $H_2$ (2), HF (3) have a significant influence on the composition profiles in the effective diffusion layer between the bulk gas phase and the surface of the wafer. We take the opportunity to note that the effective diffusivity calculations presented in earlier work [8] are erroneous.

In order to demonstrate this, let us consider transient diffusion equilibration of two compartments containing of gaseous mixtures of two different compositions. The left compartment, taken to be representative of the bulk gas mixture in a CVD reactor, has the initial composition $x_{1,L} = 0.2$; $x_{2,L} = 0.4$,

$x_{3,L} = 0.1$, $x_{4,L} = 0.3$. The right compartment has the initial compositions $x_{1,R} = 0.02$, $x_{2,R} = 0.1$, $x_{3,R} = 0.6$, $x_{4,R} = 0.28$; these are representative of the gaseous compositions at the gas/wafer interface.

The transient equilibration process is described by

$$x_i(t) = \frac{1}{2}\left(x_{i,L} + x_{i,R}\right) + \frac{1}{2} erf\left[-\frac{z}{\sqrt{4D_{i,eff}t}}\right]\left(x_{i,R} - x_{i,L}\right) \tag{74}$$

In equation (74), the effective diffusivities are evaluated at the average composition $x_{1,eq} = 0.11$, $x_{2,eq} = 0.25$, $x_{3,eq} = 0.35$, $x_{4,eq} = 0.29$, and assumed to be composition independent.

Figure 30a show the composition trajectories followed during equilibration plotted as a function of the dimensionless distance coordinate $\frac{z}{\sqrt{4D_{ref}t}}$ where the reference diffusivity value $D_{ref} = 1 \quad \mathrm{m^2\ s^{-1}}$. In ternary composition space, the equilibration trajectory follows a serpentine diffusion path; see Figure 30b. If each of the diffusivities of the transferring components were assumed to be identical, and equal to $D_{ref} = 1 \quad \mathrm{m^2\ s^{-1}}$, the equilibration path is linear, as indicated by the dashed line in Figure 30b.

Implicit in the results present in Figure 30 is the fluxes of each component is "coupled" to the driving forces of the partner species in the mixtures; such coupling effects have an influence on the predictions of the deposition rates in CVD reactors.[42]

## 12. Analysis of ultracenfrifugation

Equation (45) is the appropriate starting point for the analysis of separations in an ultracentrifuge.

The centrifugal force exerted per kg of component *i* in a multicomponent mixture is $\tilde{F}_i = \Omega^2 r$ where *r* is the distance from the axis of rotation, and $\Omega$ is the angular velocity: $\Omega = 2\pi(\text{rotational speed expressed in revolutions per second})$. Equation (45) yields

$$d_i \equiv \frac{x_i}{RT}\frac{d\mu_i}{dr} + \frac{1}{c_t RT}\left(c_i \overline{V_i} - \omega_i\right)\frac{dp}{dr} - \frac{\rho_i}{c_t RT}\left(\Omega^2 r - \Omega^2 r\right) = \frac{x_i}{RT}\frac{d\mu_i}{dr} + \frac{1}{c_t RT}\left(c_i \overline{V_i} - \omega_i\right)\frac{dp}{dr} \tag{75}$$

Mechanical equilibrium is established quickly in relation to thermodynamic equilibrium in an ultracentrifuge. At mechanical equilibrium we have

$$\frac{dp}{dr} = \rho_t \sum_{i=1}^{n} \omega_i \tilde{F}_i = \rho_t \Omega^2 r \tag{76}$$

Substituting in equation (75) results in

$$d_i = \frac{x_i}{RT}\frac{d\mu_i}{dr} + \frac{1}{c_t RT}\left(c_i \overline{V_i} - \omega_i\right)\rho_t \Omega^2 r \tag{77}$$

At thermodynamic equilibrium, the driving forces vanish and therefore the composition distribution is described by

$$\frac{x_i}{RT}\frac{d\mu_i}{dr} = -\frac{1}{c_t RT}\left(c_i \overline{V_i} - \omega_i\right)\rho_t \Omega^2 r \tag{78}$$

The ultracentrifuge induces a separation provided that the volume fraction $c_i \overline{V_i}$ is different from the mass fraction $\omega_i$. As illustration, consider the separation of the gaseous isotopes $U^{235}F_6(1)/U^{238}F_6(2)$ at 293.15 K as described in Example 2.3.2 of Taylor and Krishna;[6] see Figure 31.The molar masses are $M_1$=0.34915 kg mol$^{-1}$; $M_2$=0.35215 kg mol$^{-1}$. The centrifuge rotates at 40000 rpm. The separation takes place within the annular space between $r = r_0 = 10$ mm and $r = r_1 = 60$ mm. The mole fraction distribution of component 1 within the annular space as a function of the radial distance *r* is

$$\frac{x_{r=r}}{1-x_{r=r}}\frac{1-x_{r=r0}}{x_{r=r0}} = \exp\left[\left(M_1 - M_2\right)\frac{\Omega^2\left(r^2 - r_0^2\right)}{2RT}\right] \tag{79}$$

The composition profiles within the annular space are shown in Figure 31; the heavier isotope concentrates near the periphery. An uranium enrichment industrial facility will have a few million centrifuges to achieve the desired degree of separation.[6]

# 13. Segregation in hydrocarbon reservoirs; influence of gravity

Equation (51) is the appropriate starting point for the analysis of gravitational segregation in hydrocarbon reservoirs.[7] The analysis below essentially follows the treatment of separations in a centrifuge as described in our earlier works.[6, 8]

For gravitational segregation, the pressure gradient is

$$\frac{dp}{dz} = -\rho_t g \tag{80}$$

Setting the fluxes to zero in Equation (51), the steady-state mole fraction profiles are described by

$$\frac{x_i}{RT}\frac{d\mu_i}{dz} = \frac{1}{c_t RT}\left(c_i \overline{V_i} - \omega_i\right)\rho_t g = \frac{1}{c_t RT}\left(c_i \overline{V_i} - \frac{x_i M_i}{\overline{M}}\right)\rho_t g; \quad i = 1,2,,,n \tag{81}$$

Introducing the thermodynamic correction factors, we write the relations for the ($n$-1) independent mole fractions

$$\sum_{j=1}^{n-1} \Gamma_{ij}\frac{dx_j}{dz} = \left(\frac{\rho_t c_i}{c_t}\overline{V_i} - \frac{x_i M_i}{\overline{M}}\frac{\rho_t}{c_t}\right)\frac{g}{RT} = \left(\rho_t \overline{V_i} - M_i\right)\frac{x_i g}{RT}; \quad i = 1,2,,n-1 \tag{82}$$

in which we have used the equality, $\rho_t = c_t \overline{M}$. The partial molar volume $\overline{V_i}$ can be determined from the PR EOS, by analytic differentiation of the expression for the molar volume of the mixture, $\overline{V} = \overline{V_1} + \overline{V_2} = \frac{ZRT}{p}$. The explicit formulae are $\overline{V_1} = \frac{RT}{p}\left[Z + \left(1 - x_1\right)\frac{\partial Z}{\partial x_1}\right]$ and $\overline{V_2} = \frac{RT}{p}\left[Z + \left(1 - x_2\right)\frac{\partial Z}{\partial x_2}\right] = \frac{RT}{p}\left[Z - x_1\frac{\partial Z}{\partial x_1}\right]$. The total molar concentration of the mixture, $c_t = \frac{p}{ZRT}$. The mixture mass density is determined from $\rho_t = c_t \overline{M}$.

The "driving force" for gravitational segregation is essentially the difference between the volume fraction and the mass fraction. To illustrate these differences, Figure 32a presents PR EOS calculations of the volume fractions and mass fractions as a function of the binary mixture $C_2H_6$/$nC_{10}H_{22}$ at a pressure $p$ = 20 MPa and temperature $T$ = 440 K. There is a large difference between the volume

fraction and the mass fraction of either component, and this leads to segregation. Figure 32b presents calculations of the partial molar volumes of ethane and n-decane, along with molar volume of mixture. Figure 32c show the variation of the compressibility factor, Z, and thermodynamic factor, Γ, with mole fraction of ethane. Both *Z*-corrections and Γ-corrections are of significance.

For thermodynamically ideal mixtures, equation (82) reduces to yield

$$\frac{dx_i}{dz} = \left(\rho_t \overline{V_i} - M_i\right)\frac{x_i g}{RT}; \quad i = 1,2,,n-1 \tag{83}$$

Equation (83) can be solved analytically to yield the composition profiles

$$x_i(z) = \exp\left[\left(\rho_t \overline{V_i} - M_i\right)\frac{g}{RT} z\right]; \quad i = 1,2,,n-1 \tag{84}$$

For a binary mixture, including thermodynamic non-idealities, equation (82) simplifies to yield

$$\frac{dx_1}{dz} = \frac{1}{\Gamma}\left(\rho_t \overline{V_1} - M_1\right)\frac{x_1 g}{RT} \tag{85}$$

As illustration, we consider gravitational segregation for the binary mixture $C_2H_6/nC_{10}H_{22}$ in a reservoir of 600 m depth at a pressure $p$ = 20 MPa and temperature $T$ = 440 K. The mixture composition at depth z = 300 m from the surface ($z$ = 600 m) is $x_1$ = 0.5, $x_2$ = 0.5. The composition distribution along the reservoir depth is shown in Figure 33. The continuous solid lines are calculations using Γ correction. The dashed lines are calculations that ignore Γ corrections. The thermodynamic correction factors cannot be ignored. The profiles show a higher concentration of the lighter ethane at the top, whereas the heavier $nC_{10}H_{22}$ hydrocarbon concentrates at the well bottom.

Figure 34 presents the solutions to equation (82) for gravitational segregation for the ternary mixture $CH_4/nC_4H_{10}/nC_{12}H_{26}$ in a reservoir of 600 m depth at a pressure $p$ = 35 MPa and temperature $T$ = 333.15 K. The mixture composition at depth z = 300 m from the surface (z = 0) is $x_1$ = 0.2, $x_2$ = 0.4, $x_3$ = 0.4. The binary interaction parameters in PR EOS, are $k_{12}$ = 0.019, $k_{13}$ = 0.008, and $k_{23}$ = 0.0. Both the lightest component (methane), and the heaviest component (nC12) experience significant segregation.

The lighter $CH_4$ concentrates at the top layers, and nC12 concentrates in the bottom layers. Our results are in agreement with the MD simulations of Touzet et al.[43]

## 14. Segregation in hydrocarbon reservoirs; influence of both gravity and thermal diffusion

The Soret effect, also called thermal diffusion, is the tendency of a mixture of two or more components to separate due to a temperature gradient. In 1879 Charles Soret discovered that a salt solution contained in a tube with the two ends at different temperatures did not remain uniform in composition; the salt was more concentrated near the cold end than near the hot end of the tube; for a review of the history and applications see Platten.[44] In hydrocarbon reservoirs, the temperature gradient $\frac{dT}{dz} \approx -0.03$ K m$^{-1}$;[43] i.e. the temperature increases along the reservoir depth. Segregation is also induced due to thermal diffusion. The M-S equations can be extended to account for thermal diffusion in the following manner[3]

$$-d_i = -\frac{x_i}{RT}\frac{d\mu_i}{dz} - \frac{1}{c_t RT}\left(c_i \overline{V}_i - \omega_i\right)\frac{dp}{dz} - \sum_{\substack{j=1 \\ j\neq i}}^{n} \frac{x_i x_j}{Đ_{ij}}\left(\frac{D_i^T}{\rho_i} - \frac{D_j^T}{\rho_j}\right)\frac{1}{T}\frac{dT}{dz} = \sum_{\substack{j=1 \\ j\neq i}}^{n} \frac{x_i x_j \left(u_i - u_j\right)}{Đ_{ij}} \tag{86}$$

The thermal diffusion coefficients $D_i^T$ have the units of kg m$^{-1}$ s$^{-1}$. The terms $\frac{D_i^T}{\rho_i}$ have the units of m$^2$ s$^{-1}$. The thermal diffusion coefficients are not all independent; we have the constraint

$$\sum_{j=1}^{n} D_i^T = 0 \tag{87}$$

For the special case of a binary mixture, we write

$$-d_1 = -\frac{x_1}{RT}\frac{d\mu_1}{dz} - \frac{1}{c_t RT}\left(c_1 \overline{V}_1 - \omega_1\right)\frac{dp}{dz} - \frac{x_1 x_2}{Đ_{12}}\left(\frac{D_1^T}{\rho_1} - \frac{D_2^T}{\rho_2}\right)\frac{1}{T}\frac{dT}{dz} = \frac{x_1 x_2 \left(u_1 - u_2\right)}{Đ_{12}} \tag{88}$$

Introducing the constraint $D_1^T = -D_2^T$, we obtain

$$-d_1-\frac{x_1x_2D_1^T}{Đ_{12}}\left(\frac{\rho_t}{\rho_1\rho_2}\right)\frac{1}{T}\frac{dT}{dz}=\frac{x_1x_2(u_1-u_2)}{Đ_{12}} \tag{89}$$

Equation (89) may be re-written as

$$-d_1-\frac{x_1x_2D_1^T}{Đ_{12}}\left(\frac{\rho_t}{\rho_1\rho_2}\right)\frac{1}{T}\frac{dT}{dz}=\frac{(x_2c_1u_1-x_1c_2u_2)}{c_tĐ_{12}} \tag{90}$$

Introducing the diffusion fluxes

$$J_1=c_tx_1(u_1-u) \tag{91}$$

we derive

$$-d_1-\frac{x_1x_2D_1^T}{Đ_{12}}\left(\frac{\rho_t}{\rho_1\rho_2}\right)\frac{1}{T}\frac{dT}{dz}=\frac{(x_2J_1-x_1J_2)}{c_tĐ_{12}} \tag{92}$$

Since, the diffusion fluxes sum to zero, $-J_1=J_2$, we get

$$-d_1-\frac{x_1x_2D_1^T}{Đ_{12}}\left(\frac{\rho_t}{\rho_1\rho_2}\right)\frac{1}{T}\frac{dT}{dz}=\frac{J_1}{c_tĐ_{12}} \tag{93}$$

Define the thermal diffusion ratio

$$k_{T1}=\frac{x_1x_2D_1^T}{Đ_{12}}\left(\frac{\rho_t}{\rho_1\rho_2}\right)=\frac{D_1^T}{\rho_tĐ_{12}}\left(\frac{x_1x_2}{\omega_1\omega_2}\right) \tag{94}$$

The thermal diffusion ratio $k_{T1}$ is dimensionless.

Other quantities encountered are the thermal diffusion factor $\alpha_T$

$$\alpha_{T1}=\frac{k_{T1}}{x_1x_2}=\frac{D_1^T}{\rho_tĐ_{12}}\left(\frac{1}{\omega_1\omega_2}\right)=\frac{D_1^T}{Đ_{12}}\left(\frac{\rho_t}{\rho_1\rho_2}\right) \tag{95}$$

The Soret coefficient is defined as

$$S_{T1}=\frac{k_{T1}}{x_1x_2T}=\frac{D_1^T}{\rho_tĐ_{12}T}\left(\frac{1}{\omega_1\omega_2}\right)=\frac{D_1^T}{Đ_{12}T}\left(\frac{\rho_t}{\rho_1\rho_2}\right) \tag{96}$$

Equation (93) reduces to yield

$$-d_1 = \frac{J_1}{c_t Đ_{12}} + k_{T1}\frac{1}{T}\frac{dT}{dz}; \quad J_1 = -c_t Đ_{12}\left(d_1 + k_{T1}\frac{1}{T}\frac{dT}{dz}\right) \tag{97}$$

For segregation due to gravity, and thermal diffusion the flux expression is therefore

$$J_1 = -c_t Đ_{12}\left(\frac{x_1}{RT}\frac{d\mu_1}{dz} - \frac{1}{c_t RT}\left(c_1\overline{V_1} - \omega_1\right)\rho g + k_{T1}\frac{1}{T}\frac{dT}{dz}\right) \tag{98}$$

Setting the fluxes equal to zero, the steady-state the steady-state mole fraction profiles are described by

$$\frac{x_1}{RT}\frac{d\mu_1}{dz} = \frac{1}{c_t RT}\left(c_1\overline{V_1} - \omega_1\right)\rho g - k_{T1}\frac{1}{T}\frac{dT}{dz} \tag{99}$$

Introducing the thermodynamic correction factor $\Gamma \equiv \left(1 + \frac{\partial \ln \phi_1}{\partial \ln x_1}\right)$ we write the steady-state mole fraction profile as

$$\Gamma\frac{dx_1}{dz} = \left(\rho_t\overline{V_1} - M_1\right)\frac{x_1 g}{RT} - k_{T1}\frac{1}{T}\frac{dT}{dz} \tag{100}$$

Let us examine the influence of thermal diffusion for situations in which gravitational segregation effects are negligible. When $D_1^T > 0; \quad S_{T1} > 0; \quad k_{T1} > 0; \quad \frac{dx_1}{dT} < 0$; this implies that the component 1 segregates towards the cold end; in this scenario, thermal diffusion serves to enhance the gravitational segregation effect. Conversely, when $D_1^T < 0; \quad S_{T1} < 0; \quad k_{T1} < 0; \quad \frac{dx_1}{dT} > 0$, the component 1 segregates towards the hot end; in this scenario, thermal diffusion acts in a direction opposite to the gravitational segregation.

To illustrate the relative influences of gravity, and thermal diffusion on segregation in petroleum reservoirs, we revisit the segregation for the binary mixture $C_2H_6/nC_{10}H_{22}$ in a reservoir of 600 m depth at a pressure $p$ = 20 MPa and temperature $T$ = 440 K. The mixture composition at depth z = 300 m from the surface ($z$ = 600 m) is $x_1$ = 0.5, $x_2$ = 0.5. The composition distribution along the reservoir depth is

shown in Figure 35 for three different scenarios. Figure 35a shows segregation due to gravity effects alone; here we solve $\Gamma \frac{dx_1}{dz} = \left(\rho_t \overline{V_1} - M_1\right)\frac{x_1 g}{RT}$. Figure 35b shows segregation due to thermal diffusion effects alone; here we solve $\Gamma \frac{dx_1}{dz} = -k_{T1}\frac{1}{T}\frac{dT}{dz}$, taking $\alpha_{T1} = \frac{k_{T1}}{x_1 x_2} = -2$. Figure 35c shows segregation due to combined effects of gravity and thermal diffusion; here we solve $\Gamma \frac{dx_1}{dz} = \left(\rho_t \overline{V_1} - M_1\right)\frac{x_1 g}{RT} - k_{T1}\frac{1}{T}\frac{dT}{dz}$, taking $\alpha_{T1} = \frac{k_{T1}}{x_1 x_2} = -2$.

## 15. Notation

| | |
|---|---|
| $a_i$ | activity of species *i*, dimensionless |
| $[B]$ | matrix defined by Equations (19), $m^{-2}$ s |
| $c_i$ | molar concentration of species *i*, mol $m^{-3}$ |
| $c_t$ | total molar concentration of mixture, mol $m^{-3}$ |
| $d_i$ | generalized driving force, $m^{-1}$ |
| $Đ_{ij}$ | M-S diffusivity for binary pair *i*-*j*, $m^2$ $s^{-1}$ |
| $D_{12}$ | Fick diffusivity for binary mixture, $m^2$ $s^{-1}$ |
| $D_{i,eff}$ | effective diffusivity in mixture, $m^2$ $s^{-1}$ |
| $[D]$ | Fick diffusivity matrix, $m^2$ $s^{-1}$ |
| $\lvert D \rvert$ | Determinant of the Fick diffusivity matrix, $m^4$ $s^{-2}$ |
| $\lvert D \rvert^{1/2}$ | Square-root of determinant of $[D]$, $m^2$ $s^{-1}$ |
| $D_i^T$ | thermal diffusion coefficients, kg $m^{-1}$ $s^{-1}$ |
| $E_i$ | Component Murphree efficiency, dimensionless |
| $f_i$ | fugacity of species *i*, Pa |
| F | Faraday constant, $9.65\times10^4$ C $mol^{-1}$ |
| $F_i$ | Body force acting per mole of species *i*, N $mol^{-1}$ |
| $\tilde{F}_i$ | Body force acting per kg of species *i*, N $kg^{-1}$ |
| Fo | Fourier number, dimensionless |
| $g$ | gravitational acceleration, 9.81 m $s^{-2}$ |
| $J_i$ | molar diffusion flux of species *i* with respect to $u$, mol $m^{-2}$ $s^{-1}$ |
| $k_{12}$ | binary interaction parameter in PR EOS, dimensionless |
| $k_{T1}$ | thermal diffusion ratio, dimensionless |
| $[L]$ | Onsager diffusivity matrix in fluid phases, $m^2$ $s^{-1}$ |
| $M$ | excess amount injected in Taylor dispersion experiment, mol |

$M_i$ molar mass of species *i*, kg mol$^{-1}$

$\overline{M}$ mean molar mass of mixture, kg mol$^{-1}$

$n$ number of species in the mixture, dimensionless

$N_i$ molar flux of species *i* in laboratory fixed reference frame, mol m$^{-2}$ s$^{-1}$

$N_t$ molar flux of total mixture in laboratory fixed reference frame, mol m$^{-2}$ s$^{-1}$

$p$ total system pressure, Pa

$P_c$ critical pressure, Pa

$[Q]$ matrix quantifying fractional unaccomplished change, dimensionless

$r$ radial direction coordinate, m

$R$ gas constant, 8.314 J mol$^{-1}$ K$^{-1}$

$R$ radius of tube in Taylor dispersion studies, m

$S_{T1}$ Soret coefficient, K$^{-1}$

$t$ time, s

$T$ absolute temperature, K

$T_c$ critical temperature, K

$x_i$ mole fraction of component *i* in fluid phase, dimensionless

$y_i$ mole fraction of component *i* in vapor phase, dimensionless

$u$ cross-sectional averaged velocity in dispersion tube, m s$^{-1}$

$u$ molar average mixture velocity, m s$^{-1}$

$\overline{V_i}$ partial molar volume of species *i,* m$^3$ mol$^{-1}$

$z$ direction coordinate, m

$z_i$ charge on species *i*, dimensionless

$Z$ compressibility factor, dimensionless

***Greek letters***

$\alpha_T$ thermal diffusion factor, dimensionless

$\delta$ slab thickness, m

$\delta_{ij}$ Kronecker delta, dimensionless

| | |
|---|---|
| $\phi_i$ | fugacity coefficient of component *i*, dimensionless |
| $\Gamma_{ij}$ | thermodynamic factors, dimensionless |
| $[\Gamma]$ | matrix of thermodynamic factors, dimensionless |
| $[\Lambda]$ | matrix defined by Equations (19), (**21**), $m^2\ s^{-1}$ |
| $\lvert\Lambda\rvert^{1/2}$ | Square-root of determinant of $[\Lambda]$, $m^2\ s^{-1}$ |
| $\Phi$ | electrostatic potential, V |
| $\mu_i$ | molar chemical potential, J $mol^{-1}$ |
| $\omega_i$ | mass fraction of component *i*, dimensionless |
| $\mu_i^0$ | molar chemical potential at standard state, J $mol^{-1}$ |
| $\rho_i$ | mass density of component *i*, kg $m^{-3}$ |
| $\rho_t$ | mass density of mixture, kg $m^{-3}$ |
| $\sigma$ | rate of entropy production, J $m^{-3}\ s^{-1}\ K^{-1}$ |

***Subscripts***

| | |
|---|---|
| c | referring to critical parameter |
| i | referring to component *i* |
| n | referring to component *n* |
| t | referring to total mixture |

Table 1. Self-diffusivities $D_{i,self}^{x_j \to 1}$ in units of $10^{-8}$ m$^2$ s$^{-1}$ for linear alkanes at 333 K and 30 MPa. The rows indicate species *i* and the columns, species *j*. The tabulated data is from Krishna and van Baten.[19]

| | C1 | C2 | C3 | nC4 | nC5 | nC6 | nC7 | nC8 | nC9 | nC10 |
|---|---|---|---|---|---|---|---|---|---|---|
| C1 | 7.00 | 2.58 | 1.50 | 1.05 | | 1.05 | | 1.05 | | 1.05 |
| C2 | 5.30 | 1.95 | 1.23 | 0.92 | | 0.84 | | 0.83 | | 0.83 |
| C3 | 4.52 | 1.63 | 1.03 | 0.79 | 0.72 | 0.75 | | | | |
| nC4 | 3.83 | 1.44 | 0.92 | 0.69 | 0.65 | | | | | |
| nC5 | | | 0.83 | 0.62 | 0.59 | | | | | |
| nC6 | 3.00 | 1.09 | 0.77 | | | 0.56 | | | | |
| nC7 | | | | | | | 0.44 | | | |
| nC8 | 2.36 | 0.97 | | | | | | 0.40 | | |
| nC9 | | | | | | | | | 0.34 | |
| nC10 | 1.86 | 0.82 | | | | | | | | 0.34 |

As illustration, for the system, C1/C3/nC6, we have

$$D_{1,self}^{x_2 \to 1} = 7; \quad D_{1,self}^{x_2 \to 1} = 1.5; \quad D_{1,self}^{x_3 \to 1} = 1.05;$$
$$D_{2,self}^{x_2 \to 1} = 4.52; \quad D_{2,self}^{x_2 \to 1} = 1.03; \quad D_{2,self}^{x_3 \to 1} = 0.75$$
$$D_{3,self}^{x_2 \to 1} = 3; \quad D_{3,self}^{x_2 \to 1} = 0.77; \quad D_{3,self}^{x_3 \to 1} = 0.56$$

Table 2. PR EOS binary interaction parameters[45] for linear alkanes using in the simulations presented here.

| | C1 | C2 | C3 | nC4 | nC5 | nC6 | nC10 |
|---|---|---|---|---|---|---|---|
| C1 | | -0.003 | 0.016 | 0.019 | 0.026 | 0.04 | 0.0411 |
| C2 | | | 0.001 | 0.01 | 0.008 | -0.04 | |
| C3 | | | | 0.003 | 0.027 | 0.001 | |
| nC4 | | | | | 0.017 | | |
| nC6 | | | | | | | 0 |

Table 3. Estimated values of self-diffusivities $D_{i,self}^{x_j \to 1}$ in units of $10^{-8}$ $m^2$ $s^{-1}$ for linear alkanes at 333 K and 8.5 MPa. The rows indicate species *i* and the columns, species *j*. The tabulated data is from Krishna and van Baten.[19]

| | C1 | C2 | C3 | nC4 | nC5 | nC6 | nC10 |
|---|---|---|---|---|---|---|---|
| C1 | 35 | 12.9 | 7.5 | 5.25 | 0 | 5.25 | 5.25 |
| C2 | 26.5 | 9.75 | 6.15 | 4.6 | 0 | 4.2 | |
| C3 | 22.6 | 8.15 | 5.15 | 3.95 | 3.6 | 3.75 | |
| nC4 | 19.15 | 7.2 | 4.6 | 3.45 | 3.25 | 0 | |
| nC5 | 0 | 0 | 4.15 | 3.1 | 2.95 | 0 | |
| nC6 | 15 | 5.45 | 3.85 | 0 | 0 | 2.8 | 1.7 |
| nC10 | 9.3 | | | | | 1.7 | 1.7 |

Table 4. Flory-Huggins parameters for permeation of penetrants $CO_2$ (component 1) and $C_2H_6$ (Component 2) across a cross-linked polyethylene oxide (XLPEO) membrane (indicated by subscript m). The temperature is 298.15 K.

Input data:

$f_{1,sat} = 58\times10^5$ Pa

$f_{2,sat} = 40\times10^5$ Pa

$\chi_{12} = 1.52$

$\chi_{1m} = 0.9085$

$\chi_{2m} = 2.084$

$\overline{V_1} = 4.174\times10^{-5}$

$\overline{V_2} = 6.04\times10^{-5}$

Table 5. Flory-Huggins parameters for permeation of penetrants $CO_2$ (component 1) and $C_2H_6$ (Component 2) across a cross-linked polyethylene oxide (XLPEO) membrane (indicated by subscript m). The temperature is 263.15 K.

$f_{1,sat} = 24.5\times10^5$ Pa

$f_{2,sat} = 14.5\times10^5$ Pa

$\chi_{12} = -28.2 - \dfrac{44.3}{\ln(\phi_1)}$

$\chi_{1m} = 1.0421 + 12.3\phi_2$

$\chi_{2m} = 2.421 + 4.76\sqrt{\phi_1}$

$\overline{V_1} = 3.31\times10^{-5}$

$\overline{V_2} = 4.14\times10^{-5}$

Table 6. Modified Maxwell-Stefan diffusivities for permeation of penetrants $CO_2$ (component 1) and $C_2H_6$ (Component 2) across a cross-linked polyethylene oxide (XLPEO) membrane (indicated by subscript m). The temperature is 298.15 K.

Input data:

$$Đ_{1m}^{V} = 1.069\times10^{-10}\exp\left(6.86\phi_1\right)$$
$$Đ_{2m}^{V} = 3.756\times10^{-11}\exp\left(11.4\left(\phi_2+\phi_1\right)\right)$$
$$Đ_{12}^{V} = 2.82\times10^{-11}$$

Table 7. Modified Maxwell-Stefan diffusivities for permeation of penetrants $CO_2$ (component 1) and $C_2H_6$ (Component 2) across a cross-linked polyethylene oxide (XLPEO) membrane (indicated by subscript m). The temperature is 263.15 K.

Input data:

$$Đ_{1m}^{V} = 8.5\times10^{-12}\exp\left(18.45\left(\phi_1+0.76\phi_2\right)\right)$$
$$Đ_{2m}^{V} = 1.489\times10^{-12}\exp\left(11.4\left(\phi_2+0.832\phi_1\right)\right)$$
$$Đ_{12}^{V} = 2.82\times10^{-11}\exp\left(109\left(\phi_1+\phi_2\right)\right)$$

# 16. References


(1) PTC MathCad 15.0. http://www.ptc.com/, PTC Corporate Headquarters, Needham, 3 November 2015.

(2) de Groot, S. R.; Mazur, P. *Non-Equilibrium Thermodynamics*; North-Holland Publishing Co.: Amsterdam, 1962.

(3) Standart, G. L.; Taylor, R.; Krishna, R. The Maxwell-Stefan formulation of irreversible thermodynamics for simultaneous heat and mass transfer. *Chem. Eng. Commun.* **1979**, *3*, 277-289.

(4) Hirschfelder, J. O.; Curtiss, C. F.; Bird, R. B. *Molecular theory of gases and liquids*; Second Corrected Printing, John Wiley: New York, USA, 1964.

(5) Tuan, D. Q.; Zollweg, J. A.; Rizvi, S. S. H. Concentration Dependence of the Diffusion Coefficient of Lipid in Supercritical Carbon Dioxide. *Ind. Eng. Chem. Res.* **1999**, *38*, 2787-2793.

(6) Taylor, R.; Krishna, R. *Multicomponent mass transfer*; John Wiley: New York, 1993.

(7) Galliéro, G.; Montel, F. Nonisothermal gravitational segregation by molecular dynamics simulations. *Phys. Rev. E* **2008**, *78*, 041203.

(8) Krishna, R.; Wesselingh, J. A. The Maxwell-Stefan Approach to Mass Transfer. *Chem. Eng. Sci.* **1997**, *52*, 861-911.

(9) Lightfoot, E. N. *Transport phenomena and living systems*; John Wiley: New York, 1974.

(10) Fuller, E. N.; Schettler, P. D.; Giddings, J. C. A New Method for Prediction of Binary Gas-phase Diffusion Coefficients. *Ind. Eng. Chem.* **1966**, *58*, 19-27.

(11) Reid, R.C.; Prausnitz, J. M.; Poling, B. E. *The Properties of Gases and Liquids*; 4th Edition, McGraw-Hill: New York, 1986.

(12) Takahashi, S. Preparation of a Generalized Chart for the Diffusion Coefficients of Gases at High Pressures. *J. Chem. Eng. Japan.* **1974**, *7*, 417-420.

(13) Takahashi, S.; Hongo, M. Diffusion Coefficients of Gases at High Pressures in the $CO_2$ - $C_2H_4$ System. *J. Chem. Eng. Japan.* **1982**, *15*, 57-59.

(14) Krishna, R.; van Baten, J. M. Unified Maxwell-Stefan Description of Binary Mixture Diffusion in Micro- and Meso- Porous Materials. *Chem. Eng. Sci.* **2009**, *64*, 3159-3178.

(15) Higashi, H.; Iwai, Y.; Oda, T.; Nakamura, Y.; Arai, Y. Concentration dependence of diffusion coefficients for supercritical carbon dioxide + naphthalene system. *Fluid Phase Equilib.* **2002**, *194-197*, 1161-1167.

(16) Ago, K.; Nishiumi, H. Calculation of Mutual Diffusion Coefficients near the Critical Region from the Peng-Robinson Equation of State. *Ind. Eng. Chem. Res.* **1998**, *37*, 1692-1695.

(17) Nishiumi, H.; Kubota, T. Fundamental behavior of benzene–$CO_2$ mutual diffusion coefficients in the critical region of $CO_2$. *Fluid Phase Equilib.* **2007**, *261*, 146-151.

(18) Wilke, C. R.; Chang, P. Correlation of Diffusion Coefficients in Dilute Solutions. *A.I.Ch.E.J.* **1955**, *1*, 264-270.

(19) Krishna, R.; van Baten, J. M. The Darken relation for multicomponent diffusion in liquid mixtures of linear alkanes. An investigation using Molecular Dynamics (MD) simulations. *Ind. Eng. Chem. Res.* **2005**, *44*, 6939-6947.

(20) Leahy-Dios, A.; Firoozabadi, A. Unified Model for Nonideal Multicomponent Molecular Diffusion Coefficients. *A.I.Ch.E.J.* **2007**, *53*, 2932-2939.

(21) Dysthe, D. K.; Hafskjold, B. Inter- and Intradiffusion in Liquid Mixtures of Methane and n-Decane. *Int. J. Thermophys.* **1995**, *16*, 1213-1224.

(22) Kett, T. K.; Anderson, D. K. Ternary Isothermal Diffusion and the Validity of the Onsager Reciprocal Relations in Nonassociating Systems. *J. Phys. Chem.* **1969**, *73*, 1268-1274.

(23) Leahy-Dios, A.; Bou-Ali, M. M.; Platten, J. K.; Firoozabadi, A. Measurements of molecular and thermal diffusion coefficients in ternary mixtures. *J. Chem. Phys.* **2005**, *122*, 234502.

(24) Wesselingh, J. A.; Bollen, A. M. Multicomponent diffusivities from the free volume theory. *Chem. Eng. Res. Des.* **1997**, *75*, 590-602.

(25) Krishna, R. Serpentine Diffusion Trajectories and the Ouzo Effect in Partially Miscible Ternary Liquid Mixtures. *Phys. Chem. Chem. Phys.* **2015**, *17*, 27428-27436.

(26) Crank, J. *The Mathematics of Diffusion*; 2nd Edition, Clarendon Press: Oxford, 1975.

(27) Krishna, R. An alternative linearized theory of multicomponent mass transfer. *Chem. Eng. Sci.* **1981**, *36*, 219-222.

(28) Krishna, R. Diffusing Uphill with James Clerk Maxwell and Josef Stefan. *Curr. Opin. Chem. Eng.* **2016**, *12*, 106-119.

(29) Krishna, R. Uphill Diffusion in Multicomponent Mixtures. *Chem. Soc. Rev.* **2015**, *44*, 2812-2836.

(30) Krishna, R. Highlighting Diffusional Coupling Effects in Ternary Liquid Extraction and Comparisons with Distillation. *Ind. Eng. Chem. Res.* **2016**, *55*, 1053-1063.

(31) Krishna, R. Tracing the Origins of Transient Overshoots for Binary Mixture Diffusion in Microporous Crystalline Materials. *Phys. Chem. Chem. Phys.* **2016**, *18*, 15482-15495.

(32) Murphree, E. V. Graphical rectifying column calculations. *Ind. Eng. Chem.* **1925**, *17*, 960-964.

(33) Murphree, E. V. Rectifying column calculations with particular reference to n-component mixtures. *Ind. Eng. Chem.* **1925**, *17*, 747-750.

(34) Treybal, R. E. *Mass-Transfer Operations*; 3rd Edition, McGraw-Hill: New York, 1980.

(35) Robbins, L. A.; Cusack, R. W. *Chaper 15, Liquid-Liquid Extraction Operations and Equipment*. Perry's Chemical Engineers' Handbook; 7th Edition, Edited by R.H. Perry and D.W. Green, McGraw-Hill: New York, 1999.

(36) Seader, J. D.; Henley, E. J.; Roper, D. K. *Separation Process Principles*; 3rd Edition, John Wiley: New York, 2011.

(37) Price, W. F. Theory of the Taylor Dispersion Technique for Three-component-system Diffusion Measurements. *J. Chem. Soc.-Faraday Trans. 1* **1988**, *84*, 2431-2439.

(38) Rutten, P. W. M. *Diffusion in Liquids*. Ph.D. Dissertation, Delft University of Technology, Delft, 1992.

(39) Dyson, D. C.; Simon, J. M. A Kinetic Expression with Diffusion Correction for Ammonia Synthesis on Industrial Catalyst. *Ind. Eng. Chem. Fundamentals* **1968**, *7*, 605-610.

(40) Wilke, C. R. Diffusional Properties of Multicomponent Gases. *Chem. Eng. Prog.* **1950**, *46*, 95-104.

(41) Krishna, R. Comments on "Simulation and Optimization of an Industrial Ammonia Reactor". *Ind. Eng. Chem. Res.* **1989**, *28*, 1266.

(42) Kuijlaars, K. J.; Kleijn, C. R.; Van Den Akker, H. E. A. Multi-component Diffusion Phenomena in Multiple-Wafer Chemical Vapor Deposition Reactors. *Chem. Eng. J.* **1995**, *57*, 127-136.

(43) Touzet, M.; Galliero, G.; Lazzeri, V.; Saghir, M. Z.; Montel, F.; Legros, J.-C. Thermodiffusion: From microgravity experiments to the initial state of petroleum reservoirs. *C.R. Mecanique* **2011**, *339*, 318-323.

(44) Platten, J. K. The Soret Effect: A Review of Recent Experimental Results. *J. Appl. Mech.* **2006**, *73*, 5-15.

(45) Sandler, S. I. *Chemical, Biochemical, and Engineering Thermodynamics*; 3rd Edition, John Wiley: New York, 1999.

# 17. Captions for Figures

Figure 1. Calculations of combined FSG and PR EOS models for thermodynamics and diffusion in $CO_2(1)/C_2H_4(2)$ mixtures at $T$ = 323.2 K with varying compositions $x_1$, and total pressure, $p$. (a) Compressibility factor, $Z$. (b) Thermodynamic correction factor, $\Gamma$. (c) Maxwell-Stefan diffusivity, $Đ_{12}$. (d) Fick diffusivity, $D_{12}$. The PR EOS calculations presented here use a binary interaction parameter $k_{12}$ = 0.0.

Figure 2. Calculations of combined FSG and PR EOS models for thermodynamics and diffusion in $CO_2(1)/C_2H_4(2)$ mixtures ($x_1$=0.5) with varying reduced pressures $p_r$ and reduced temperatures $T_r$. (a) Compressibility factor, $Z$. (b) Thermodynamic correction factor, $\Gamma$. (c) Maxwell-Stefan diffusivity, $Đ_{12}$. (d) Fick diffusivity, $D_{12}$. The reduced pressure is calculated from $p_r = \dfrac{p}{x_1 P_{c1} + x_2 P_{c2}}$. The reduced temperature is calculated from $T_r = \dfrac{T}{x_1 T_{c1} + x_2 T_{c2}}$. The PR EOS calculations presented here use a binary interaction parameter $k_{12}$ = 0.0.

Figure 3. (a, b, c) Experimental data of Takahashi and Hongo[13] for M-S diffusivities of $CO_2$(trace amounts)/$C_2H_4$ mixtures, and $CO_2/C_2H_4$(trace amounts) mixtures at (a) 298.2 K, (b) 323.2 K, and (c)

348.2 K for a range of pressures. The dashed lines are the estimations using the FSG equation (52). The continuous solid lines are the estimations of the M-S diffusivities using Equation (53). (d, e, f) Calculations of the compressibility factor using the Peng-Robinson Equation of State (PR EOS) of $CO_2$(trace amounts)/$C_2H_4$ mixtures, and $CO_2$/$C_2H_4$(trace amounts) mixtures at (d) 298.2 K, (e) 323.2 K, and (f) 348.2 K for a range of pressures. The PR EOS calculations presented here use a binary interaction parameter $k_{12}$ = 0.0. The mole fraction of the trace component is taken to be 0.005.

Figure 4. Data on MD simulations for the Maxwell-Stefan diffusivity, $Đ_{12}$, culled from Krishna and van Baten[14], for binary (a) $CH_4(1)/C_2H_6(2)$, (b) $CH_4(1)/C_3H_8(2)$, (c) $CH_4(1)/N_2(2)$, (d) $CO_2(1)/CH_4(2)$, (e) $CO_2(1)/N_2(2)$, and (d) $CO_2(1)$/Ar(2) mixtures at 300 K. For MD simulation data, the $x$-axis is the total molar concentration, $c_t$, in the simulation box; note that this value is *not* calculated from the ideal gas law. The continuous solid lines are the estimations of the M-S diffusivities using Equation (53); in this case the $x$-axis is calculated using $c_t = \frac{p}{ZRT}$.

Figure 5. MD simulations for the Maxwell-Stefan diffusivity, $Đ_{12}$, for binary $CH_4(1)/C_2H_6(2)$ mixtures at 333 K at (a) 5 MPa, (b) 10 MPa, (c) 20 MPa, (d) 30 MPa, and (e) 40 MPa and with varying compositions of methane $x_1$. The simulation methodology is the same as that used in the work of Krishna and van Baten.[19] The continuous solid lines are the estimations of the M-S diffusivities using Equation (53). Also shown by the dashed lines are the FSG estimations, using equation (52).

Figure 6. (a) Experimental data of Tuan et al.[5] for the dependence of the Fick diffusivity of methyl oleate (MO) (component 1) in supercritical $CO_2$ (component 2), on the mole fraction of MO for $T$ = 313.15 K, $p$ = 10.6 MPa, and $p$ = 11.5 MPa. Also shown by the continuous solid lines are the estimations of the Fick diffusivity using Equation (54). (b, c) Calculations of the (b) compressibility factor, Z, and the (c) thermodynamic factor, $\Gamma$ using the PR EOS. The critical parameters for the PR EOS calculations are taken from Table 2 of Tuan et al;[5] the binary interaction parameter, $k_{12}$ = 0.063.

Figure 7. Calculations of the thermodynamic factor, $\Gamma$, for naphthalene (component 1) in supercritical $CO_2$ (component 2), as a function of the mole fraction of naphthalene, at $p$ = 8.25 MPa, and $p$ = 10.4 MPa. The temperature $T$ = 308.2 K. The PR EOS calculations use the binary interaction parameter, $k_{12}$ = 0.016, calculated by Higashi et al.[15]

Figure 8. (a) Experimental data of Ago and Nishiumi[16] for diffusivity of benzene (component 1) in supercritical $CO_2$ (component 2) as a function of the reduced pressure, $p_r = \frac{p}{P_{c2}}$ where $P_{c2}$ = 7.28 MPa is the critical pressure of $CO_2$. The measurements were made in a Taylor dispersion tube with varying amounts of benzene injection into the tube. (b) Calculations of the compressibility factor using the Peng-Robinson Equation of State (PR EOS). (c) Calculations of the thermodynamic factor, $\Gamma$, using PR EOS. (d) Calculations of the Fick diffusivities as a function of $p/p_c$ and composition of benzene in the mixture using the PR EOS. The PR EOS calculations presented here use a binary interaction parameter $k_{12}$ = 0.0774.

Figure 9. (a, b) Experimental data of Nishiumi and Kubota[17] for diffusivity of benzene (component 1) in supercritical $CO_2$ (component 2) as a function of the reduced pressure, $p_r = \frac{p}{P_{c2}}$ where $P_{c2}$ = 7.28 MPa is the critical pressure of $CO_2$. The measurements were made in a Taylor dispersion tube with varying amounts of benzene injection into the tube. The solid lines are the calculations of the Fick diffusivities as a function of $p/p_c$ and composition of benzene in the mixture using the PR EOS. The PR EOS calculations presented here use a binary interaction parameter $k_{12}$ = 0.0774.

Figure 10. PR EOS calculations for thermodynamics in $CH_4(1)/C_3H_8(2)$ mixture ($x_1$=0.7) with varying reduced pressures $p_r$ and reduced temperatures $T_r$. (a) Compressibility factor, $Z$. (b) Thermodynamic correction factor, Γ. The reduced pressure is calculated from $p_r = \frac{p}{x_1 P_{c1} + x_2 P_{c2}}$. The reduced temperature is calculated from $T_r = \frac{T}{x_1 T_{c1} + x_2 T_{c2}}$. The PR EOS calculations presented here use a binary interaction parameter $k_{12}$ = 0.016.

Figure 11. PR EOS calculations for thermodynamics in $CH_4(1)/C_3H_8(2)$ mixtures at $T$ = 298.15 K with varying compositions $x_1$, and total pressure, $p$. (a) Compressibility factor, $Z$. (b) Thermodynamic correction factor, Γ. The PR EOS calculations presented here use a binary interaction parameter $k_{12}$ = 0.016.

Figure 12. MD simulation data of Krishna and van Baten[19] on $Đ_{ij}$ for the binary methane(1)/ethane(2), methane(1)/n-hexane(3), and ethane(2)/n-hexane(3) mixtures at 333 K and 30 MPa. The continuous solid lines are the calculations of $Đ_{ij}$ using the Vignes interpolation formula (56). The values of the self-diffusivities at the limiting compositions, $D_{i,self}^{x_j \to 1}$, are provided in Table 1. The M-S diffusivities at the limiting compositions, calculated from Table 1, are (units of $10^{-8}$ $m^2$ $s^{-1}$):

$$Đ_{12}^{x_1 \to 1} = 5.3; \quad Đ_{12}^{x_2 \to 1} = 2.5; \quad Đ_{13}^{x_1 \to 1} = 3; \quad Đ_{13}^{x_3 \to 1} = 1.05; \quad Đ_{23}^{x_2 \to 1} = 1.09; \quad Đ_{23}^{x_3 \to 1} = 0.84.$$

Figure 13. MD simulation data of Krishna and van Baten[19] on $Đ_{ij}$ for the binary methane(1)/ethane(2), methane(1)/propane(3), and ethane(2)/propane (3) mixtures at 333 K and 30 MPa.. The continuous solid lines are the calculations of $Đ_{ij}$ using the Vignes interpolation formula (56). The values of the self-diffusivities at the limiting compositions, $D_{i,self}^{x_j \to 1}$, are provided in Table 1. The M-S diffusivities at the limiting compositions, calculated from Table 1, are (units of $10^{-8}$ $m^2$ $s^{-1}$):

$$Đ_{12}^{x_1 \to 1} = 5.3; \quad Đ_{12}^{x_2 \to 1} = 2.5; \quad Đ_{13}^{x_1 \to 1} = 4.52; \quad Đ_{13}^{x_3 \to 1} = 1.5; \quad Đ_{23}^{x_2 \to 1} = 1.63; \quad Đ_{23}^{x_3 \to 1} = 1.23.$$

Figure 14. MD simulation data of Krishna and van Baten[19] on $Đ_{ij}$ for the binary methane(1)/propane(2), methane(1)/n-hexane(3), and propane(2)/n-hexane (3) mixtures at 333 K and 30 MPa.. The continuous solid lines are the calculations of $Đ_{ij}$ using the Vignes interpolation formula (56). The values of the self-diffusivities at the limiting compositions, $D_{i,self}^{x_j \to 1}$, are provided in Table 1. The M-S diffusivities at the limiting compositions, calculated from Table 1, are (units of $10^{-8}$ $m^2$ $s^{-1}$):

$$Đ_{12}^{x_1 \to 1} = 4.52; \quad Đ_{12}^{x_2 \to 1} = 1.5; \quad Đ_{13}^{x_1 \to 1} = 3; \quad Đ_{13}^{x_3 \to 1} = 1.05; \quad Đ_{23}^{x_2 \to 1} = 0.77; \quad Đ_{23}^{x_3 \to 1} = 0.75.$$

Figure 15. MD simulation data of Krishna and van Baten[19] on $Đ_{ij}$ for the binary ethane(1)/propane(2), ethane(1)/n-butane(3), and propane(2)/n-butane (3) mixtures at 333 K and 30 MPa.. The continuous solid lines are the calculations of $Đ_{ij}$ using the Vignes interpolation formula (56). The values of the self-diffusivities at the limiting compositions, $D_{i,self}^{x_j \to 1}$, are provided in Table 1. The M-S diffusivities at the limiting compositions, calculated from Table 1, are (units of $10^{-8}$ $m^2$ $s^{-1}$):

$$Đ_{12}^{x_1\to 1} = 1.63; \quad Đ_{12}^{x_2\to 1} = 1.23; \quad Đ_{13}^{x_1\to 1} = 1.44; \quad Đ_{13}^{x_3\to 1} = 0.92; \quad Đ_{23}^{x_2\to 1} = 0.92; \quad Đ_{23}^{x_3\to 1} = 0.79.$$

Figure 16. MD simulation data of Krishna and van Baten[19] on $Đ_{ij}$ for the binary propane(1)/n-butane(2), propane(1)/n-pentane(3), and n-butane(2)/n-pentane (3) mixtures at 333 K and 30 MPa.. The continuous solid lines are the calculations of $Đ_{ij}$ using the Vignes interpolation formula (56). The values of the self-diffusivities at the limiting compositions, $D_{i,self}^{x_j \to 1}$, are provided in Table 1. The M-S diffusivities at the limiting compositions, calculated from Table 1, are (units of $10^{-8}$ $m^2$ $s^{-1}$):

$$Đ_{12}^{x_1\to 1} = 0.92; \quad Đ_{12}^{x_2\to 1} = 0.79; \quad Đ_{13}^{x_1\to 1} = 0.83; \quad Đ_{13}^{x_3\to 1} = 0.72; \quad Đ_{23}^{x_2\to 1} = 0.62; \quad Đ_{23}^{x_3\to 1} = 0.65.$$

Figure 17. (a) MD simulation data of Krishna and van Baten[19] on $Đ_{ij}$ for the binary mixtures of methane with ethane, propane, n-butane, n-hexane, and n-decane at 333 K and 30 MPa as function of the mole fraction of methane. The continuous solid lines are the calculations of $Đ_{ij}$ using the Vignes interpolation formula (56). (b) Calculations of the Fick diffusivity using Equation (57), where the thermodynamic factor is calculated using the PR EOS, using the binary interaction parameters in Table 2.

Figure 18. (a, b) Thermodynamics and diffusion in $CH_4(1)/C_3H_8(2)$ mixtures at $T$ = 311 K and 206.8 bar. (a) Calculations of the thermodynamic factor, Γ, using PR EOS. (b) Experimental data of Sigmund, as reported in Figure 2c of Leahy-Dios and Firoozabadi,[20] for Fick diffusivities of $CH_4(1)/C_3H_8(2)$ mixtures at $T$ = 311 K and $p$ = 206.8 bar. The continuous solids lines are the estimations using Equation (57), along with limiting M-S diffusivities determined from MD simulations (units of $10^{-8}$ $m^2$ $s^{-1}$): $Đ_{12}^{x_1\to 1} = 4.52$; $Đ_{12}^{x_2\to 1} = 1.5$. The PR EOS calculations presented here use the binary interaction parameters in Table 2.

Figure 19. (a) Experimental data of Dysthe and Hafskjold[21] for Fick diffusivities of $CH_4(1)$/n-$C_{10}H_{22}(2)$ mixtures at $T$ = 303.5 K and $p$ = 40 MPa. (b) Experimental data of Dysthe and Hafskjold[21] for Fick diffusivities of $CH_4(1)$/n-$C_{10}H_{22}(2)$ mixtures at $T$ = 303.5 K and $p$ = 40, 50 and 60 MPa. (c) Calculations of the thermodynamic factor, Γ, using PR EOS at $p$ = 20, 25, 30, 35, 40, 50 and 60 MPa. (d) Spinodal compositions for $CH_4(1)$/n-$C_{10}H_{22}(2)$ mixtures at $T$ = 303.5 K. (e) Experimental data of Dysthe and Hafskjold[21] for Fick diffusivities of $CH_4(1)$/n-$C_{10}H_{22}(2)$ mixtures at $T$ = 303.5 K with varying total pressures; the mole fractions of methane $x_1$ = 0.903. The PR EOS calculations use the binary interaction parameters in Table 2.

Figure 20. Transformation of Fick diffusivity matrix from mass average reference velocity to molar average reference velocity, and vice versa.

Figure 21. Calculations for the determinant $|\Gamma|$ for the ternary mixture of $nC_8H_{18}(1)/nC_{10}H_{22}(2)/1$-methylnapthalene(3) as a function of the composition of 1MN, $x_3$, keeping the ratio $x_1/x_2$ at a constant value of unity. The calculations are presented for three different temperatures $T$ = 295.65 K, 240 K, and 200 K. The PR EOS calculations presented here use the binary interaction parameters = 0 for all three binary pairs.

Figure 22. MD simulated values[19] (shown by red circles) of $|\Lambda|^{1/2}$ for (a) methane(1)/ethane(2)/n-hexane(3), (b) methane(1)/ethane(2)/propane (3), and (c) methane(1)/propane(2)/n-hexane (3) at 333 K. The open circles represent calculations using Equations (31), (59), and (61).

Figure 23. Ternary diagram delineating the two-phase V/L region for methane(1)/propane(2)/n-hexane (3) mixtures at 333 K and 8.5 MPa. The compositions of the vapor and liquid phases in equilibrium with each other are indicated by the tie-lines. The region to the left of the two-phase region consists of the liquid region. The inset shows the calculations for the determinant $|\Gamma|$ as a function of the composition of n-hexane, $x_3$, keeping the ratio $x_1/x_2$ at a constant value of unity. The PR EOS calculations presented here use the binary interaction parameters in Table 2.

Figure 24. Schematic for transient diffusion of methane(1)/propane(2)/n-hexane (3) mixtures at 333 K and 8.5 MPa into a liquid phase slab of half-thickness $\delta$. The surfaces on either side of the liquid slab consists of ternary vapor phase mixture of constant composition. At time $t$ = 0, a liquid slab of composition $x_{10}$ = 0.05, $x_{20}$ = 0.55, $x_{30}$ = 0.4 is exposed to a vapor phase mixture of composition $y_1$ = 0.659033, $y_2$ = 0.318393, $y_3$ = 0.022574; this composition is held constant during the equilibration process. The composition of the liquid phase in equilibrium with the vapor phase is $x_{1\delta}$ = 0.333532, $x_{2\delta}$ = 0.521103, $x_{3\delta}$ = 0.145365.

Figure 25. (a) Transient equilibration for liquid phase diffusion in methane(1)/propane(2)/n-hexane (3) mixtures at 333 K and 8.5 MPa using Equation (29) for the estimation of the elements of the Fick diffusivity matrix $[D]$. (b) The equilibration trajectory plotted in composition space. (c) Component Murphree efficiencies plotted as a function of the Fourier number, $\frac{4|D|^{1/2}t}{\delta^2}$, wherein the value of the characteristics diffusivity is chosen as the square root of the determinant of the Fick matrix, $|D|^{1/2} = 5.5\times10^{-8}$ m$^2$ s$^{-1}$. The M-S diffusivities at the limiting compositions are calculated from Table 3 as guidelines. The PR EOS calculations presented here use the binary interaction parameters in Table 2.

Figure 26. Simulation results for Taylor dispersion for liquid phase methane(1)/propane(2)/n-hexane (3) mixtures at 333 K and 8.5 MPa, using Equation (29) for the estimation of the elements of the Fick diffusivity matrix $[D]$. The liquid mixture flowing in the tube has the (cross-sectional averaged) composition $x_1$ = 0.4, $x_2$ = 0.4, $x_3$ = 0.2. At time $t$ = 0, Dirac $\delta$-pulses M1 = M2 = $10^{-7}$ moles of components 1 and 2 are injected at the inlet. The M-S diffusivities at the limiting compositions are

calculated from Table 3 as guidelines. The PR EOS calculations presented here use the binary interaction parameters in Table 2.

Figure 27. Simulation results for Taylor dispersion for liquid phase (a) methane(1)/ethane(2)/n-hexane (3), (b) methane(1)/ethane(2)/propane (3), (c) propane(1)/n-butane(2)/n-pentane, and (d) methane(1)/n-hexane(2)/n-decane (3) mixtures at 333 K and 8.5 MPa, using Equation (29) for the estimation of the elements of the Fick diffusivity matrix $[D]$. The liquid mixture flowing in the tube has the (cross-sectional averaged) compositions (a) $x_1 = 0.4$, $x_2 = 0.3$, $x_3 = 0.2$, (b) $x_1 = 0.3$, $x_2 = 0.3$, $x_3 = 0.4$, (d) $x_1 = 0.7$, $x_2 = 0.2$, $x_3 = 0.1$, and(d) $x_1 = 0.5$, $x_2 = 0.4$, $x_3 = 0.1$. At time $t = 0$, Dirac $\delta$-pulses M1 = M2 = $10^{-7}$ moles of components 1 and 2 are injected at the inlet. The M-S diffusivities at the limiting compositions are calculated from Table 3 as guidelines. The PR EOS calculations presented here use the binary interaction parameters in Table 2.

Figure 28. (a) Calculation of the compressibility factor, $Z$, and the determinant $|\Gamma|$ in the gaseous mixture $N_2/H_2/NH_3$ at a temperature of 500 K and total pressure of 25 MPa. In these calculations, the ratio of the compositions $x_2/x_1 = 3$. (b) Calculation of the effective diffusivities in the gaseous mixture $N_2/H_2/NH_3$ at a temperature of 500 K and total pressure of 25 MPa. In these calculations, the M-S pair diffusivities are calculated using Equation (53).

Figure 29. Calculation of the effective diffusivities in the gaseous mixture $WF_6/H_2/HF/Ar$ at a temperature of 673 K and total pressure 100 Pa. In these calculations, the ratio of the compositions $x_2/x_1 = 3$, and the composition of Ar is held constant at $x_4 = 0.3$.

Figure 30. (a) Transient equilibration between the left and right compartments of gaseous mixtures $WF_6/H_2/HF/Ar$ at a temperature of 673 K and total pressure 100 Pa. The left compartment has the initial composition $x_{1,L} = 0.2$; $x_{2,L} = 0.4$, $x_{3,L} = 0.1$, $x_{4,L} = 0.3$. The right compartment has the initial compositions $x_{1,R} = 0.02$, $x_{2,R} = 0.1$, $x_{3,R} = 0.6$, $x_{4,R} = 0.28$. The $x$-axis is $\frac{z}{\sqrt{4D_{ref}t}}$ where the reference diffusivity value $D_{ref} = 1 \quad m^2\ s^{-1}$. (b) The equilibration trajectories are plotted in ternary composition space. The dashed line represents the trajectory followed if each component has the same effective diffusivity with a value $D_{ref} = 1 \quad m^2\ s^{-1}$.

Figure 31. Separation of gaseous uranium isotopes $U^{235}F_6(1)/U^{238}F_6(2)$ by ultracentrifugation as described in Example 2.3.2 of Taylor and Krishna.[6]

Figure 32. Composition dependence of the thermodynamic properties binary mixture $C_2H_6/nC_{10}H_{22}$ at a pressure $p = 20$ MPa and temperature $T = 440$ K. (a) Volume fractions and mass fractions as a function of the mixture mole fractions. (b) Partial molar volumes of ethane and n-decane, along with molar volume of mixture. (c) Variation of the compressibility factor, Z, and thermodynamic factor, Γ, with mole fraction of ethane. The binary interaction parameter in PR EOS, $k_{12} = 0.014$.

Figure 33. Gravitational segregation for the binary mixture $C_2H_6/nC_{10}H_{22}$ in a reservoir of 600 m depth at a pressure $p$ = 20 MPa and temperature $T$ = 440 K. The mixture composition at depth z = 300 m from the surface (z = 0) is $x_1$ = 0.5, $x_2$ = 0.5. The binary interaction parameter in PR EOS, $k_{12}$ = 0.014. The continuous solid lines are calculations using Γ correction. The dashed lines are calculations that ignore Γ corrections.

Figure 34. Gravitational segregation for the ternary mixture $CH_4/nC_4H_{10}/nC_{12}H_{26}$ in a reservoir of 600 m depth at a pressure $p$ = 35 MPa and temperature $T$ = 333.15 K. The mixture composition at depth z = 300 m from the surface (z = 0) is $x_1$ = 0.2, $x_2$ = 0.4, $x_3$ = 0.4. The binary interaction parameters in PR EOS, are $k_{12}$ = 0.019, $k_{13}$ = 0.008, and $k_{23}$ = 0.0. The continuous solid lines are model calculations using Γ correction.

Figure 35. Segregation for the binary mixture $C_2H_6/nC_{10}H_{22}$ in a reservoir of 600 m depth at a pressure $p$ = 20 MPa and temperature $T$ = 440 K. The mixture composition at depth z = 300 m from the surface (z = 0) is $x_1$ = 0.5, $x_2$ = 0.5. The binary interaction parameter in PR EOS, $k_{12}$ = 0.014. (a) Segregation due to gravity effects alone, (b) Segregation due to thermal diffusion alone. (c) Segregation due to a combination of gravity and thermal diffusion.

Fig. S1

# $CO_2/C_2H_4$ mixtures: Influence of $x_1$ and ***p***

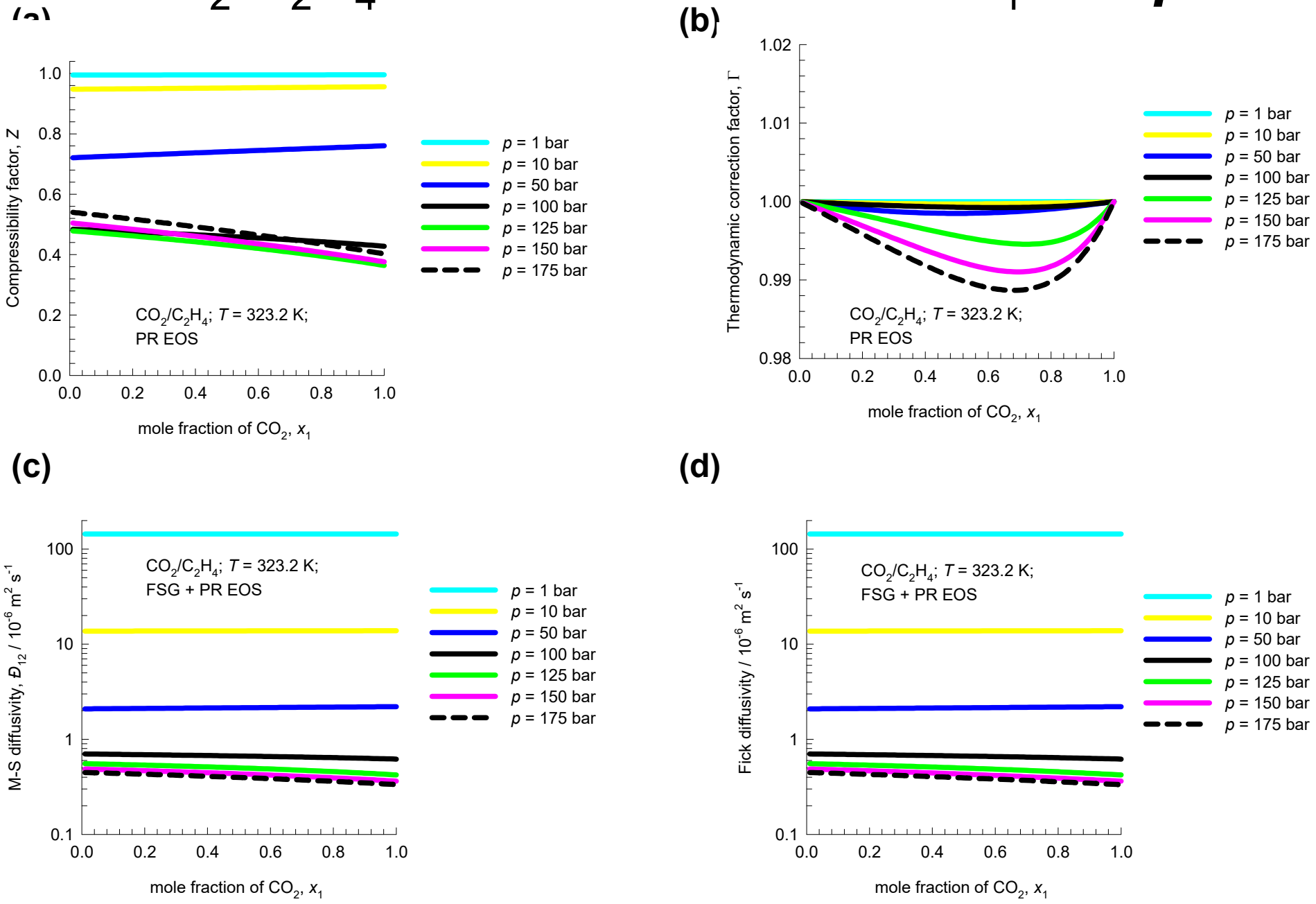

Fig. S2

# $CO_2/C_2H_4$ mixtures: Influence of $p$ and $T$

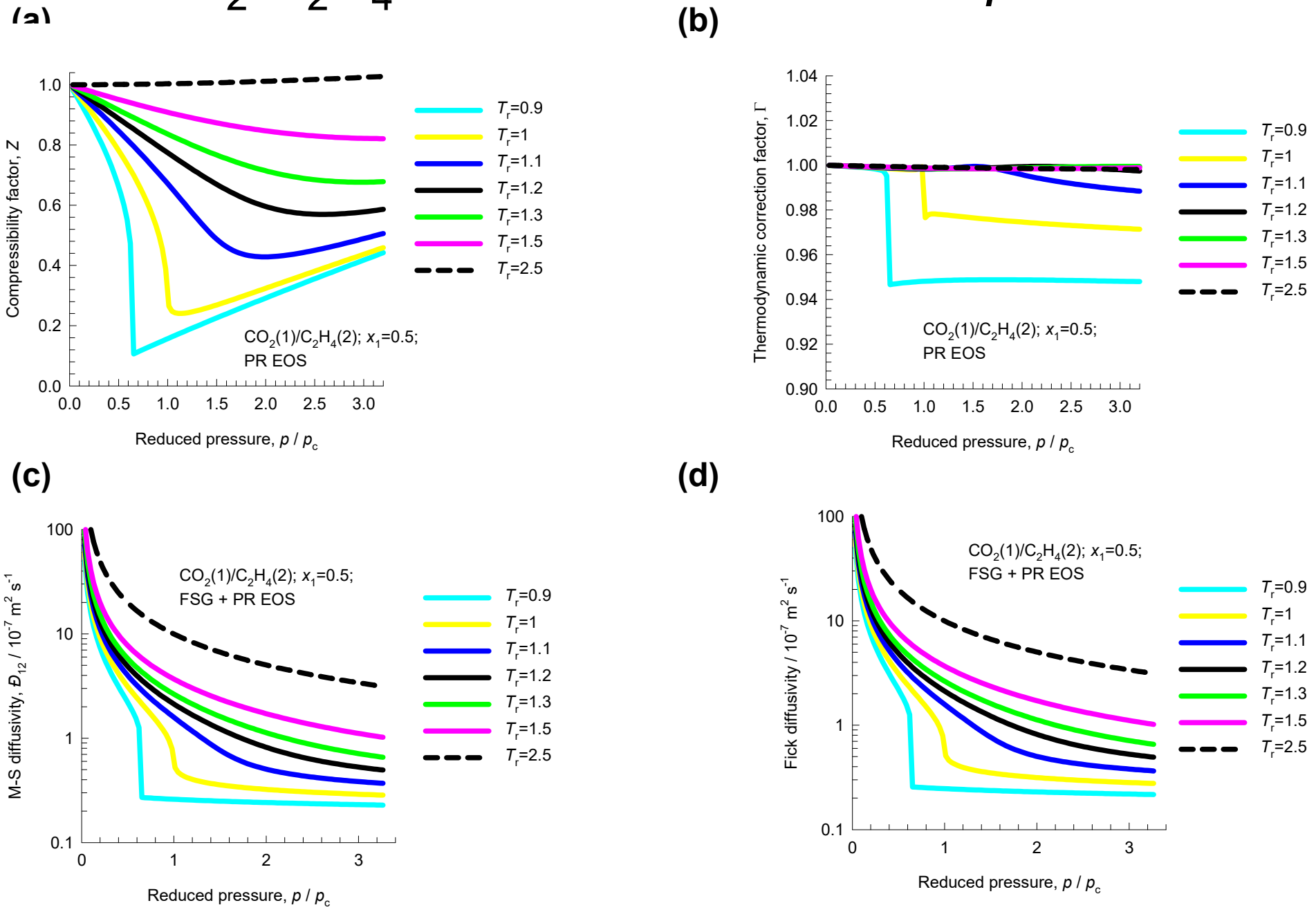

# Binary gas mixtures at High Pressures

Fig. S3

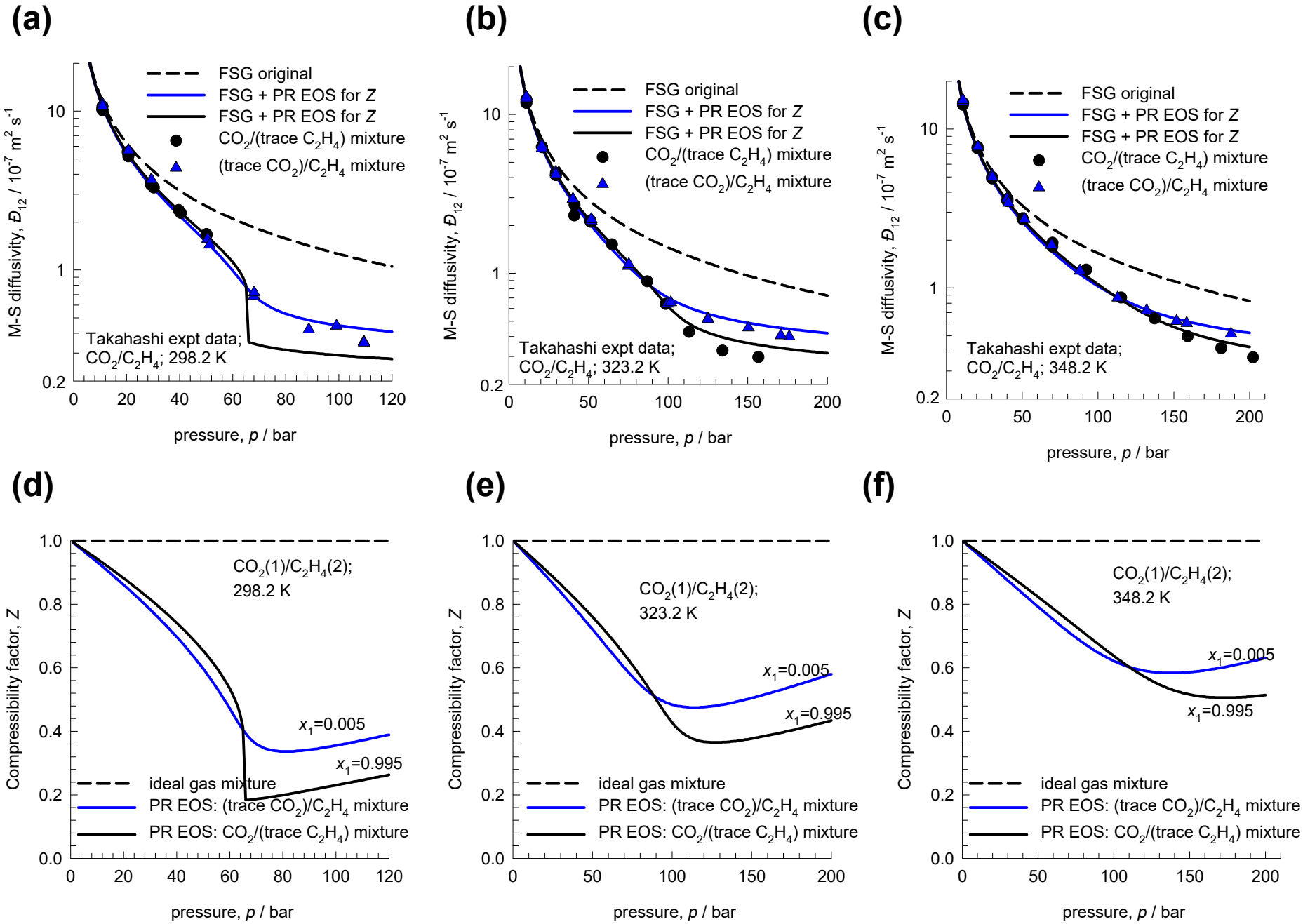

# Influence of increased molar density

Fig. S4

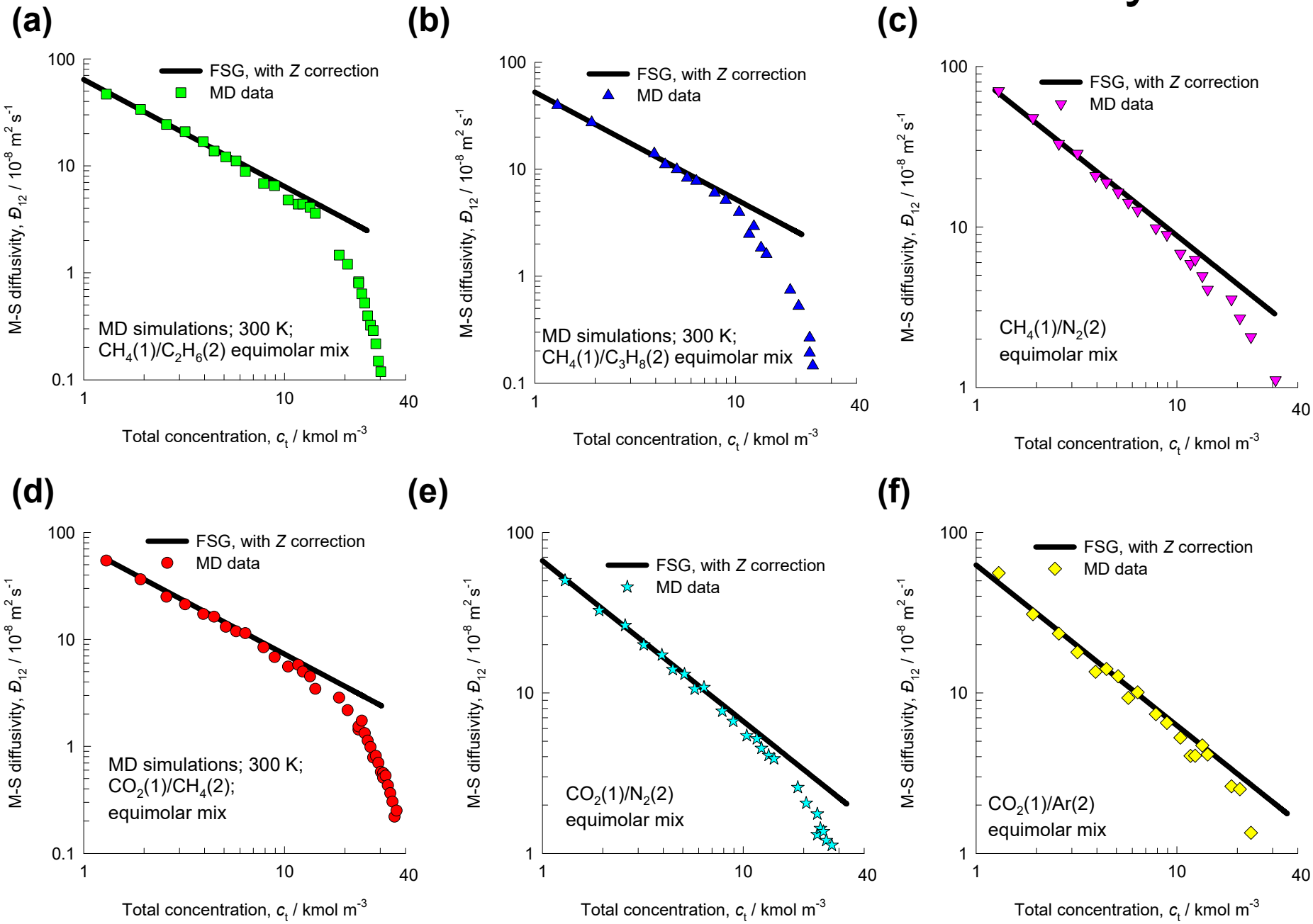

Fig. S5

# C1/C2 mixture diffusion at varying pressures

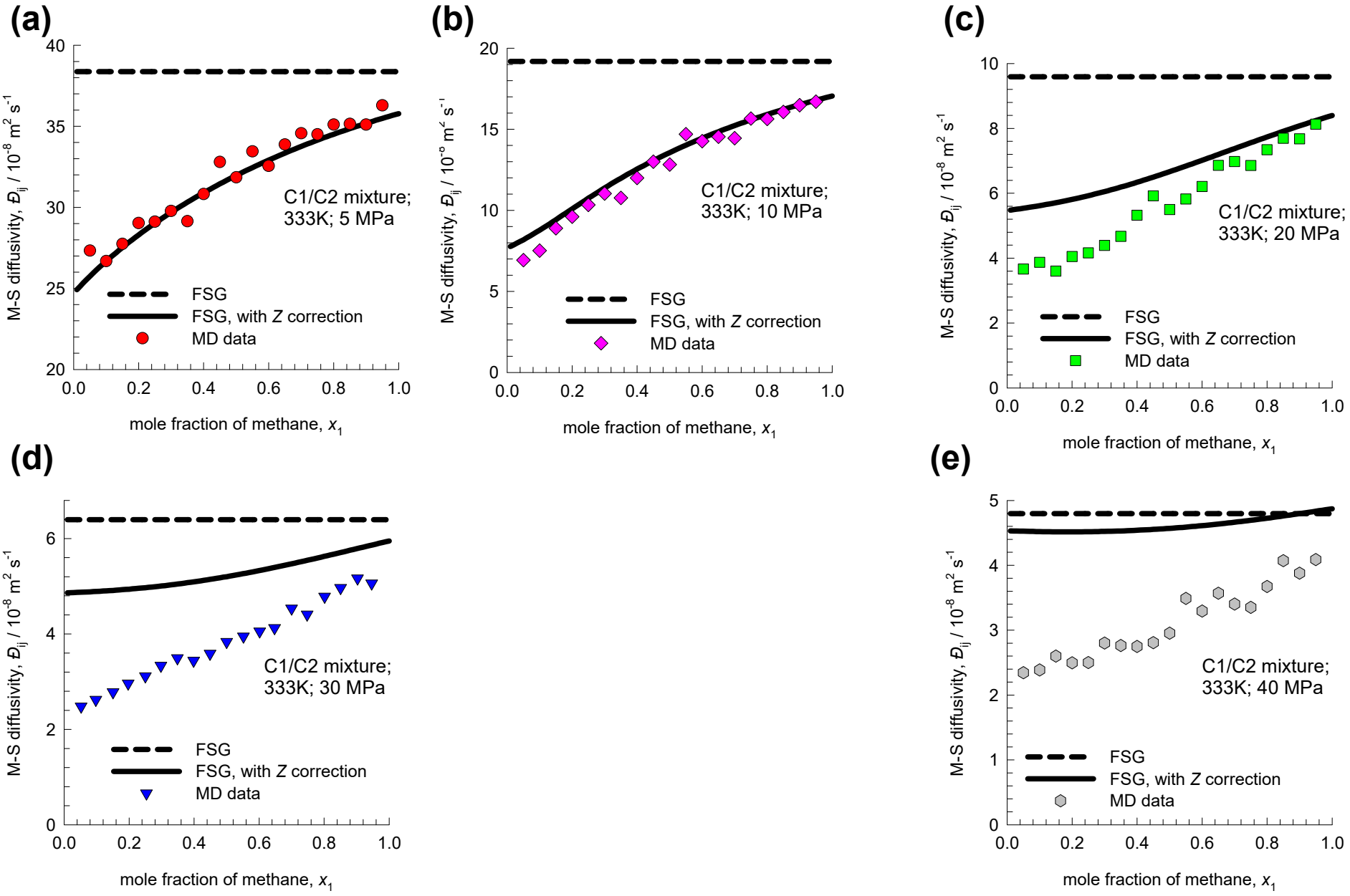

Fig. S6

# Diffusion of methyl oleate in supercritical $CO_2$

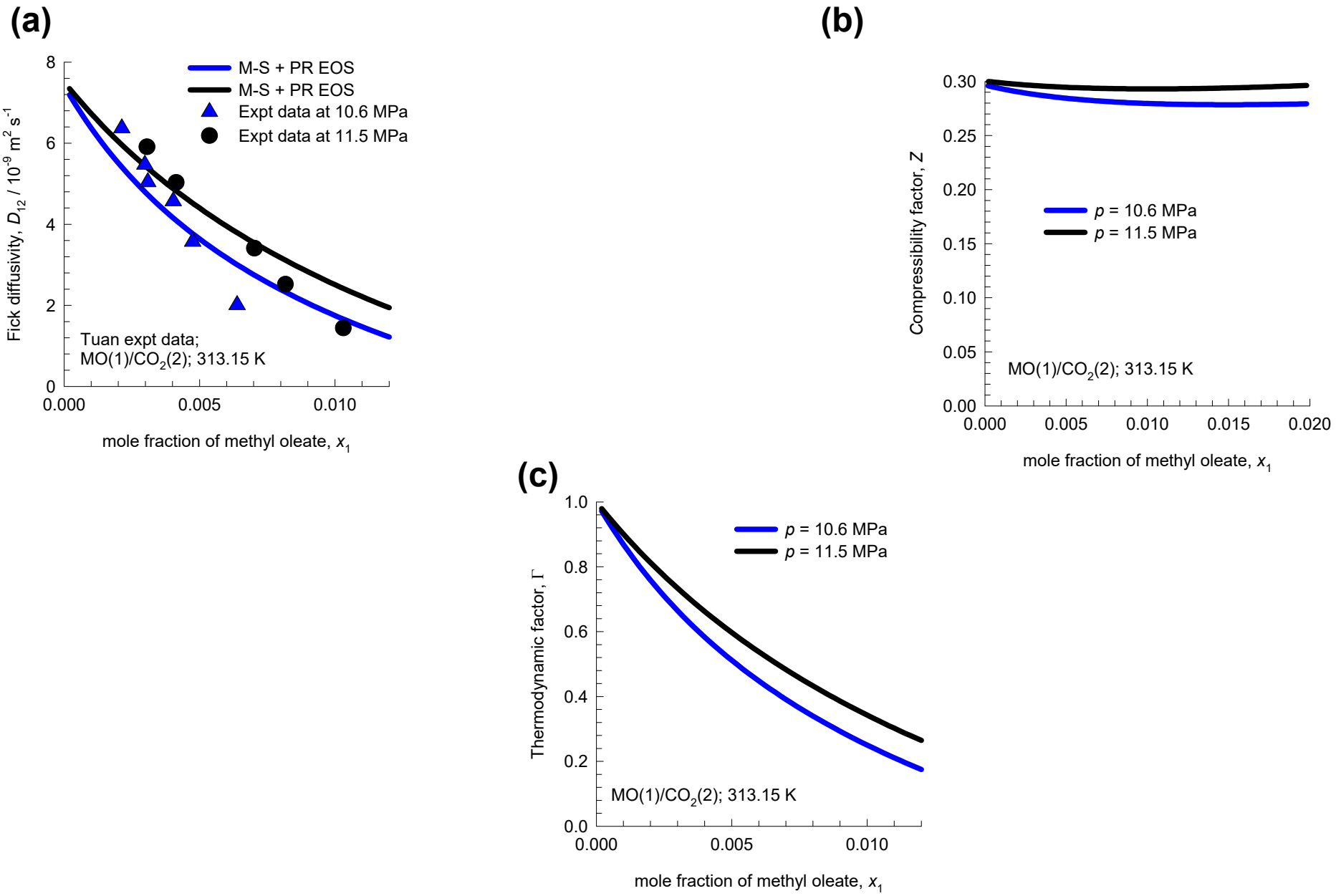

Fig. S7

# Diffusion of naphthalene in supercritical $CO_2$

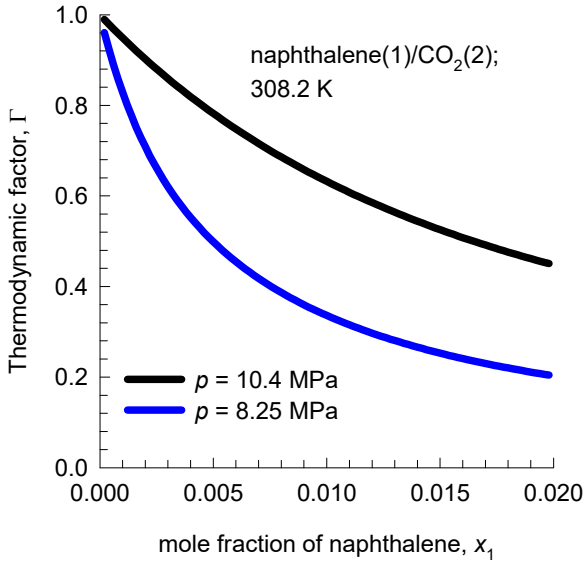

# Diffusion in benzene/$CO_2$ mixtures

Fig. S8

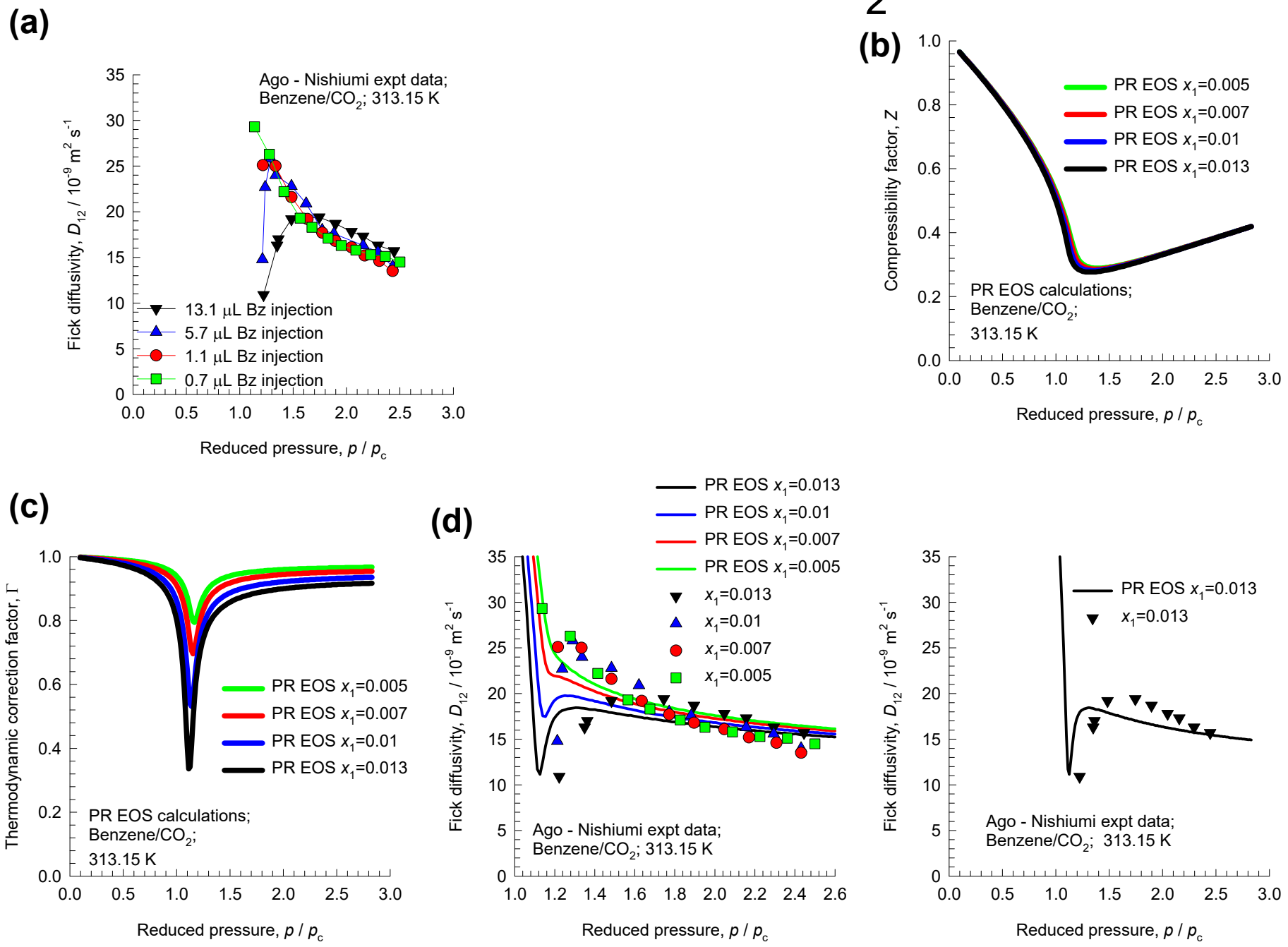

# Diffusion in benzene/$CO_2$ mixtures

Fig. S9

**(a)**

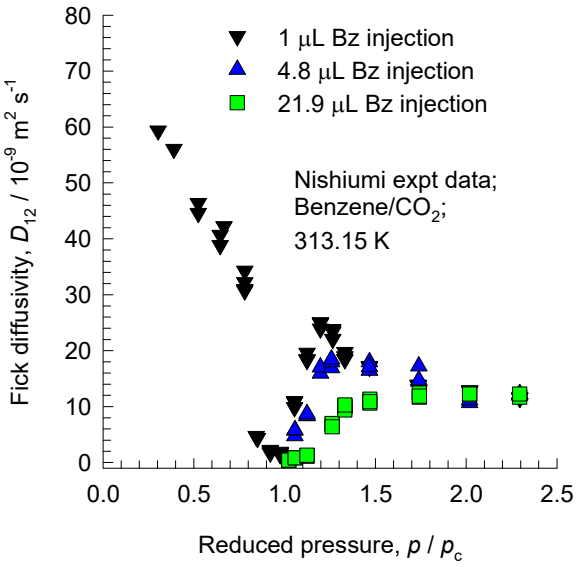


**(b)**

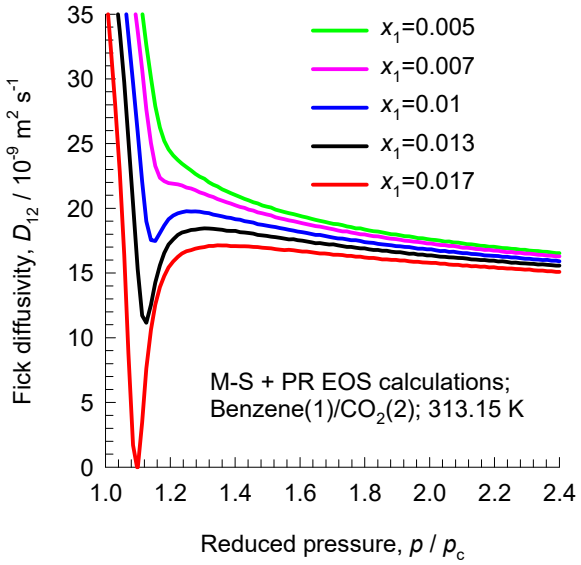

# C1/C3 mixtures: Influence of *p* & *T*

Fig. S10

**(a)**

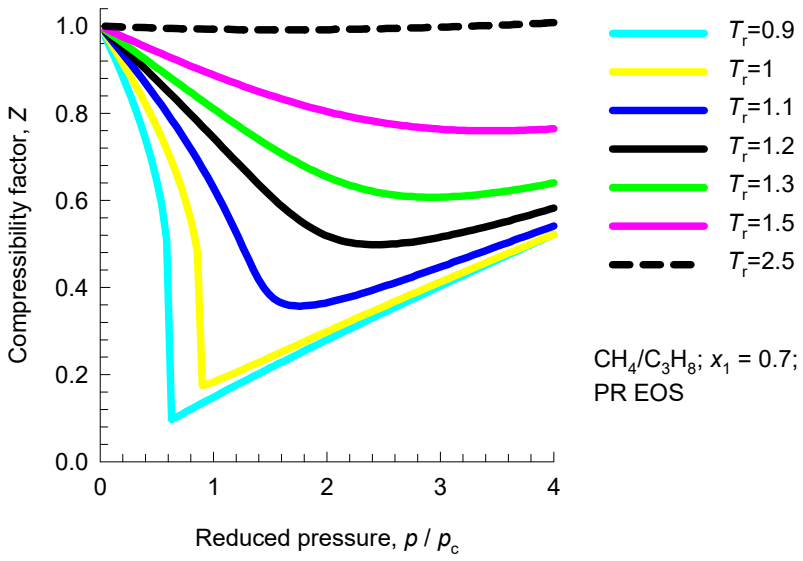


**(b)**

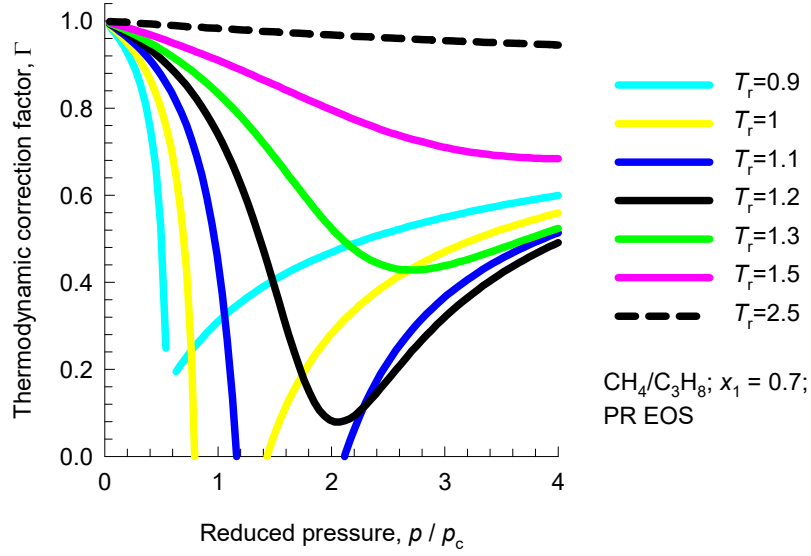

# Influence of $x_1$ & $p$

Fig. S11

**(a)**

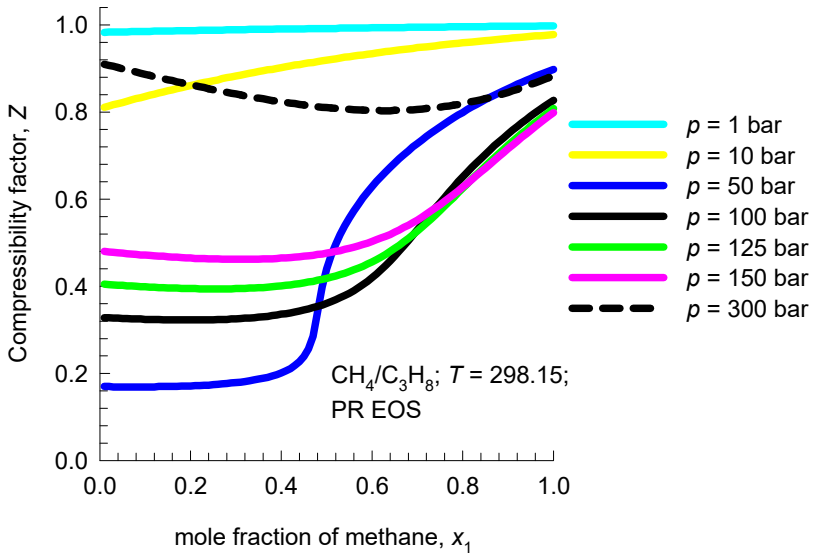


**(b)**

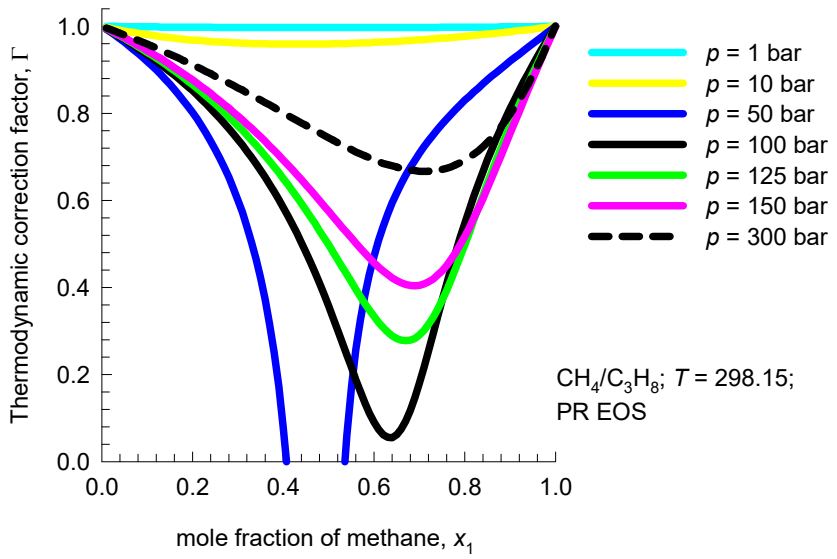

# C1/C2; C1/nC6; C2/nC6 mixtures: Vignes interpolation

Fig. S12

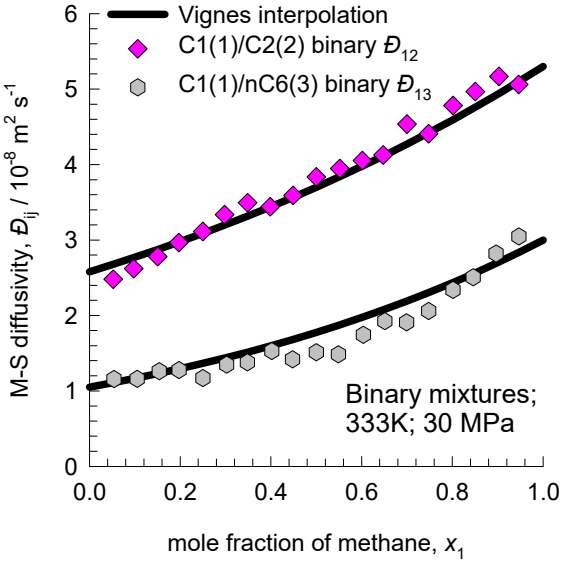


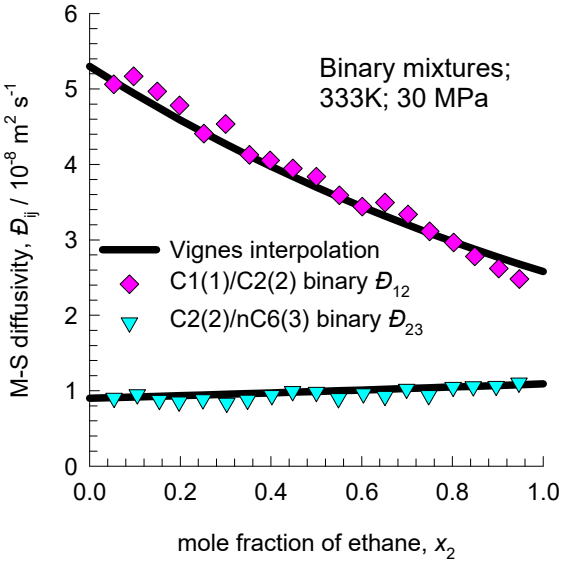


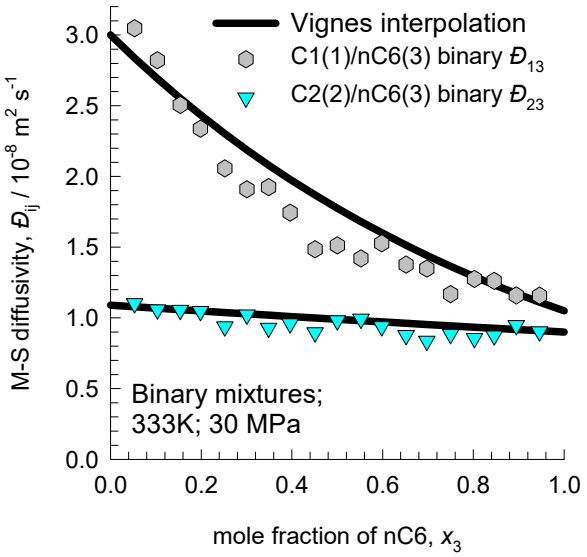


$$Đ_{12}^{x_1\to 1}=5.3;\quad Đ_{12}^{x_2\to 1}=2.5;\quad Đ_{13}^{x_1\to 1}=3;\quad Đ_{13}^{x_3\to 1}=1.05;\quad Đ_{23}^{x_2\to 1}=1.09;\quad Đ_{23}^{x_3\to 1}=0.84.$$

# C1/C2; C1/C3; C2/C3 mixtures: Vignes interpolation

Fig. S13

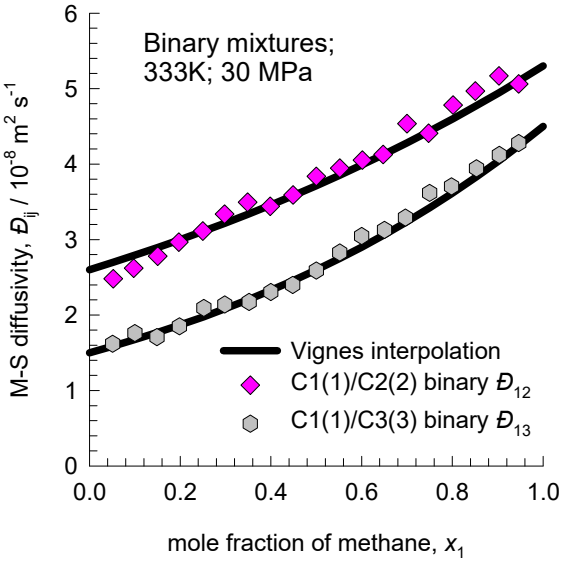


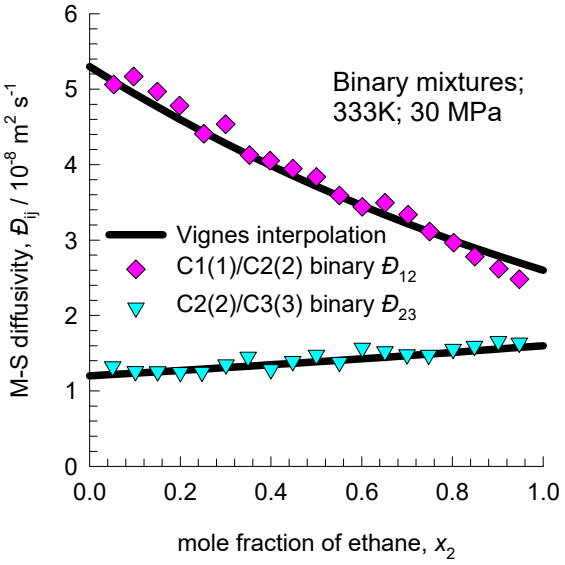


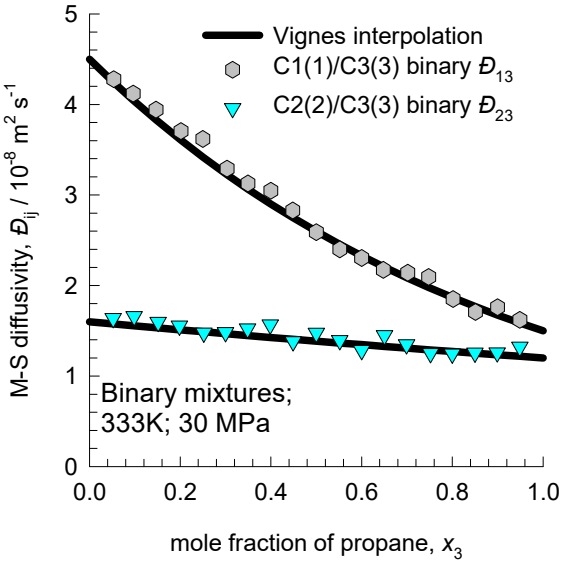


$$Đ_{12}^{x_1\to 1}=5.3;\quad Đ_{12}^{x_2\to 1}=2.5;\quad Đ_{13}^{x_1\to 1}=4.52;\quad Đ_{13}^{x_3\to 1}=1.5;\quad Đ_{23}^{x_2\to 1}=1.63;\quad Đ_{23}^{x_3\to 1}=1.23.$$

# C1/C3; C1/nC6; C3/nC6 mixtures: Vignes interpolation

Fig. S14

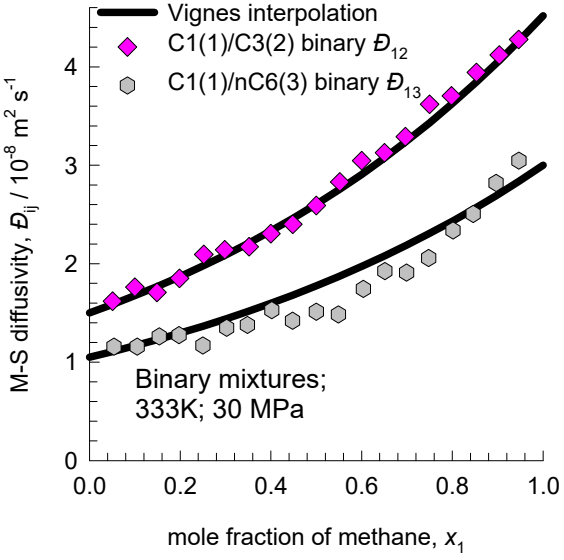


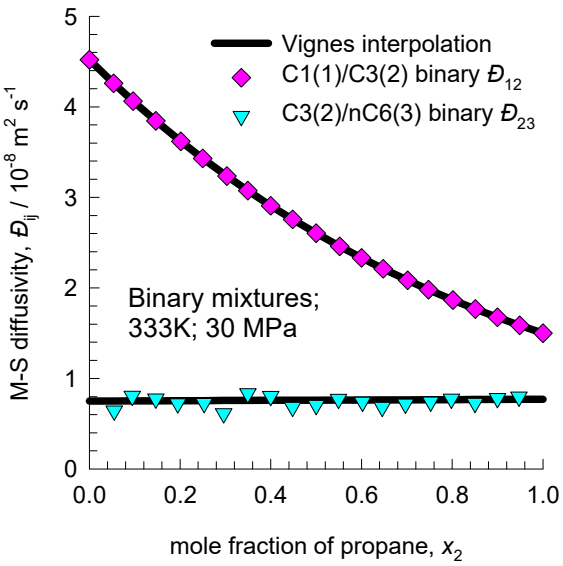


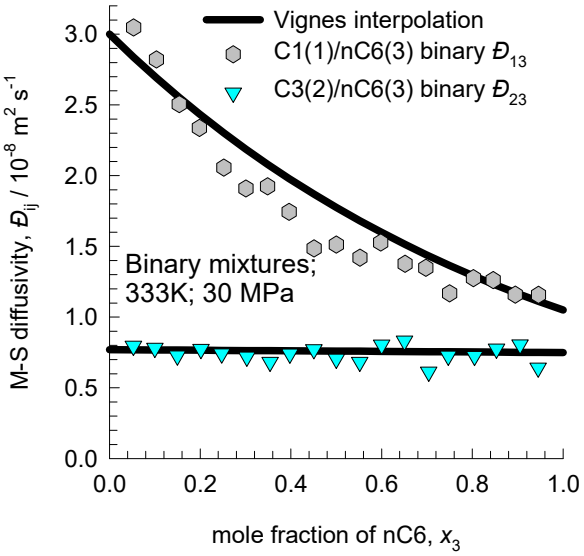


$$Đ_{12}^{x_1\to 1} = 4.52; \quad Đ_{12}^{x_2\to 1} = 1.5; \quad Đ_{13}^{x_1\to 1} = 3; \quad Đ_{13}^{x_3\to 1} = 1.05; \quad Đ_{23}^{x_2\to 1} = 0.77; \quad Đ_{23}^{x_3\to 1} = 0.75.$$

# C2/C3; C2/nC4; C3/nC4 mixtures: Vignes interpolation

Fig. S15

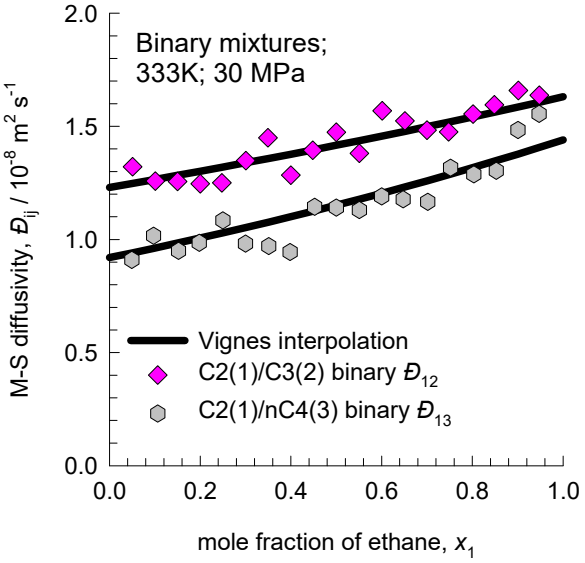


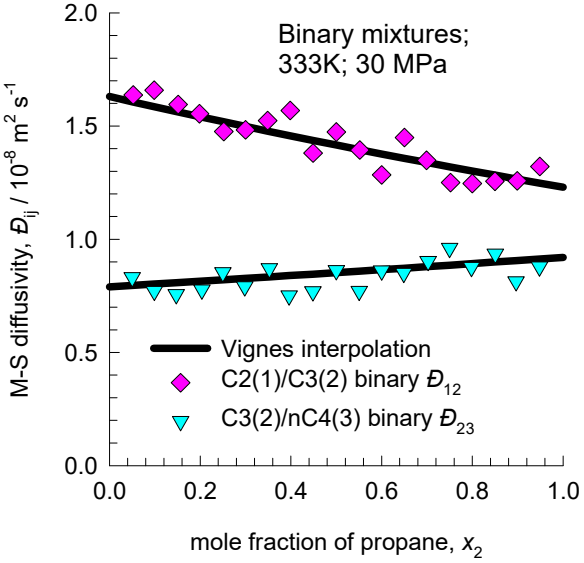


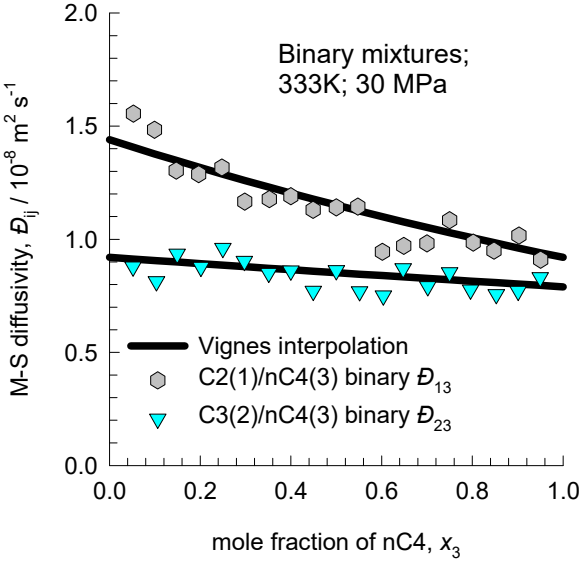


$$Đ_{12}^{x_1\to 1}=1.63;\quad Đ_{12}^{x_2\to 1}=1.23;\quad Đ_{13}^{x_1\to 1}=1.44;\quad Đ_{13}^{x_3\to 1}=0.92;\quad Đ_{23}^{x_2\to 1}=0.92;\quad Đ_{23}^{x_3\to 1}=0.79.$$

# C3/nC4; C3/nC5; nC4/nC5 mixtures: Vignes interpolation

Fig. S16

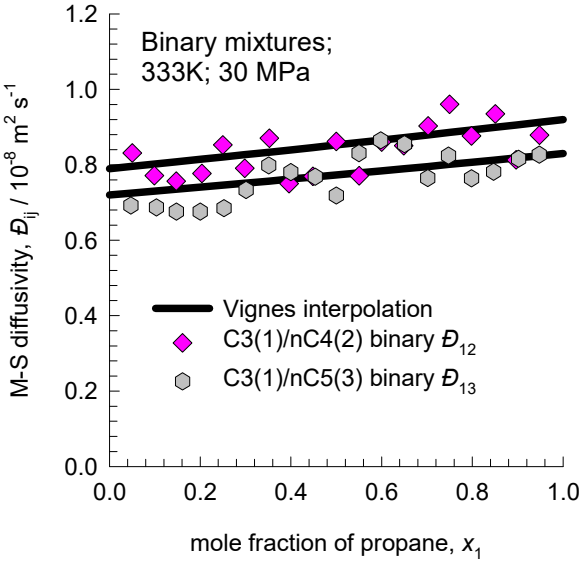


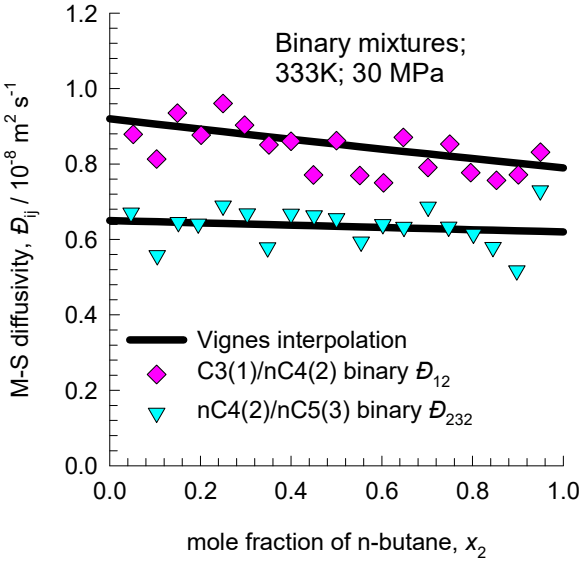


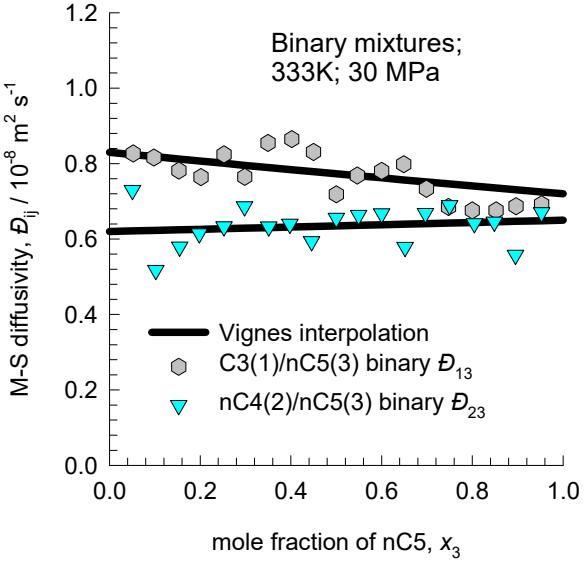


$$Đ_{12}^{x_1\to 1} = 0.92; \quad Đ_{12}^{x_2\to 1} = 0.79; \quad Đ_{13}^{x_1\to 1} = 0.83; \quad Đ_{13}^{x_3\to 1} = 0.72; \quad Đ_{23}^{x_2\to 1} = 0.62; \quad Đ_{23}^{x_3\to 1} = 0.65.$$

# Binary mixtures containing methane: Vignes interpolation

Fig. S17

**(a)**

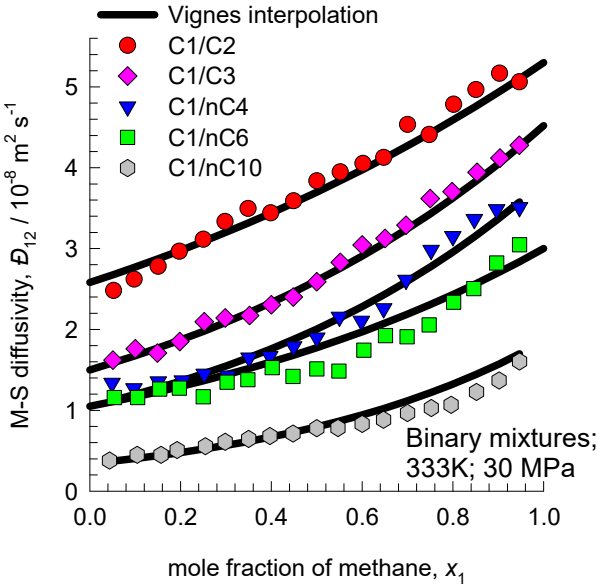


**(b**

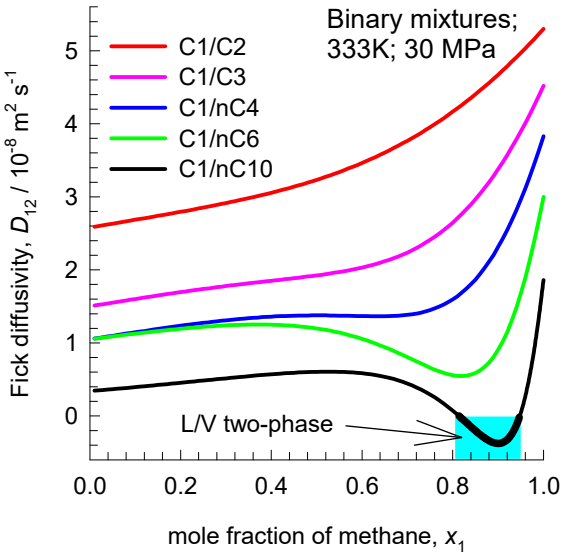

# Diffusivities in C1/C3 liquid mixture

Fig. S18

**(a)**

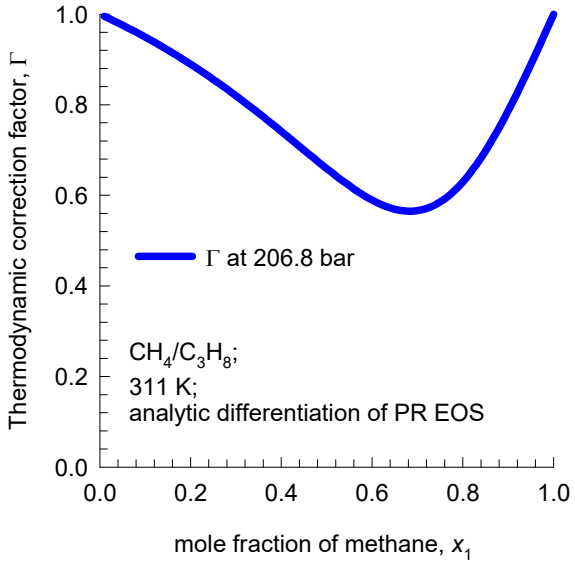


**(b)**

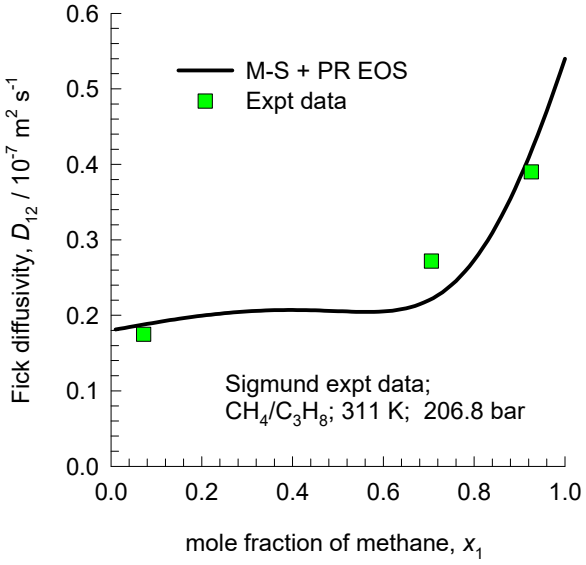

# Vapor/liquid phase transitions

Fig. S19

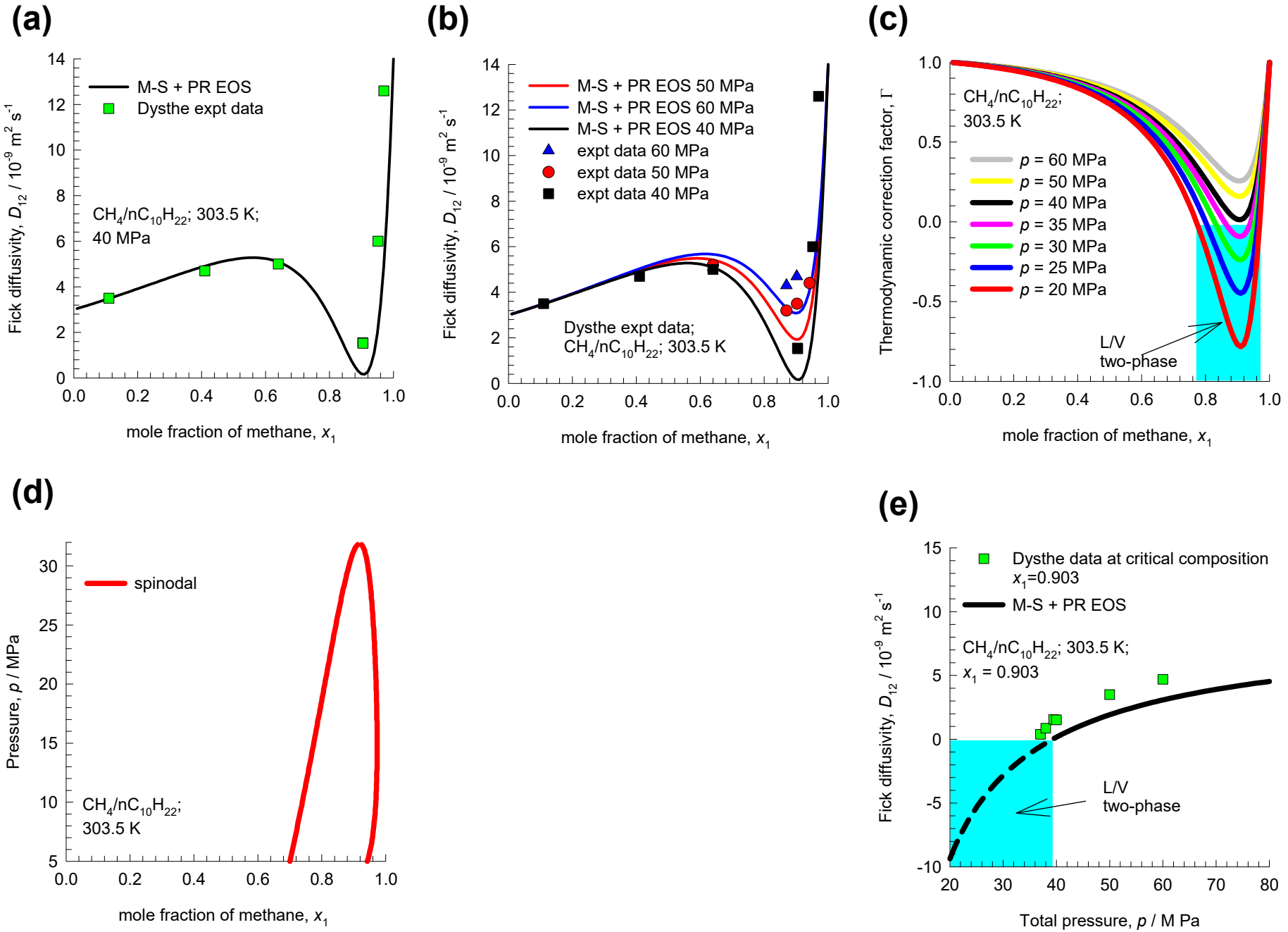

Fig. S20

# nC8/nC10/1MN mixtures: Transforming reference velocity frames

Fick matrix in mass average reference velocity frame

$$[D]=\begin{bmatrix} x_1 & 0 \\ 0 & x_2 \end{bmatrix}\begin{bmatrix} \omega_1 & 0 \\ 0 & \omega_2 \end{bmatrix}^{-1}\begin{bmatrix} 1-\omega_1\left(\frac{x_1}{\omega_1}-\frac{x_3}{\omega_3}\right) & -\omega_1\left(\frac{x_2}{\omega_2}-\frac{x_3}{\omega_3}\right) \\ -\omega_2\left(\frac{x_1}{\omega_1}-\frac{x_3}{\omega_3}\right) & 1-\omega_2\left(\frac{x_2}{\omega_2}-\frac{x_3}{\omega_3}\right) \end{bmatrix}[D^{mass}]^{-1}\begin{bmatrix} 1-\omega_1\left(1-\frac{x_1}{\omega_1}\frac{\omega_3}{x_3}\right) & -\omega_1\left(1-\frac{x_2}{\omega_2}\frac{\omega_3}{x_3}\right) \\ -\omega_2\left(1-\frac{x_1}{\omega_1}\frac{\omega_3}{x_3}\right) & 1-\omega_2\left(1-\frac{x_2}{\omega_2}\frac{\omega_3}{x_3}\right) \end{bmatrix}^{-1}\begin{bmatrix} \omega_1 & 0 \\ 0 & \omega_2 \end{bmatrix}\begin{bmatrix} x_1 & 0 \\ 0 & x_2 \end{bmatrix}^{-1}$$

Fick matrix in molar average reference velocity frame

$$[D^{mass}]=\begin{bmatrix} 1-\omega_1\left(\frac{x_1}{\omega_1}-\frac{x_3}{\omega_3}\right) & -\omega_1\left(\frac{x_2}{\omega_2}-\frac{x_3}{\omega_3}\right) \\ -\omega_2\left(\frac{x_1}{\omega_1}-\frac{x_3}{\omega_3}\right) & 1-\omega_2\left(\frac{x_2}{\omega_2}-\frac{x_3}{\omega_3}\right) \end{bmatrix}^{-1}\begin{bmatrix} \omega_1 & 0 \\ 0 & \omega_2 \end{bmatrix}\begin{bmatrix} x_1 & 0 \\ 0 & x_2 \end{bmatrix}^{-1}[D]\begin{bmatrix} x_1 & 0 \\ 0 & x_2 \end{bmatrix}\begin{bmatrix} \omega_1 & 0 \\ 0 & \omega_2 \end{bmatrix}^{-1}\begin{bmatrix} 1-\omega_1\left(1-\frac{x_1}{\omega_1}\frac{\omega_3}{x_3}\right) & -\omega_1\left(1-\frac{x_2}{\omega_2}\frac{\omega_3}{x_3}\right) \\ -\omega_2\left(1-\frac{x_1}{\omega_1}\frac{\omega_3}{x_3}\right) & 1-\omega_2\left(1-\frac{x_2}{\omega_2}\frac{\omega_3}{x_3}\right) \end{bmatrix}$$

Fig. S21

# nC8/nC10/1MN mixtures: L/S phase transitions

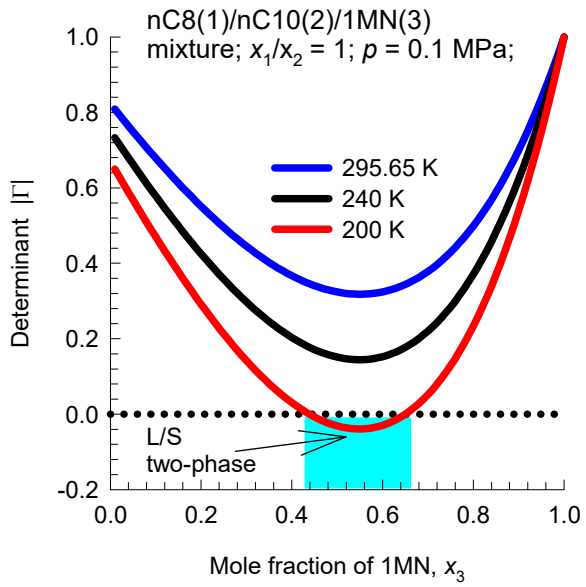

Fig. S22

# Ternary mixtures: Vignes interpolation

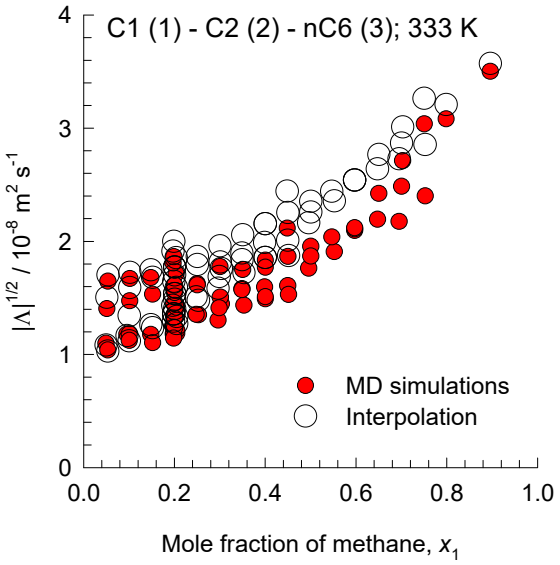


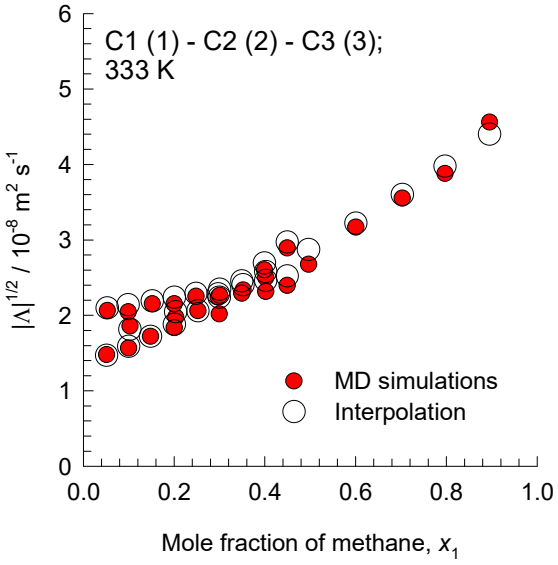


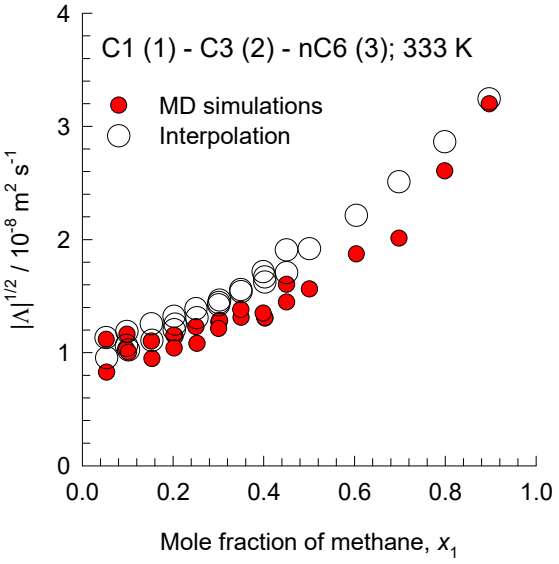

Fig. S23

# C1/C3/nC6 mixtures: V/L phase transitions

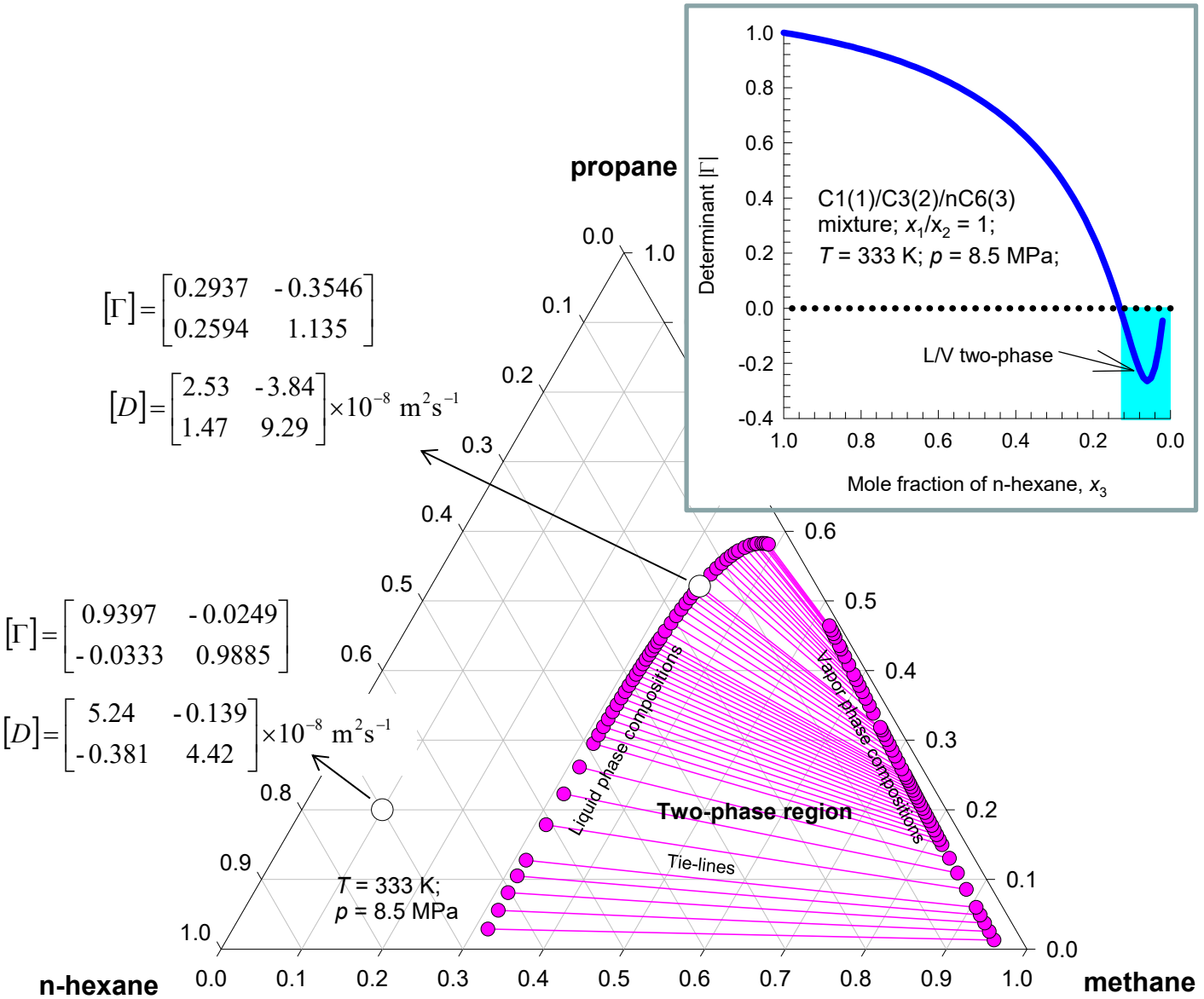

Fig. S24

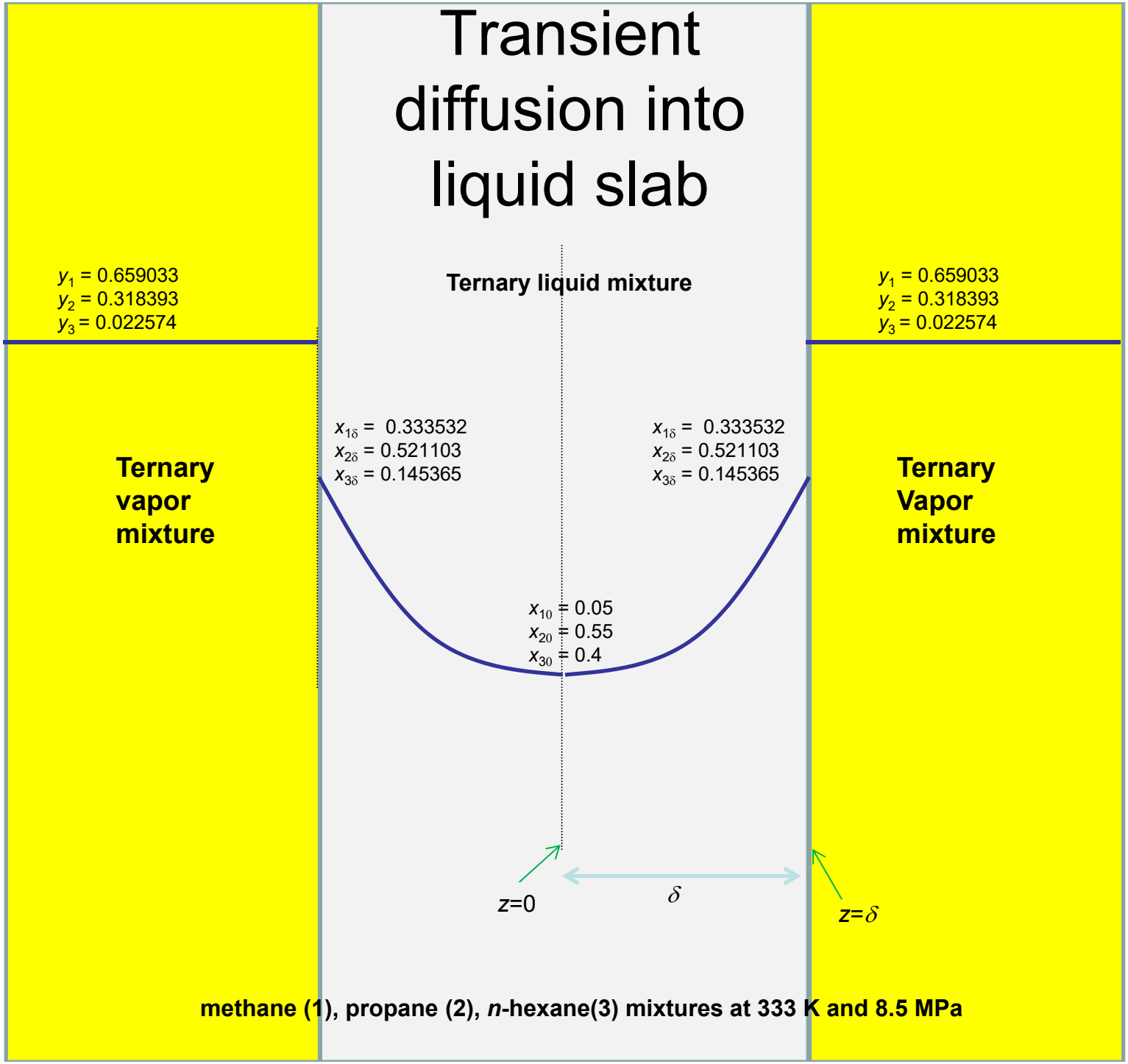
Transient diffusion into liquid slab
$y_1$ = 0.659033
$y_2$ = 0.318393
$y_3$ = 0.022574
Ternary liquid mixture
$y_1$ = 0.659033
$y_2$ = 0.318393
$y_3$ = 0.022574
$x_{1\delta}$ = 0.333532
$x_{2\delta}$ = 0.521103
$x_{3\delta}$ = 0.145365
$x_{1\delta}$ = 0.333532
$x_{2\delta}$ = 0.521103
$x_{3\delta}$ = 0.145365
Ternary vapor mixture
Ternary Vapor mixture
$x_{10}$ = 0.05
$x_{20}$ = 0.55
$x_{30}$ = 0.4
z=0
$\delta$
z=$\delta$
methane (1), propane (2), n-hexane(3) mixtures at 333 K and 8.5 MPa

Fig. S25

# C1/C3/nC6 mixtures: liquid equilibration trajectories

**(a)**

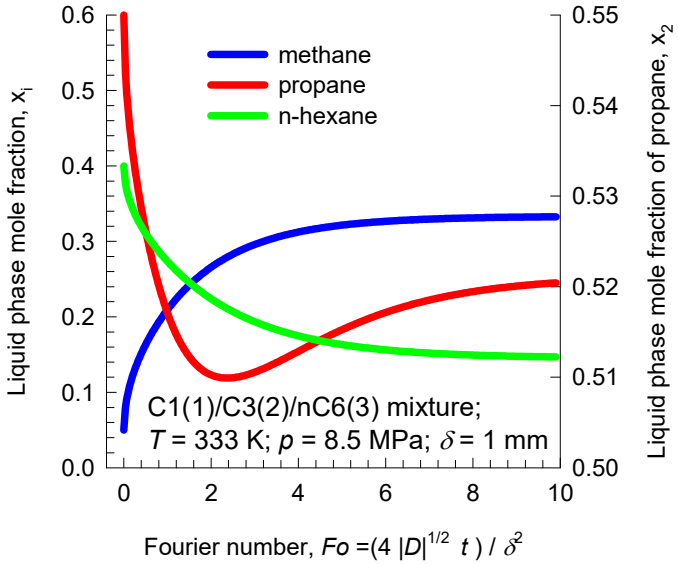


**(b)**

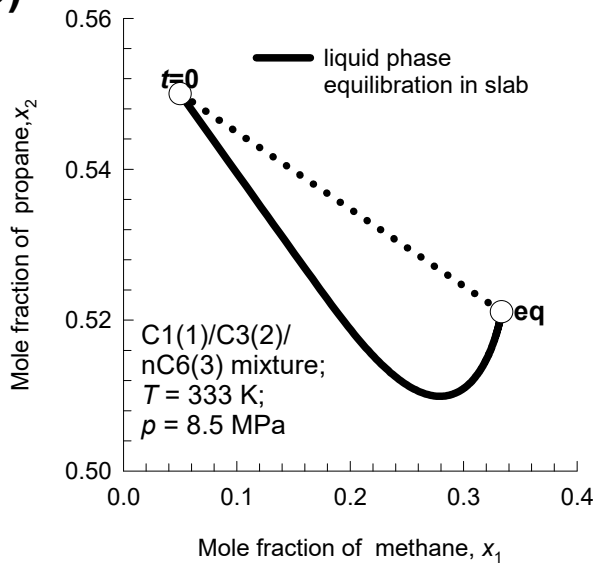


**(c)**

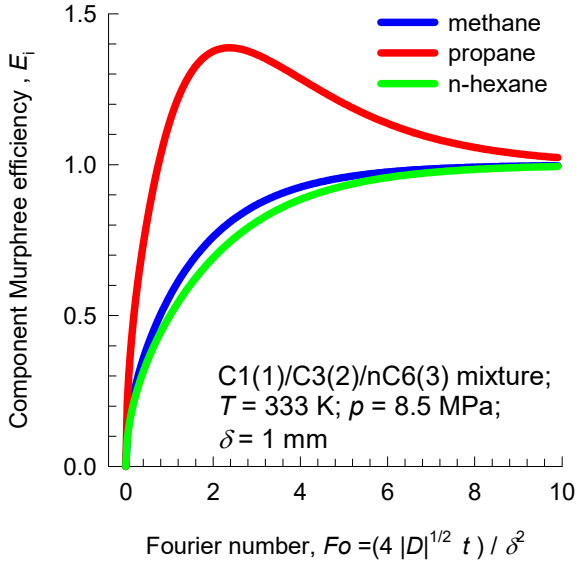

# C1/C3/nC6 mixture: Taylor dispersion

Fig. S26

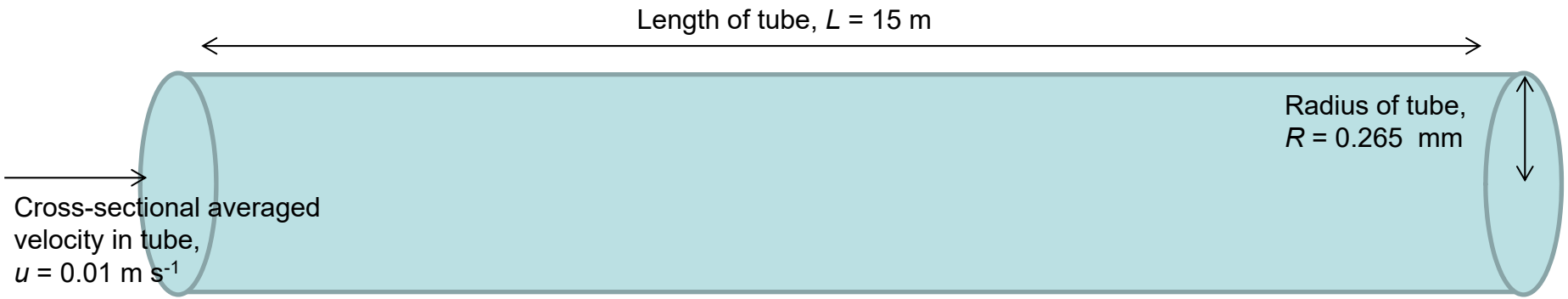


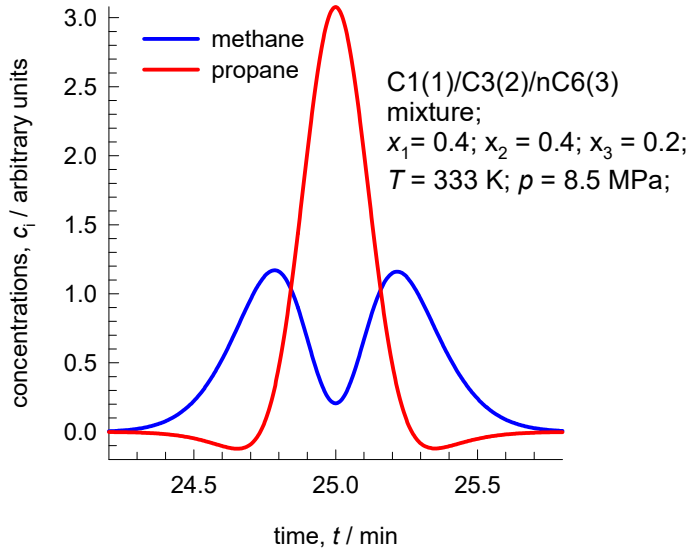

Fig. S27

# Ternary hydrocarbon mixtures: Taylor dispersion

**(a)**

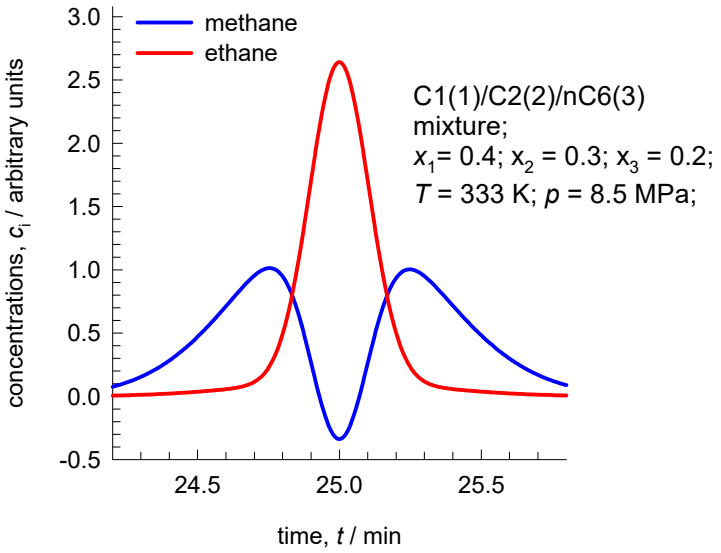


**(b)**

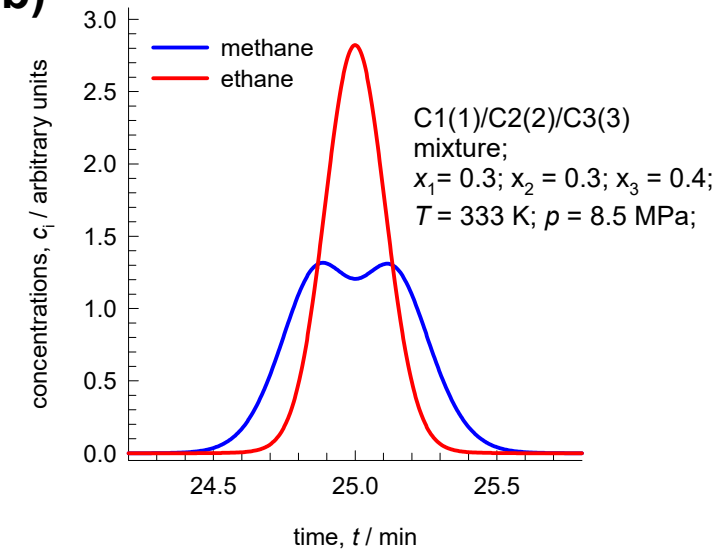


**(c)**

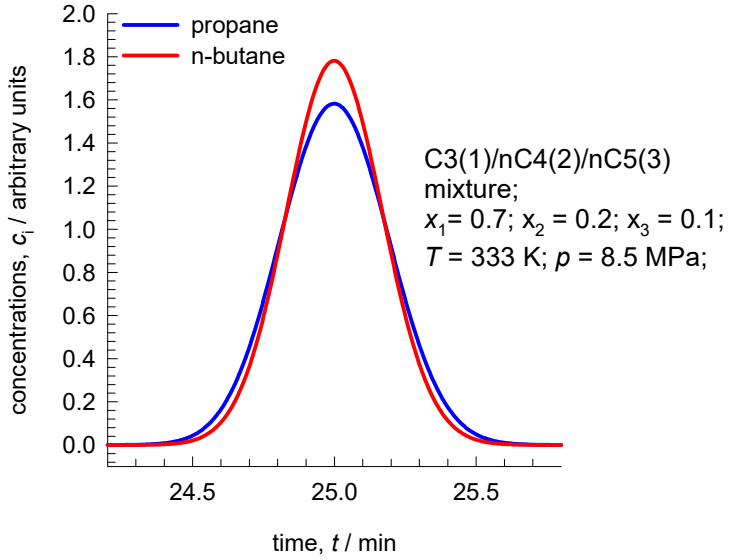


**(d)**

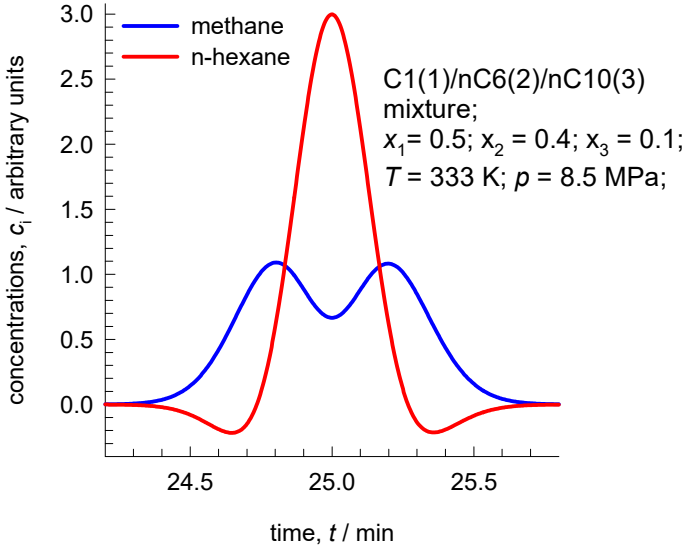

Fig. S28

# Effective diffusivities in Ammonia Synthesis

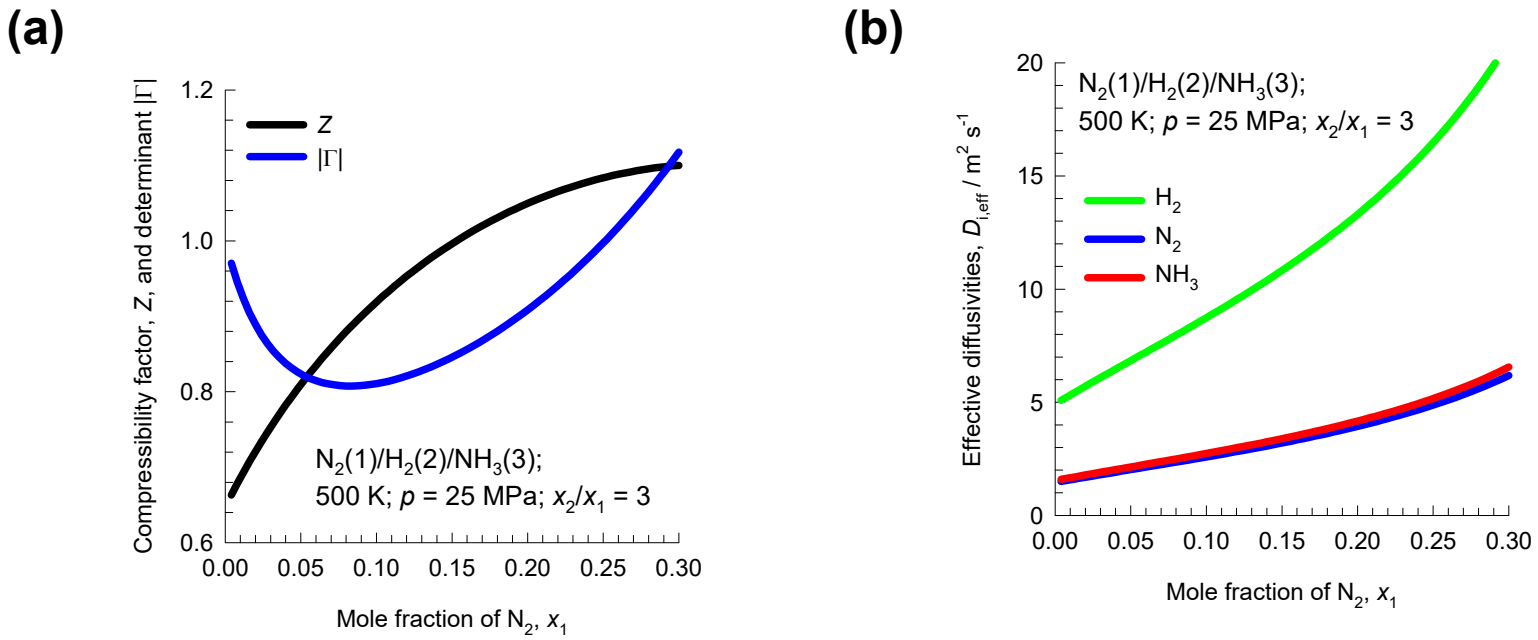

Fig. S29

# Effective diffusivities in CVD reactor

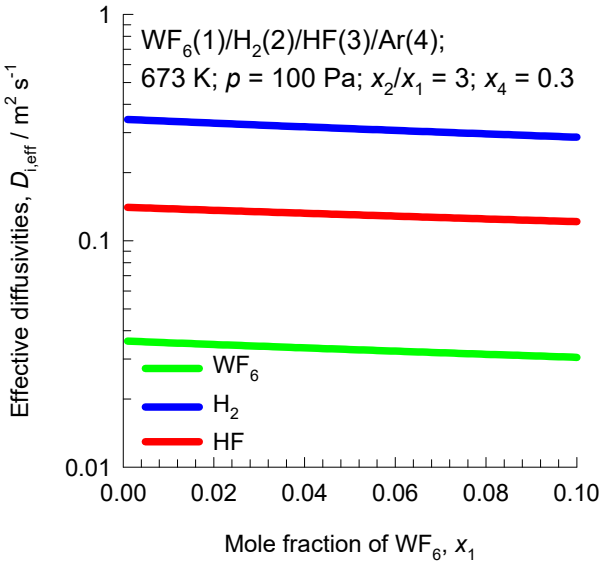

# Diffusion trajectories in CVD reactor

Fig. S30

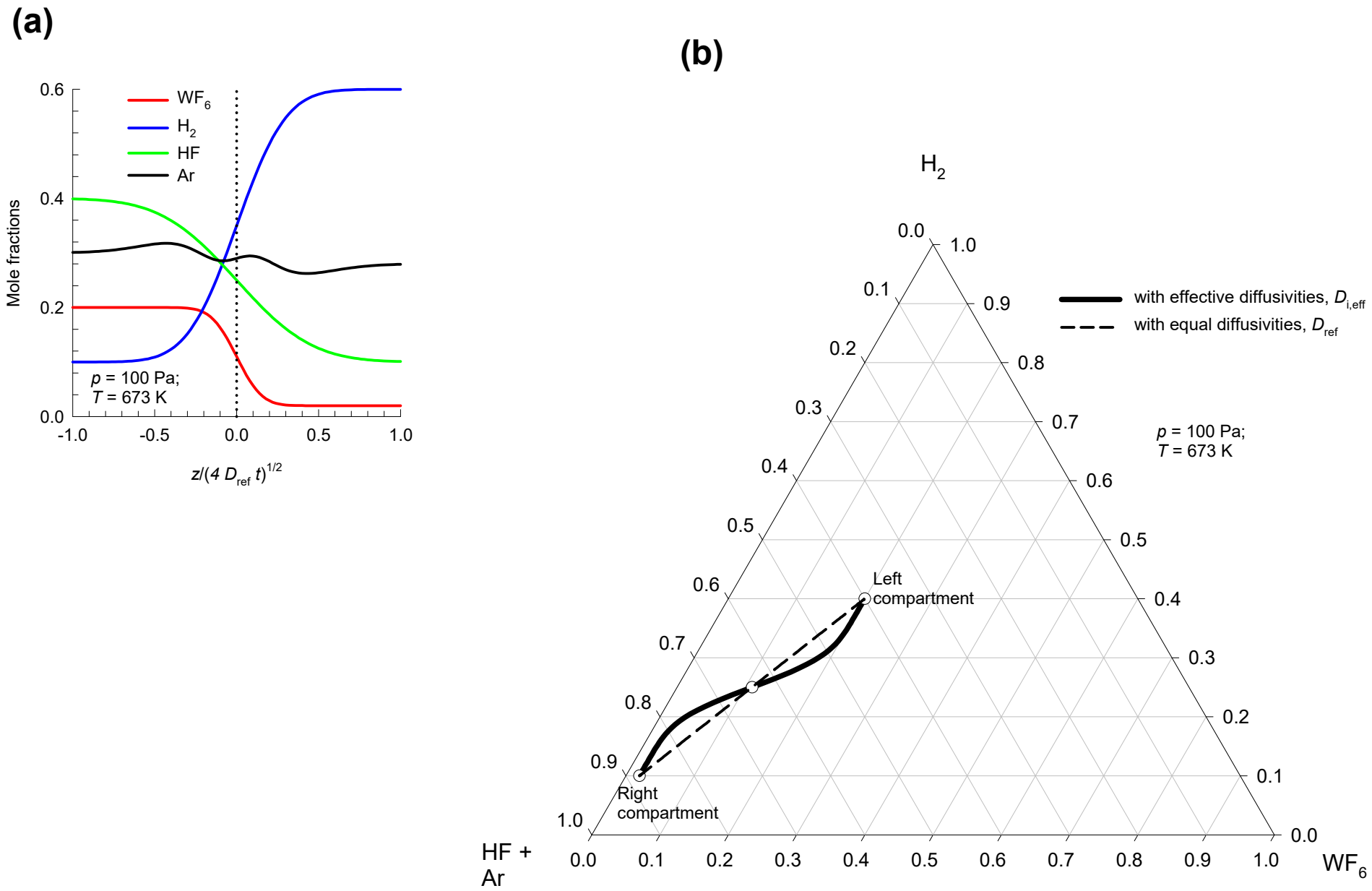

# Ultracentrifugation

Fig. S31

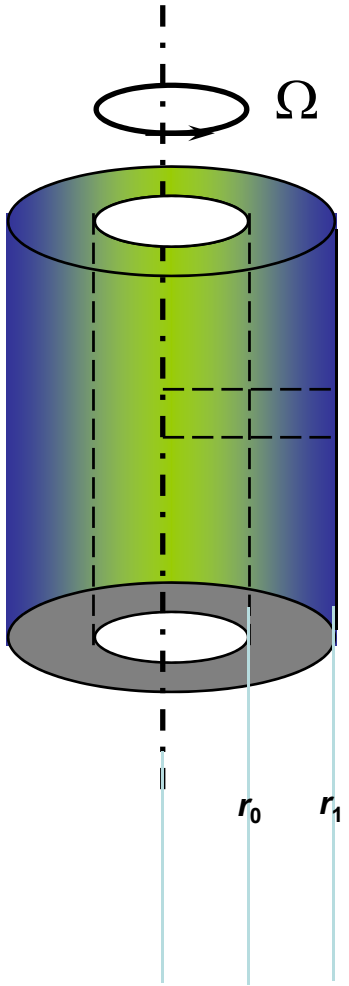


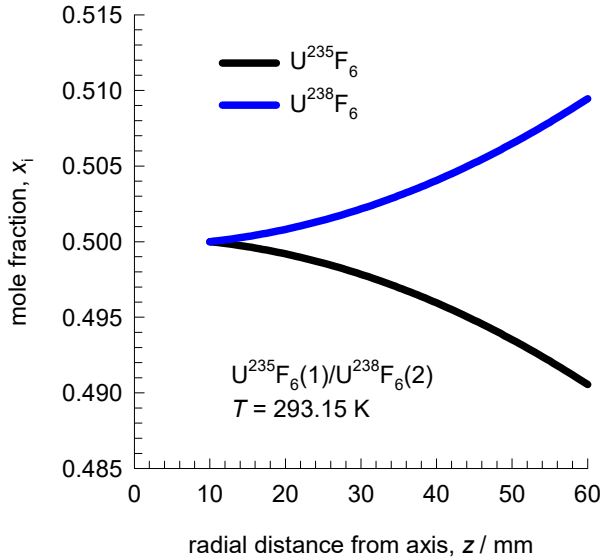

Fig. S32

# Ethane/n-decane mixture thermodynamics

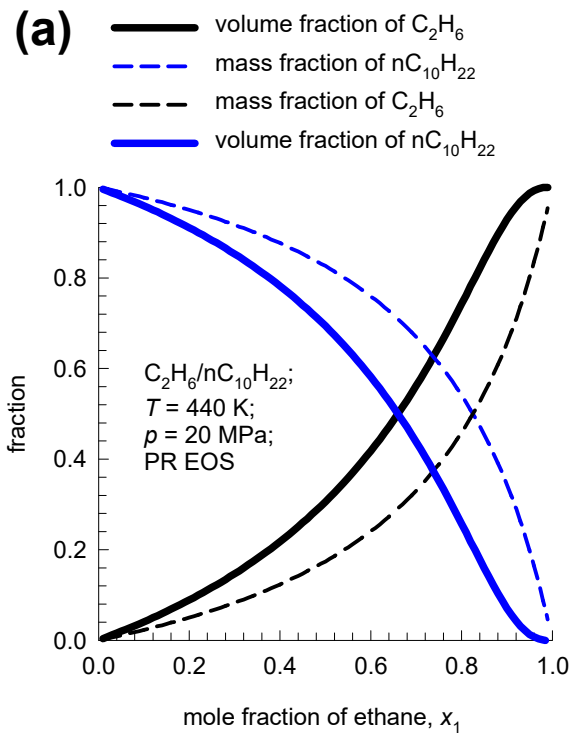


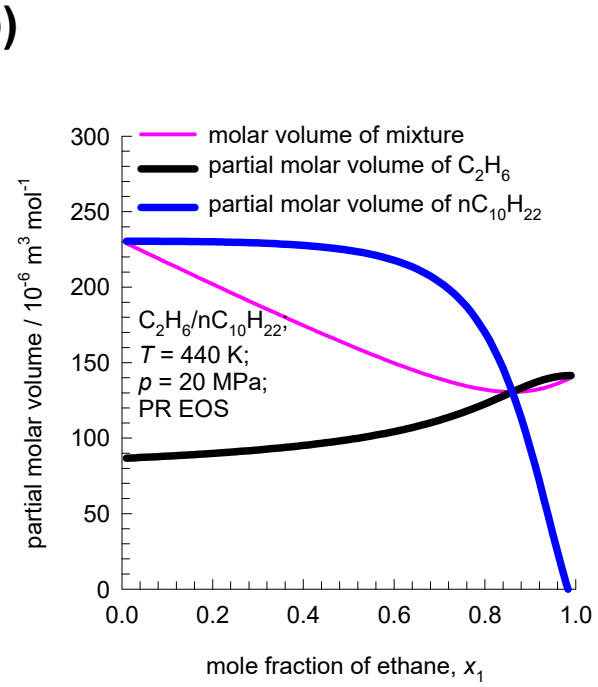


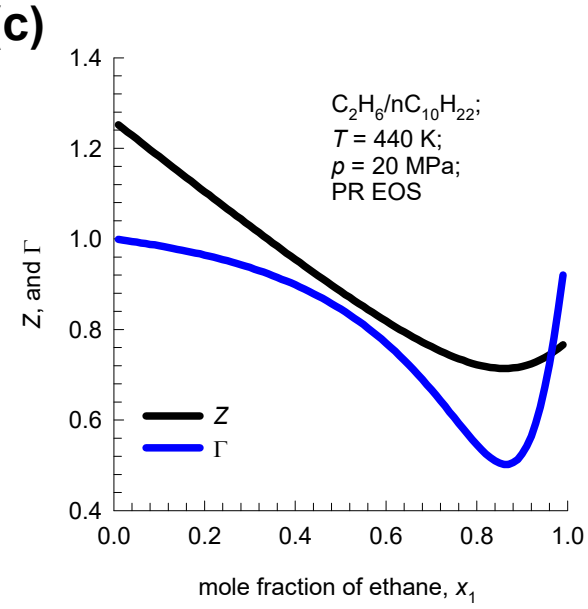

# Gravitational segregation

Fig. S33

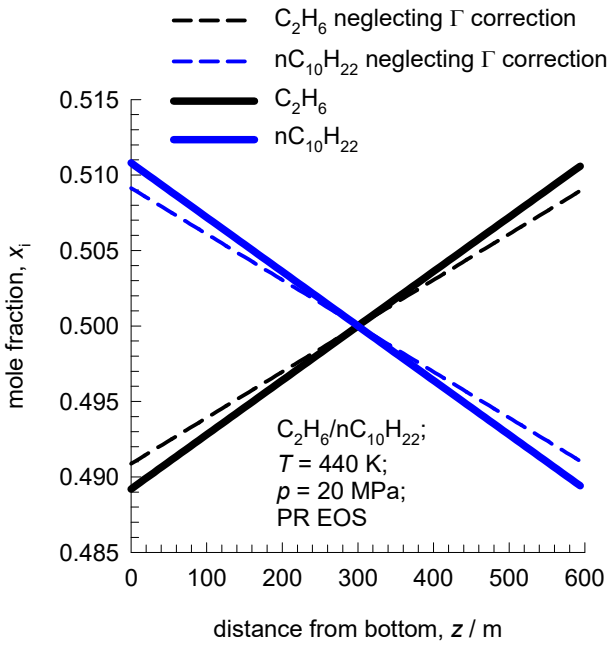


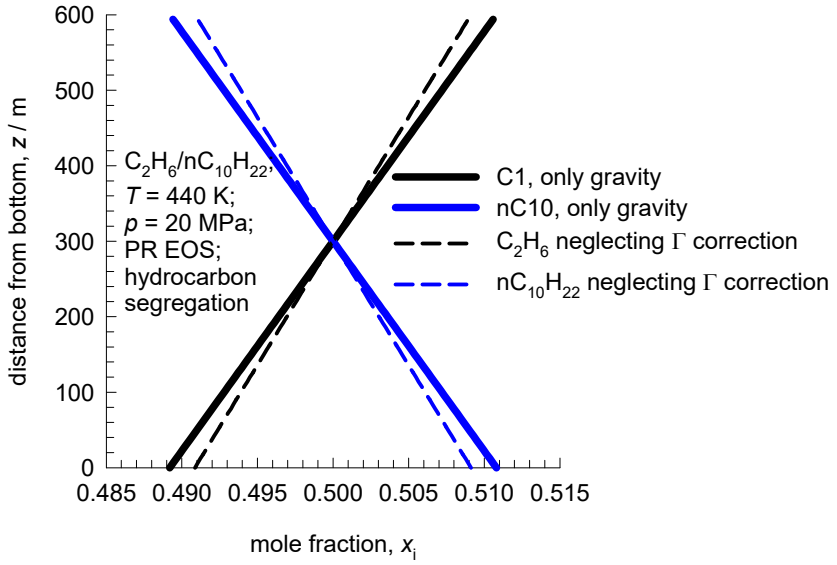

# Gravitational segregation

Fig. S34

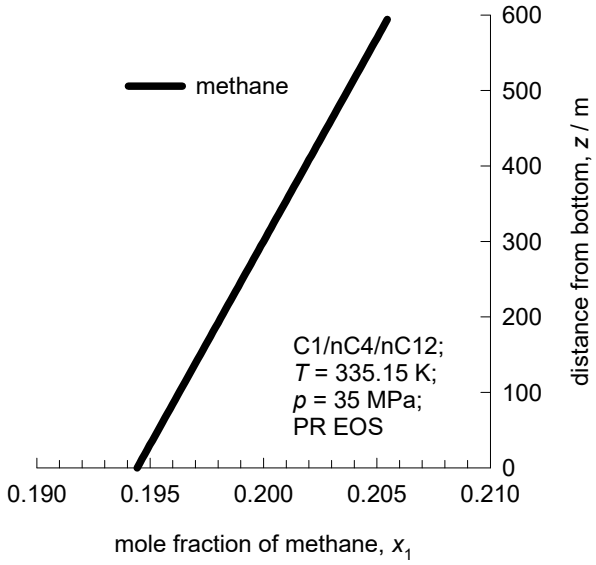


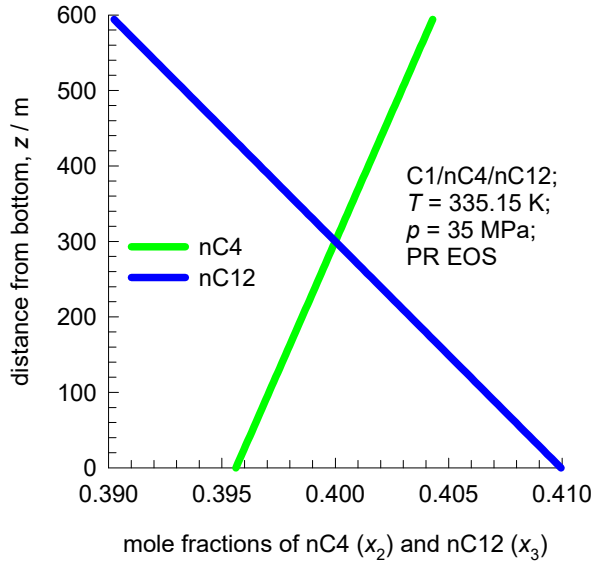

# Gravitational+ Thermo-diffusional segregation

Fig. S35